

INFORMATION TO USERS

This manuscript has been reproduced from the microfilm master. UMI films the text directly from the original or copy submitted. Thus, some thesis and dissertation copies are in typewriter face, while others may be from any type of computer printer.

The quality of this reproduction is dependent upon the quality of the copy submitted. Broken or indistinct print, colored or poor quality illustrations and photographs, print bleedthrough, substandard margins, and improper alignment can adversely affect reproduction.

In the unlikely event that the author did not send UMI a complete manuscript and there are missing pages, these will be noted. Also, if unauthorized copyright material had to be removed, a note will indicate the deletion.

Oversize materials (e.g., maps, drawings, charts) are reproduced by sectioning the original, beginning at the upper left-hand corner and continuing from left to right in equal sections with small overlaps. Each original is also photographed in one exposure and is included in reduced form at the back of the book.

Photographs included in the original manuscript have been reproduced xerographically in this copy. Higher quality 6" x 9" black and white photographic prints are available for any photographs or illustrations appearing in this copy for an additional charge. Contact UMI directly to order.

U·M·I

University Microfilms International
A Bell & Howell Information Company
300 North Zeeb Road, Ann Arbor, MI 48106-1346 USA
313/761-4700 800/521-0600



Order Number 9124406

Ultrasonic absorption in soft and hard fetal tissues

Drewniak, James Lewis, Ph.D.

University of Illinois at Urbana-Champaign, 1991

U·M·I
300 N. Zeeb Rd.
Ann Arbor, MI 48106



ULTRASONIC ABSORPTION IN SOFT AND HARD FETAL TISSUES

BY

JAMES LEWIS DREWNIAK

B.S., University of Illinois, 1985
M.S., University of Illinois, 1987

THESIS

Submitted in partial fulfillment of the requirements
for the degree of Doctor of Philosophy in Electrical Engineering
in the Graduate College of the
University of Illinois at Urbana-Champaign, 1991

Urbana, Illinois

UNIVERSITY OF ILLINOIS AT URBANA-CHAMPAIGN

THE GRADUATE COLLEGE

NOVEMBER 1990

WE HEREBY RECOMMEND THAT THE THESIS BY

JAMES LEWIS DREWNIAK

ENTITLED ULTRASONIC ABSORPTION IN SOFT AND HARD FETAL TISSUES

BE ACCEPTED IN PARTIAL FULFILLMENT OF THE REQUIREMENTS FOR
THE DEGREE OF DOCTOR OF PHILOSOPHY

Director of Thesis Research

Head of Department

Committee on Final Examination†

Chairperson

† Required for doctor's degree but not for master's.

ULTRASONIC ABSORPTION IN SOFT AND HARD FETAL TISSUES

James Lewis Drewniak, Ph.D.
Department of Electrical and Computer Engineering
University of Illinois at Urbana-Champaign, 1991
F. Dunn, Advisor

Although the use of ultrasound as a diagnostic modality in obstetrics has become ubiquitous, concern that harmful effects may occur under special circumstances continues. A physical mechanism by which biological effects could occur is the deposition of heat in the tissue as a result of the energy absorbed from the acoustic wave. Because the teratogenicity of hyperthermia has been well-established and concerns of more subtle effects of elevated fetal temperature exist, there is currently a concerted effort to provide manufacturers of medical diagnostic ultrasound instrumentation and clinicians with guidelines for the use of ultrasound during pregnancy. The temperature elevation in fetal soft tissue is estimated analytically from simple heat transfer models and simple assumptions concerning the ultrasound propagation and beam. Experimental animal studies exist to support the calculations. There is a need, however, to continue developing heat transfer models that better reflect the actual problem, such that more accurate estimates of the temperature elevation upon exposure to ultrasound can be made. Included in such models would be the absorption properties of fetal soft tissue and fetal bone as a function of gestational age. The absorption of ultrasound in fetal tissues and the resulting temperature elevation are studied in this thesis. The temperature elevation in fetal mice exposed to 1 *MHz* ultrasound is measured, and the results are compared with analytical values of the temperature increase that are calculated using a simple heat transfer model. The transient thermoelectric method for measuring the absorption coefficient of liquids and soft tissues is also analyzed. The results provide an

experimental guide for more accurate measurements of the absorption coefficient in fetal soft tissue. Finally, the absorption in fetal bone as a function of gestational age is considered. The acoustic propagation properties in bone are as yet unknown. The velocity and absorption are expected to be a function of the mode and direction of propagation because of the anisotropy of the bone. In the absence of specific knowledge regarding the acoustic properties of fetal bone, from which the temperature increase might be calculated, the temperature rise resulting from exposure to ultrasound can be measured. The temperature elevation in fetal bone exposed to 1 *MHz* ultrasound is measured for a range of gestational ages. An equivalent heat source obtained from the measurements, which might be used in numerical and analytical calculations, is given.

DEDICATION

in memory of my father

ACKNOWLEDGEMENTS

I would like to thank my advisor Professor Floyd Dunn for his encouragement and guidance throughout the course of this work. I learned a very scholarly approach to science from him for which I will always be grateful. I would also like to thank Professors Leon Frizzell, Paul Mayes, and Michael Chen for serving on my graduate committee. I am grateful to Professor Frizzell for the guidance and insight he provided into several aspects of this work. I am deeply indebted to Professor Mayes for the time he has always made for discussions, and the encouragement and support he has given me. I owe to him my enthusiasm for Maxwell's equations and wave motion, and the joy they give me. I am very grateful to Professor Gregory Stillman, who as my undergraduate advisor provided constant encouragement that propelled me toward graduate school. I thank Professor John Harris for the many discussions I had with him. His courses in acoustics and wave propagation provided me with a great deal of insight into wave motion. I also thank Professor Narayana Rao for his support and encouragement for the activities of the Electrical and Computer Engineering Student Advisory Committee when I was a member. The organizational skills that I began to develop in the course of my association with Professor Rao and the committee will benefit me greatly in the future.

I thank the staff of the Bioacoustics Research Laboratory for their assistance in the construction of hardware used in this work and in the preparation of papers that were published. The experimental portion of the study presented in Chapter 3 was conducted

in conjunction with Mrs. Kay Carnes. Her expertise in animal care and preparation, and ultrasonic bioeffects research was instrumental to the success of that work.

I thank my sisters Kathleen, Mary, and Theresa for the loving support and encouragement they provided throughout my education. Words cannot express the love and gratitude that I feel for my parents Robert and Dorothy for their loving support and encouragement of all my pursuits in the course of growing up, and for teaching me the merits of hard work and perseverance. To them I owe what success I have and will achieve. Finally, I thank my wife Mariesa for her love, encouragement, and support throughout the course of this work. I am also grateful for her assistance in typing portions of this thesis, and for help with L^AT_EX.

TABLE OF CONTENTS

CHAPTER	PAGE
1 INTRODUCTION	1
2 MEASUREMENT APPARATUS AND TECHNIQUES	12
2.1 The Ultrasound Irradiation System	12
2.2 Transducer Characterization	17
2.3 Temperature Measurement Techniques	26
3 <i>IN UTERO</i> MEASUREMENT OF THE TEMPERATURE ELEVATION IN FETAL MICE EXPOSED TO 1 MEGAHERTZ ULTRASOUND	35
3.1 Methods	36
3.2 Analytical Development	43
3.3 Results and Discussion	49
4 AN ANALYSIS FOR A MORE ACCURATE DETERMINATION OF THE ULTRASONIC ABSORPTION COEFFICIENT IN SOFT TISSUE	55
4.1 Theory	62
4.2 Results and Discussion	70
4.3 Comparison of Gaussian and UDCA Beams	85
4.4 Results for Tissues with a Thermal Diffusivity Different from Water .	89
4.5 Summary	93
5 ULTRASONIC ABSORPTION IN FETAL BONE	96
5.1 Acoustic Waves in Solids	97
5.2 Methods	107
5.3 Estimation of the Error in the Temperature Increase Measurements .	116
5.4 Temperature Increase Measurements at 1 MHz	126
6 SUMMARY AND RECOMMENDATIONS FOR FUTURE WORK	139
APPENDIX A INTEGRAL-DIFFERENTIAL RELATION BETWEEN THE IMPULSE AND UNIT STEP RESPONSES	144
APPENDIX B TRANSDUCER BEAM PROFILES	146

APPENDIX C A SIMPLE INTERPRETATION OF THE EQUIVALENT HEAT SOURCE RESULTING FROM THE ABSORPTION OF ULTRASOUND BY BIOLOGICAL TISSUE	151
REFERENCES	155
VITA	169

CHAPTER 1

INTRODUCTION

Although the use of ultrasound as a diagnostic modality in obstetrics has become ubiquitous, concern that harmful effects may occur continues. Several studies have demonstrated that lesions can be produced in soft tissue upon exposure to ultrasound for some exposure conditions [65], [80], [82], [88], [115], [167], [175]. Two mechanisms, thermal and cavitation, are considered to be of primary importance in the ultrasonic production of lesions in soft tissue [6]. The thermal mechanism is considered in the study reported herein. The deposition of acoustic energy converted to heat and the resulting temperature elevation in fetal tissues are currently of great concern to the ultrasound community, because of the well established teratogenicity of hyperthermia [71], [146] and the possibility of more subtle, as yet undetermined, effects associated with elevated fetal temperatures. The National Council on Radiation Protection and Measurements (NCRP) Committee 66 is currently preparing a document to provide information on thermal effects upon exposure to diagnostic ultrasound. The American Institute of Ultrasound in Medicine (AIUM) has convened a Thermal Index Working Group to determine ultrasound exposure conditions which would result in a temperature increase in the fetus of 1°C (a normal diurnal variation in the body temperature of the mother). The study reported herein is concerned with the conversion of acoustic energy to heat, i.e., ultrasonic absorption, and the resulting temperature elevation in fetal tissues exposed to ultrasound.

Estimations of the temperature elevation in tissue resulting from heat generation involve a correct description of the conductive and convective processes in the tissue as well as

the source of the heat generation. The bioheat transfer equation introduced by Pennes [166] for modeling heat transport in perfused media has been used extensively in calculating the temperature increase resulting from exposure of biological specimens to ultrasound [1], [30], [38], [137], [138], [139], [151], [154], [155], [177]. An assessment by Eberhart et al. [68] concluded that the bioheat equation is “an adequate model for the prediction of the macroscopic temperature distribution in several biological tissues.” The form of the bioheat equation commonly employed in the prediction of the temperature elevation in fetal tissue resulting from exposure to ultrasound is

$$\frac{\partial T(\bar{\mathbf{r}}, t)}{\partial t} = \kappa \nabla^2 T(\bar{\mathbf{r}}, t) - \frac{T(\bar{\mathbf{r}}, t)}{\tau} + \frac{q_v(\bar{\mathbf{r}}, t)}{\rho C_p} \quad (1.1)$$

where T is the temperature elevation, $\bar{\mathbf{r}}$ is the spatial coordinate (where the overbar represents a vector quantity), κ is the thermal diffusivity of the medium, τ is the perfusion time constant, $q_v(\bar{\mathbf{r}}, t)$ is the rate of heat production per unit volume, ρ is the density, and C_p is the specific heat. A thermally isotropic medium has been assumed in writing Eq. (1.1). Other forms of the bioheat equation appear in the literature [151], [177], in which the blood flow is given by a blood perfusion rate w ($\frac{gm}{cm^3-s}$), which is related to the perfusion time constant by

$$\tau = \frac{\rho C_p}{w \rho_b C_b} \quad (1.2)$$

where ρ_b is the density of blood and C_b is the specific heat of blood.

The solution to the bioheat equation depends upon the specific boundary conditions and initial values associated with a particular application and may be obtained by well-known analytical and numerical methods [113], [156], [184]. Numerical solutions to the bioheat equation are commonly sought in hyperthermia applications [66], [67], [111], [147], [177]. Whereas the analytical solutions discussed below assume a homogeneous and isotropic medium with

uniform perfusion, inhomogeneities, anisotropies and nonuniform perfusion are easily handled in numerical computations. Chan et al. [46] used a numerical method to calculate the temperature increase at a fat-muscle-bone interface. Reflections of the ultrasonic wave at interfaces were ignored, and the perfusion was chosen to provide a best fit to the available experimental data. Their calculated results were found to be in reasonable agreement, given the simplifying assumptions, with experimental results published by Lehman [131].

An analytical solution for an infinite medium with isotropic and homogeneous thermal properties can be obtained easily by the method of Green's functions [156], [190]. The Green's function for the bioheat equation is given by the solution to

$$\frac{\partial G}{\partial t} = \kappa \nabla^2 G - \frac{G}{\tau} + \delta(\bar{\mathbf{r}})\delta(t) \quad (1.3)$$

Equation (1.3) can be solved using transform techniques [54]. By introducing a time and spatial shift in the delta function, i.e., $\delta(\bar{\mathbf{r}} - \bar{\mathbf{r}}')\delta(t - \theta)$, a shift in the Green's function is introduced, and the resulting solution to Eq. (1.3) is

$$G(\bar{\mathbf{r}} - \bar{\mathbf{r}}', t - \theta) = \frac{e^{-\frac{(t-\theta)}{\tau} - \frac{|\bar{\mathbf{r}} - \bar{\mathbf{r}}'|^2}{4\kappa(t-\theta)}}}{[4\pi\kappa(t - \theta)]^{\frac{3}{2}}} \quad (1.4)$$

Let the heat source be given by

$$\frac{q_v(\bar{\mathbf{r}}, t)}{\rho C_p} = \frac{q_{v0} f(\bar{\mathbf{r}}) F(t)}{\rho C_p} = Q_0 F(t) f(\bar{\mathbf{r}}) \quad (1.5)$$

where Q_0 ($\frac{^{\circ}\text{C}}{\text{s}}$) is the magnitude of the rate of the temperature increase, q_{v0} is the volumetric rate of energy deposition, and $f(\bar{\mathbf{r}})$, and $F(t)$ are the spatial and temporal variations of $q_v(\bar{\mathbf{r}}, t) = q_{v0} f(\bar{\mathbf{r}}) F(t)$, respectively. A solution to the bioheat equation in an infinite, isotropic, and homogeneous medium for the temperature elevation at position $\bar{\mathbf{r}}$ and time t is then given by

$$T(\bar{\mathbf{r}}, t) = Q_0 \int_0^t d\theta F(\theta) \int_V d\bar{\mathbf{r}}' f(\bar{\mathbf{r}}') G(\bar{\mathbf{r}} - \bar{\mathbf{r}}', t - \theta) \quad (1.6)$$

Equation (1.6) is also a representation for the solution to the heat equation in an infinite, isotropic, and homogeneous medium in the limit as $\tau \rightarrow \infty$. Other analytical representations of the solution to the bioheat and heat equations and other boundary conditions have been considered by investigators in the ultrasound field, and are discussed below.

The bioheat and heat equations have been used to predict the temperature elevation in soft tissue exposed to ultrasound. Typically the solutions assume an infinite, isotropic, and homogeneous medium with zero initial conditions and zero temperature elevation at infinity. It is common to assume plane wave propagation in the soft tissue. The equivalent heat source is then found to be $q_{v0} = 2\alpha I$, where α is the acoustic absorption coefficient and I is the acoustic intensity. The Green's function representation given by Eq. (1.6) is then employed to calculate $T(\bar{r}, t)$.

Pond, in an attempt to discern the role of heat in the production of lesions in brain tissue *in vivo*, in the focal region of an ultrasonic transducer, calculated the temperature elevation using Eq. (1.6) with $\tau \rightarrow \infty$ [167], [168]. His experimental results compared favorably with his calculations. Robinson and Lele [175] in their investigation of lesion development in brain *in vivo* and polymethylmethacrylate also used the solution to the heat equation given by Eq. (1.6) to predict the temperature elevation resulting from exposure to high intensity ultrasound. Their experimental results compared favorably with the computed values; however, the authors noted that more accurate data for the ultrasonic and thermal properties of tissue are necessary for better estimations of the temperature elevation. Another early use of the heat equation to predict the temperature elevation in tissue was reported by Lerner et al. [135] in their assessment of the effect of temperature elevation on the frequency dependence of thresholds for ultrasonic production of thermal lesions in tissue.

The heat equation and the solution given by Eq. (1.6) have also been used in thermal modeling for the ultrasonic treatment of glaucoma and ultrasonic hyperthermia in ophthalmic therapy [137], [138], [139]. The uniform acoustical and thermal properties of the eye lend themselves particularly well to the assumptions of a thermally homogeneous, infinite medium for the times of interest in these studies. Lesions were produced by elevating the temperature in the tissue with high intensity ultrasound and exposure durations of several seconds. The predicted temperature elevation and lesion size agreed well with the experimental results in the rabbit eye.

The Green's function representation for the solution to the heat equation was used by Konopatskaya [120] to study the heating in soft tissue exposed to focused ultrasound. The equivalent heat source and source region for the focused ultrasound beam, in the focal region, were modeled as nested ellipsoids with uniform heat deposition proportional to the intensity over the particular ellipse. The product of the source and Green's function was then integrated over the source region. The temperature elevation in the rabbit brain exposed *in vitro* to focused ultrasound was found to agree well with the analytical results.

Nyborg [155] has reported analytical results, neglecting perfusion, for the temperature elevation in soft tissue upon exposure to unfocused ultrasound. The equivalent heat source resulting from ultrasonic absorption was modeled as a uniform cylinder in the near-field region of the transducer and as an adjoining cone in the far-field region. The study reported the calculated temperature increase for a variety of diameters of the transducer. An extension of this work to include perfusion was given also by Nyborg [154]. The cited work by Nyborg [154], [155], is used in a current effort to provide information concerning the temperature

increase resulting from exposure to diagnostic ultrasound [150]. Analytical results that include perfusion are presented for uniformly heated spheres and discs as well as other cases.

Wu and Du reported results for the steady state temperature increase generated by a focused Gaussian beam of ultrasound [202]. The study included perfusion, and the equivalent heat source resulting from ultrasonic absorption was derived from analytical expressions for acoustic propagation of a Gaussian beam in water. Their investigation included not only the zero boundary condition at infinity, but also Dirichlet and Neuman boundary conditions for a half-space, to illustrate the effects of a finite boundary on the temperature elevation. The complexity of the expression for the equivalent heat source of the focused Gaussian beam precluded analytical integration for the transient problem.

The studies cited above have employed the representation given by Eq. (1.6) in computing the temperature elevation resulting from ultrasonic absorption. The equivalent heat source was approximated in various manners and then the product of the source and Green's function was integrated over the source region. Other mathematical methods exist for finding the solution to the heat and bioheat equations [156], [184]. For example an early study by Filipczinski [74], [75] utilized transform methods for computing the temperature elevation resulting from a uniform cylindrical heat source approximating a focused beam of ultrasound. Wu and Du also employed transform methods to determine the temperature elevation in tissues generated by finite-amplitude tone bursts of plane wave ultrasound [201].

These studies form the basis and support for current efforts aimed at calculating the temperature increase in soft and hard fetal tissues. Experimental studies have been reported on testing the applicability of the simple models of these studies for the equivalent heat source and source region resulting from ultrasonic exposure. An experimental animal study

by Sikov et al. [185] measured the temperature rise in fetal rats during the exposure of the exteriorized uterus. Temperature increases up to $21.5\text{ }^{\circ}\text{C}$ and $17.5\text{ }^{\circ}\text{C}$ for 0.8 and 2.4 MHz ultrasound at a spatial-average, temporal-average intensity of $10\text{ }\frac{\text{W}}{\text{cm}^2}$ for an exposure time of 7.5 min were measured. The lower temperature elevation at 2.4 MHz can be attributed to a smaller beamwidth at the higher frequency. Calculations based on models given by Nyborg [152] showed reasonable agreement with the measurements; however, the authors pointed out that the number of assumptions involved in the calculations made the agreement seem somewhat surprising. A more recent study of the temperature elevation in the rat fetus exposed to ultrasound, with the uterus exteriorized, has been reported by Abraham et al. [1]. A temperature elevation in the range of $7\text{ }^{\circ}\text{C}$ to $20\text{ }^{\circ}\text{C}$ was measured in 15 to 20 day rat fetuses exposed to 1 MHz ultrasound for spatial-average, temporal-average intensities of 2, 4.2, and $7.9\text{ }\frac{\text{W}}{\text{cm}^2}$ for exposure times of 10 min . The experimental data for live and dead fetuses were compared with the analytical model of Nyborg [152], and did not include perfusion. The magnitude of the volumetric rate of heating q_{v0} is commonly taken to be $2\alpha I$ in soft tissue calculations. A best-fit analytical curve for the experimental data was drawn by Abraham et al. by choosing α appropriately. Since perfusion was neglected in the live fetuses, the resulting α was denoted as an effective absorption coefficient. The effective absorption coefficient, or absorption coefficient resulting from a best fit of the analytical model to the measurements, was greater than twice that of an adult soft tissue such as liver, for both the live and dead fetuses.

Significant temperature increases at soft tissue-bone interfaces have been reported by Hynynen and DeYoung [112]. They reported the maximum temperature rise to be at the bone surface and decrease rapidly both in front of the bone and inside it. A maximum steady

state temperature elevation of approximately $5\text{ }^{\circ}\text{C}$ was measured after 20 min of exposure to an ultrasound beam with an acoustic output power of 1.7 W and a scan diameter of 20 mm . This degree of temperature elevation is of serious concern in fetal exposures. A study of the temperature elevation in bone upon exposure to ultrasound was conducted by Carstensen et al. [38]. The skull of a young mouse was the experimental animal model employed to simulate fetal bone. A temperature elevation of approximately $5\text{ }^{\circ}\text{C}$ was measured in the adult mouse skull exposed to 3.6 MHz focused ultrasound at a spatial-peak, temporal-average intensity I_{SPTA} , of $1.5\text{ }\frac{\text{W}}{\text{cm}^2}$ for 1.5 min . The temperature elevation calculated from the analytical model given by Nyborg that included perfusion was fitted to the experimental data. The absorbed energy (proportional to q_{v0}) and τ were chosen to yield the best fit. Reasonable arguments were given for the final values chosen, and the experimental data agreed well with the calculated results.

Although few experimental studies of fetal tissues exposed to ultrasound have been reported, the results illustrate two important points. First, potentially harmful temperature elevations can be produced in soft and hard fetal tissues exposed to ultrasound under some exposure conditions. The diurnal variation in the body temperature of a human mother is approximately $1\text{ }^{\circ}\text{C}$. Thus, ultrasonic exposure conditions, in which the primary consideration for harmful effects to the fetus is heat deposition, are considered to be without risk if this temperature is not exceeded. It may, however, be possible to exceed a $1\text{ }^{\circ}\text{C}$ temperature elevation in the fetus using some diagnostic devices. Although the typical I_{SPTA} of scanning mode fetal imaging devices are well below the intensities used in the cited animal studies, the I_{SPTA} of some fetal Doppler devices presently in clinical use do exceed $1.0\text{ }\frac{\text{W}}{\text{cm}^2}$ [4], [5]. In view of the available data from animal studies, there is concern that the temperature increase

in the fetus may, under special circumstances, exceed $1\text{ }^{\circ}\text{C}$ in fetal Doppler exposures [38]. Second, insufficient knowledge of absorption in fetal tissues exists to determine accurately the volumetric rate of heat deposition, and there is insufficient knowledge of perfusion. Thus, models that more accurately reflect the complex heat transfer problem involved from which reasonable estimates of the temperature elevation might be obtained, cannot be constructed.

It is the purpose of this study to provide information on the absorption of ultrasound in soft and hard fetal tissues and to determine resulting temperature elevations for conditions which approximate those of fetal Doppler devices.

The ultrasound measurement system and the ultrasound and temperature measurement techniques employed herein are described in Chapter 2. A study of the temperature elevation in fetal mice exposed *in utero* to 1 MHz ultrasound is presented in Chapter 3. The gravid uterine environment is preserved in these measurements. The measured temperature increase is in the range of $1.5\text{ }^{\circ}\text{C}$ to $4.5\text{ }^{\circ}\text{C}$ for intensities from 0.5 to $10\text{ }\frac{\text{W}}{\text{cm}^2}$. Several exposure durations were used from 30 to 400 s . The temperature increase measured in this study is in the range of those measured by Sikov et al. [185] and Abraham et al. [1]. Analytical results with an equivalent heat source allowing for different absorption in the fetal tissue, as compared to those of the surrounding dam, are given. There is reasonable agreement between the analytical and experimental values of temperature increase. However, it is pointed out in Chapter 3 that the volumetric rate of heating q_{v0} and the blood perfusion constant τ can be chosen easily in retrospect to fit the data. Without specific knowledge of the absorption and perfusion, accurate estimates of the temperature increase for given exposure conditions are not possible.

Accurate measurement of the absorption coefficient in fetal tissues is particularly difficult because of the small size and low absorption of the tissue specimens. Heat conduction as a result of the small size can contribute a significant error to the measurement. In addition, a measurement artifact associated with the presence of the thermocouple temperature sensor can also introduce a significant error because of the low absorption of fetal soft tissue. The error resulting from heat conduction in the measurement of the ultrasonic absorption coefficient using the transient thermoelectric method is studied analytically in Chapter 4. An expression for the temperature increase in a tissue specimen *in vitro*, of finite dimensions, irradiated by a focused ultrasonic transducer, is given as a function of spatial coordinates, time, radial and axial beam dimensions, and absorption. An error is defined, and results are presented for various values of beamwidth, tissue dimensions, absorption, and time for the purpose of quantifying the experimental error due to heat conduction, and to provide guidance for minimizing this error in experimental procedures. For example, it is shown that the effect of heat conduction on the measured rate of temperature increase is less than 7% when using a transducer with a 5 mm half-power beamwidth at depths greater than 1.5 mm in the tissue. The analytical results given for the error as a function of the half-power beamwidth are shown to compare favorably with published experimental data.

Finally, temperature increase measurements in human fetal femurs exposed *in vitro* to 1 MHz ultrasound at 37 °C are presented in Chapter 5. The temperature is measured with a thermocouple probe and is given for several gestational ages. The temperature elevation measured in 59 and 108 day fetal femurs exposed at $1 \frac{W}{cm^2}$ for 20 s is found to be 0.10 °C and 2.9 °C, respectively. The initial rate of the temperature increase in the specimens is evaluated and compared to known values of absorption in soft tissue. For example, the initial

rate of temperature increase in the 108 *day* gestational age specimen resulting from exposure to ultrasound is 30 time greater in the fetal bone than that of soft tissue with an absorption coefficient of 0.05 cm^{-1} .

CHAPTER 2

MEASUREMENT APPARATUS AND TECHNIQUES

The system used for ultrasonic exposure of the tissue specimens and measurement of temperature is described in this chapter. The first of the two primary components of the apparatus to be discussed is the ultrasound irradiation system, which includes the ultrasound transducer, the RF signal driving and control circuitry, and the computer control for gating the RF and positioning the specimen relative to the acoustic beam. The means by which the transducers employed for the experimental measurements are characterized are discussed and the results presented. Finally the temperature measurement is discussed, including the temperature sensor, i.e., the thermocouple, and the amplifying and data acquisition of the thermal electromotive force (emf) output of the thermocouple. The error in the measured temperature is also discussed.

2.1 The Ultrasound Irradiation System

The schematic of the ultrasound system used for irradiating tissue specimens and characterizing the transducers is shown in Figure 2.1. The RF source is a Hewlett Packard 8660A signal generator, with a 86601A RF plug-in, having a bandwidth of 0.01 MHz – 110 MHz. The output of the signal generator is fed to a matched RF attenuator for rough amplitude control of the transducer driving signal. The RF at the output of the attenuator is gated by a double-balanced mixer (Mini Circuits Laboratory, TAK-5) before being input to the power amplifier (Amplifier Research, Model 1000L). The amplified signal is then input to a driving/matching circuit that drives the transducer crystal. A signal is fed back from

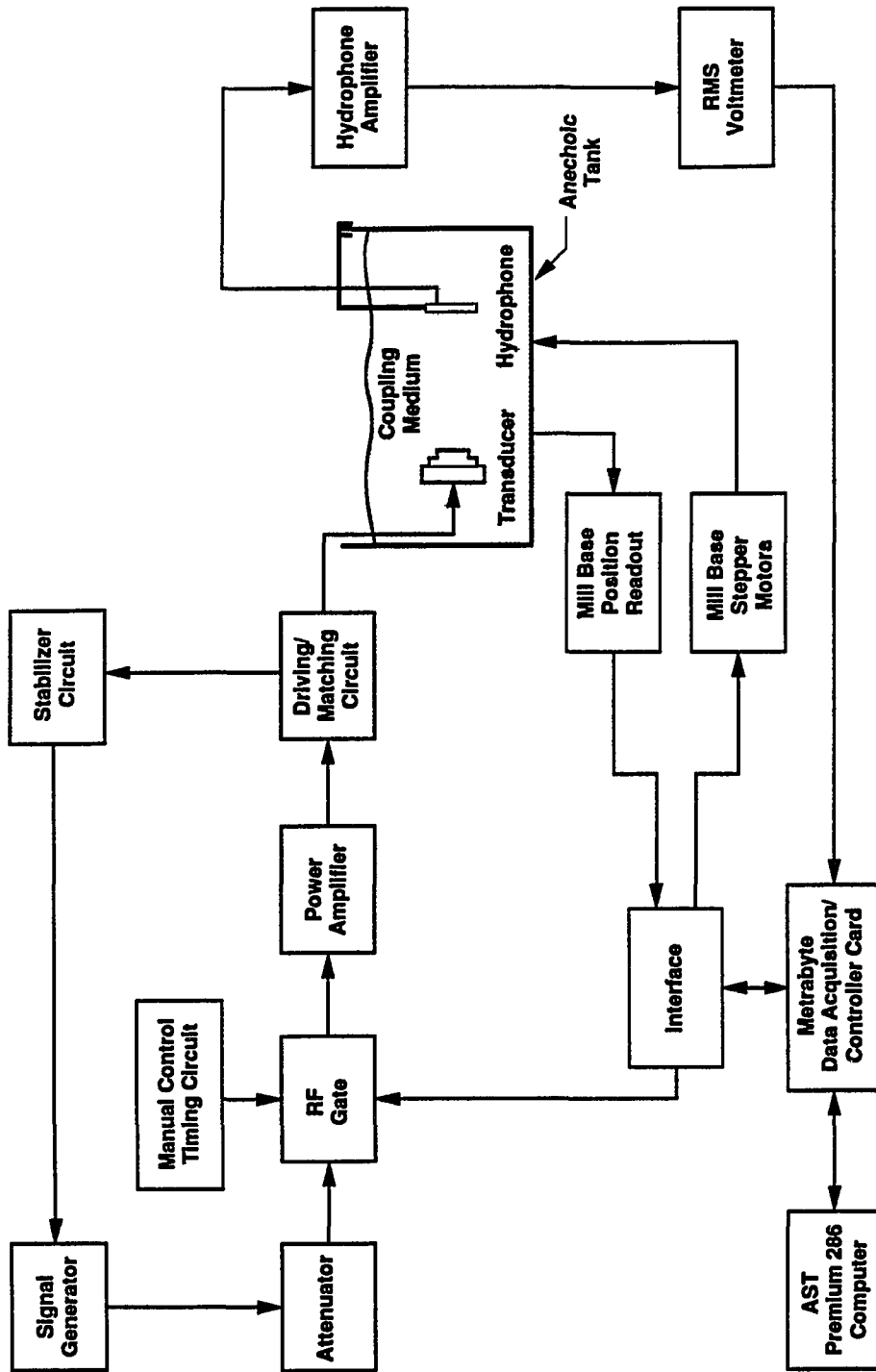


Figure 2.1: Schematic representation of the ultrasound irradiation system.

the transducer driving/matching circuit to a stabilizing circuit, the output of which is the input to the AM modulation of the signal generator. By proper design of the feedback path from the transducer driving/matching circuit to the AM modulated input of the RF source, discussed below, a very stable voltage signal is applied to the transducer.

All tissue and transducer characterization measurements are performed in a large tank of either distilled, degassed water, or degassed isotonic saline (mammalian Ringer's solution) at 37°C . The measurement tank is mounted on a mill base that can be moved manually, or by dc stepping motors in increments of 0.001 in . The transducer is mounted in a fixed position and the tank is moved relative to the transducer. The tissue specimens to be irradiated, or the acoustic field sensor employed in field measurements, are mounted fixed to the tank; hence, the tissue specimen or acoustic sensor is fixed relative to the bath coordinates. The position of the tank relative to the transducer is determined by an optical linear encoder (Dynamics Research Corporation, Model L-50) and displayed on a 3-axis digital readout (C-TEK Incorporated, Model LIN-103).

The overall system, RF triggering, relative transducer positioning, applied transducer voltage, and data acquisition, can be controlled by an AST Premium 286 personal computer (PC). The computer is interfaced to the system by a controller/data acquisition card (Metrabyte DAS-20) that is mounted in one of the PC expansion slots. Only a minimal amount of external circuitry is then required for reading the mill base position, triggering the RF signal, positioning the bath relative to the transducer, and adjusting the driving voltage for the transducer. Each of these functions can also be performed manually. The Metrabyte DAS-20 card is also used for A/D conversion.

Voltage is applied to the transducer through the driving/matching circuit shown in Figure 2.2. The parallel inductor, L , and capacitor, C_M , serve to match the 50Ω output impedance of the power amplifier to the PZT-4 and PZT-5 transducer elements. The PZT composite materials are significantly lower Q elements than a material, such as X-cut quartz, and precise matching is not a critical issue for obtaining the acoustic powers required for the applications treated herein. The Amplifier Research Model 1000L power amplifier is rated for loads with standing wave ratios (SWR) to infinity at all levels of forward electrical power, and waves that are reflected at the load are absorbed by the source. As a result, it is not necessary that the transducer be matched to exactly 50Ω , rather, C_M and L are adjusted such that up to $10 \frac{W}{cm^2}$ of acoustic power can be obtained at 1 and 3 MHz, and $3 \frac{W}{cm^2}$ can be obtained at 5 and 7 MHz for voltages less than 30 V applied to the transducer. The inductance of the parallel inductor is adjusted by changing inductors.

A stable voltage is maintained across the transducer by feedback of the signal V_c , to the stabilizer circuit which has been described elsewhere [127]. The voltage signal across the capacitor C_s is half-wave rectified by the two diodes shown in Figure 2.2. The signal V_c is then low pass filtered by the RG58 coaxial cable connecting the driving/matching circuit and the stabilizer circuit in series with the high input impedance of the stabilizer circuit. The stabilizer circuit then acts as a comparator to maintain a constant voltage of $V_D = -2.0 V$. The output of the stabilizer circuit is fed to the AM modulation input of the signal generator to increase the driving voltage V_T when V_D falls below $-2.0 V$, or to decrease it if V_D increases above $-2.0 V$. If very low driving voltages are to be applied to the transducer, the rectified and filtered voltage from the diode network is amplified by a non-inverting amplifier with a

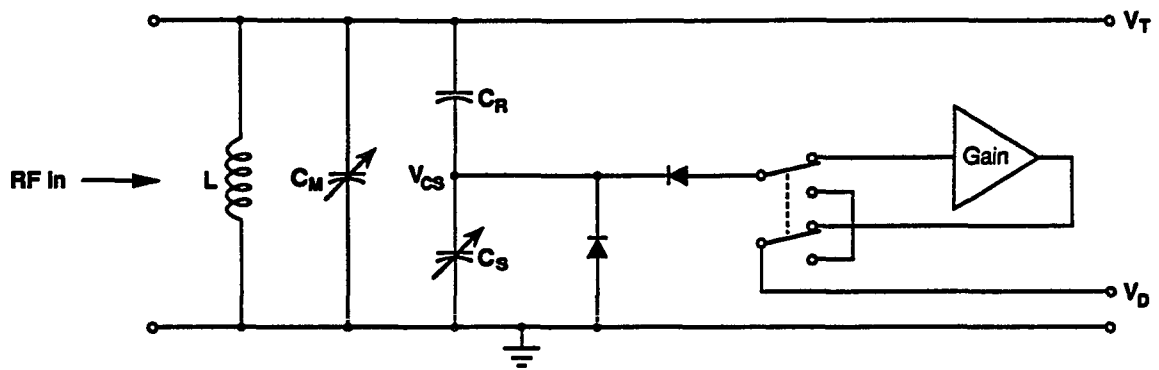


Figure 2.2: Driving/matching circuit for tuning and applying a stable voltage to the transducer.

gain of 23. The voltage applied to the transducer is then adjusted by the capacitor divider and is given by

$$V_T = V_c \left(\frac{C_s}{C_R} + 1 \right) \quad (2.1)$$

The range of the variable precision capacitor C_s (General Radio model 1422N) is 100–1150 pF . The capacitor C_R is mounted in a plug-in unit that allows it to be changed such that a range of voltages from approximately 0.5 V to several hundred volts can be applied to a transducer.

This method of driving the transducer does not require a knowledge of the incident and reflected power with the transducer connected, or accurate voltage measurements at the transducer when generating an ultrasound field. Accurate voltage measurements at the transducer V_T over a range of C_s can be performed once and related linearly to C_s . A transducer can then be calibrated by an absolute method, e.g., with a sphere radiometer [63], [103], [105], and the intensity related to the value of C_s . The ultrasound intensity I generated by the transducer at a given point in the field is found to be linear with V_T^2 . Thus, using the linear relationships between I and V_T^2 , and V_T and C_s , the desired ultrasound intensity is set by adjusting the value of C_s . Voltage measurements across the transducer as a function of C_s and absolute calibrations of the transducer are checked frequently. This method of driving a transducer provides a simple and quick means of generating a well-known ultrasound field that is to be used frequently.

2.2 Transducer Characterization

The ultrasound irradiation system described in the previous section is used to characterize the transducers employed in the experiments described herein. The acoustic radiation

pattern generated by a given transducer is determined, the intensity calibrations are performed, the amplitudes of the harmonic components of the acoustic field are measured, and the linearity of the device is tested for the transducers employed in the experimental procedures. The acoustic radiation pattern is plotted using a PVDF needle hydrophone probe (NTR Systems, Inc., Model NP-1000) with an active element of 0.5 *mm* diameter. The hydrophone output is fed to a high input impedance preamplifier (NTR Systems, Inc., Model HP-2130) with a gain of 30 *dB*. The output of the preamplifier drives an RMS voltmeter (Fluke, Model 8920A) which has a single digital output line. The digitized output of the RMS voltmeter is read by the Metrabyte data acquisition and controller card. The radiation pattern transverse to the acoustic axis of propagation is plotted by measuring the RMS voltage response of the PVDF element to a 200 *msec* ultrasound pulse at 0.5 *mm* intervals across the beam.

The acoustic beams employed in this study have half-power beamwidths (HPBW) greater than 4.5 *mm* in the far field so that the 0.5 *mm* diameter of the sensing element of the hydrophone causes no averaging of the important features of the radiation pattern. The radiation patterns were also measured with a thermocouple probe and found to agree well with those measured with a hydrophone. The hydrophone is fixed to the tank mounted on the mill base, which is moved with respect to the transducer to plot the beam profile. The beam plotting is computer controlled. One feature of the plotting program allows the beam to be centered on the sensing element by fitting a second- or fourth-order polynomial to the beam shape and positioning the acoustic axis of propagation on the maximum of the polynomial fit. The transducers employed in this study are axisymmetric. Beam profiles in two orthogonal directions that are perpendicular to the acoustic axis of propagation are

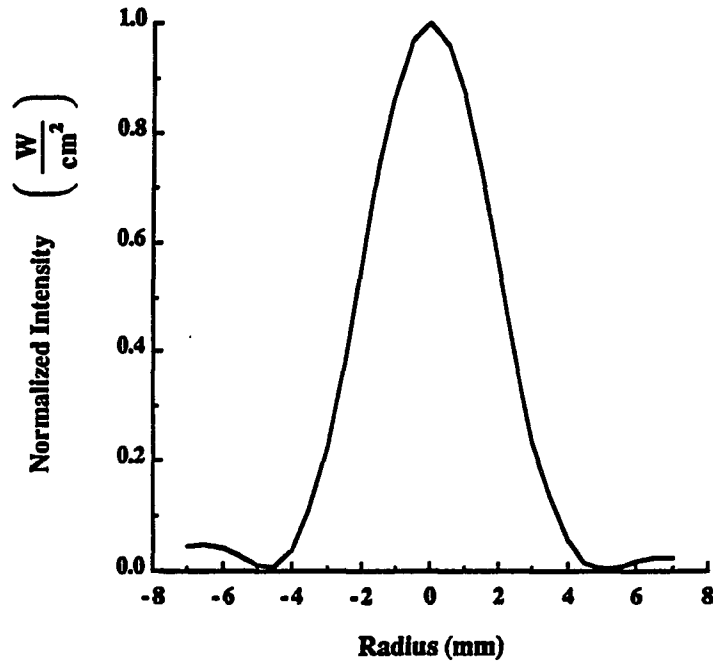


Figure 2.3: Relative intensity profile transverse to the acoustic axis of propagation at the focus of a 1 *MHz*, focused transducer measured with a PVDF needle hydrophone probe.

plotted to ensure that the transducer field is axisymmetric. A typical measurement of the beam of a focused, 1 *MHz* transducer with a 5.0 *cm* aperture and 15 *cm* focal length is shown in Figure 2.3.

The primary calibrations of acoustic intensity at the field points of interest are performed utilizing an elastic sphere radiometer [63]. The spatial peak, temporal average (SPTA) intensity is calculated from

$$I_{\text{SPTA}} = \frac{F_r c_0}{\pi a^2 Y_p A_{\text{CF}}} \quad (2.2)$$

where F_r is the acoustic radiation force, c_0 is the speed of ultrasound in the fluid medium, a is the radius of the sphere, A_{CF} is an area correction factor to account for the deviation of the cross-sectional beam profile from a uniform plane wave [84], and the dimensionless constant

Y_p is the radiation force per unit cross section per unit energy density, and can be calculated or found in the literature [104], [105]. The radiation force F_r is determined from deflection measurements of a grade 10 440C stainless steel sphere in the ultrasound field, the mass of the sphere, and the length of the suspension of the sphere. The sphere deflection is measured at points across the beam transverse to the acoustic axis of propagation, the beam profile is plotted, and the sphere is positioned at the maximum. The deflection of the steel sphere is related to the average intensity across the sphere cross-section. The intensity of the beam decreases across the diameter of the sphere for the beams employed in this study; hence, it is necessary to correct for this with the factor A_{CF} . Letting I_{SATA} denote the temporal-average intensity that is spatially averaged over the radius of the ball, the area correction factor is given by

$$A_{CF} = \frac{I_{SATA}}{I_{SPTA}} = \frac{\int_0^{2\pi} d\theta \int_0^a r dr f(r)}{\int_0^{2\pi} d\theta \int_0^a r dr} \quad (2.3)$$

where $f(r)$ is the axisymmetric intensity profile with the peak normalized to unity. In practice, the transverse beam profile is measured with a hydrophone over a width of $1\frac{1}{2}$ – 2 times the diameter of the largest sphere to be used in the procedure, a second-order polynomial is fitted to the beam and the area correction factor determined. Acoustic windows constructed from 26 μm Mylar are placed on each side of the sphere to prevent acoustic streaming and to minimize convective currents in the water bath. The windows are spaced 2.0 cm apart to allow a maximum deflection of the sphere of 1.5 cm for sphere suspension lengths of 10–11 cm [40]. The intensity as a function of the square of the voltage applied to the transducer, for a 4.2 mm HPBW at 7 MHz , is shown in Figure 2.4. The three sphere sizes used have radii of 0.099, 0.119, and 0.159 cm . The area correction factors for the described beam and 0.099, 0.119, and 0.159 cm spheres are 0.957, 0.936, and 0.887,

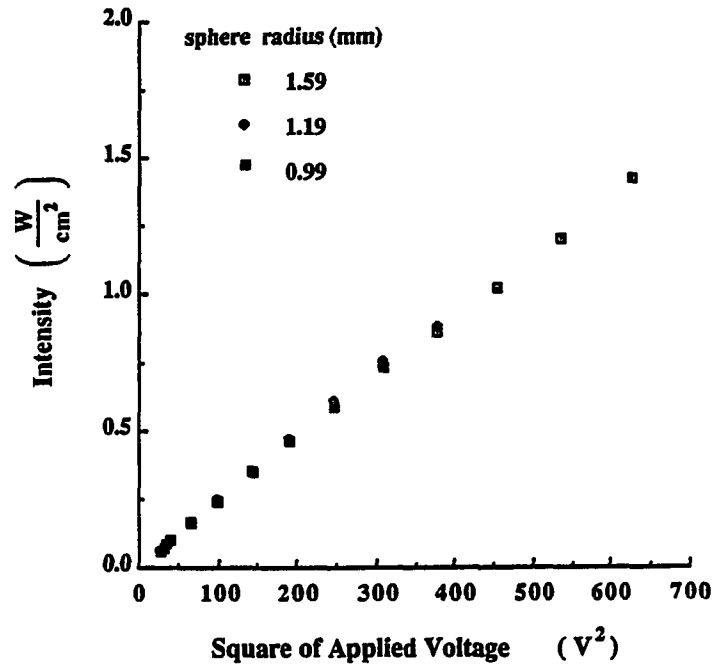


Figure 2.4: Intensity versus the square of the voltage applied to transducer 201B (see Appendix B) at 7 MHz as determined by steel sphere radiometry for 0.099, 0.119, and 0.159 cm sphere radii.

respectively. The correlation coefficient of the data for each sphere is greater than 0.99. The slopes of the three lines are then averaged to obtain the calibration number for the intensity as a function of the square of the voltage applied to the transducer. The coefficient of variation (standard deviation as a percentage of the mean) for the calibrations is typically 3–7%.

An error analysis of Eq. (2.2) yields

$$\epsilon_{I_{SPTA}} = \left(\epsilon_{F_r}^2 + \epsilon_{Y_p}^2 + \epsilon_{A_{CF}}^2 + 4\epsilon_a^2 + \epsilon_c^2 \right)^{\frac{1}{2}} \quad (2.4)$$

where ϵ_i is the relative error contributed to the total relative error $\epsilon_{I_{SPTA}}$ by the i^{th} factor. The speed of sound in water c_0 as a function of temperature and salinity is well-known [55], and the radius of the sphere can be measured accurately such that the contribution

of these two factors to the overall error $\epsilon_{I_{\text{SPTA}}}$ is negligible. The errors in determining the radiation force using a mass deflection technique have been previously reported [198]. The radiation force can be measured to an accuracy of $\pm 3\%$ if the deflection of the sphere in the ultrasound field is sufficiently small. For suspension lengths of 10 to 11 cm, greater accuracy can be achieved by limiting the deflection to less than 1.5 cm [40]. The largest error in the calibration is usually contributed by the ϵ_{Y_p} term resulting from a sphere radius and frequency such that ka ($k = \frac{2\pi f}{c_0}$) is near one of the minima of the radiation force function Y_p . A plot of Y_p as a function of ka values to 50 for a grade 10 440 C stainless steel sphere in water is shown in Figure 2.5. [The jaggedness of the lines in the Y_p curve shown in Figure 2.5 is an artifact of the plotting routine Cricket Graph and has no connection with the Y_p function.] A small error in ka can result in a significant error in Y_p for ka values near minima. An experimentally verified alternative to stainless steel spheres is the use of fused silica spheres in the calibration [105]. Whereas the Y_p function for stainless steel spheres varies rapidly as a function of ka with sharp minima, the Y_p function for fused silica spheres varies slowly for $ka < 20$ with less pronounced minima and maxima, and is nearly flat for $ka > 20$. The use of absorbing spheres of polyethylene for ultrasonic intensity measurements has been studied analytically, though not experimentally verified [103]. An advantage of absorbing spheres for intensity measurements is that the Y_p function is virtually flat for $ka > 15$, which is often the case at medical ultrasound frequencies. The slow variation in the Y_p function is also important for intensity measurements in a nonlinear ultrasound field. Different spectral components of the ultrasound field have a different ka value, hence, a different value of Y_p for each spectral component. The error introduced by harmonic components in the nonlinear acoustic field for stainless steel spheres is negligible for most purposes for $ka > 15$ because

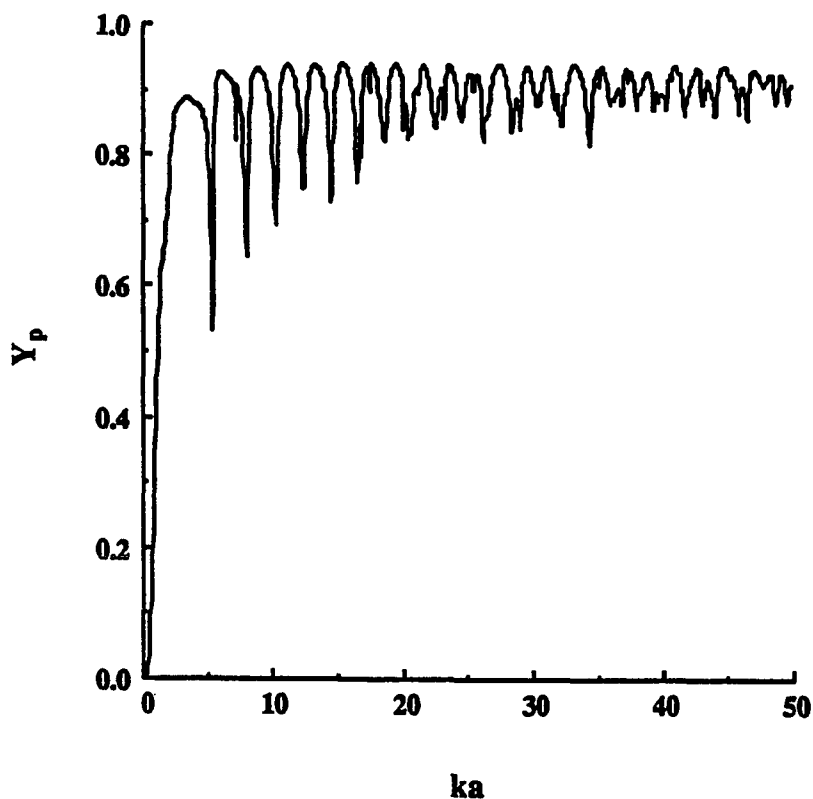


Figure 2.5: Y_p as a function of ka for grade 10 440 C stainless steel spheres.

the Y_p function does not vary by more than 15% of its maximum value. In addition, the limiting case for a nonlinear acoustic field, i.e., a sawtooth wave, has the second harmonic component 6 *dB* below the fundamental.

The harmonics of the nonlinear ultrasonic field radiated by transducers employed in this study were measured as a function of the voltage applied to the transducer and the intensity at the observation point. The transducer was driven with the system shown in Figure 2.1. The beam is plotted transversely for each transducer to determine the maximum of the main beam and the hydrophone positioned at the spatial peak. To prevent an undesired standing wave component between the transducer and membrane hydrophone, the membrane hydrophone is rotated such that the vector normal to the membrane is at an angle of approximately 15 – 20° with respect to the acoustic axis of propagation of the transducer. The

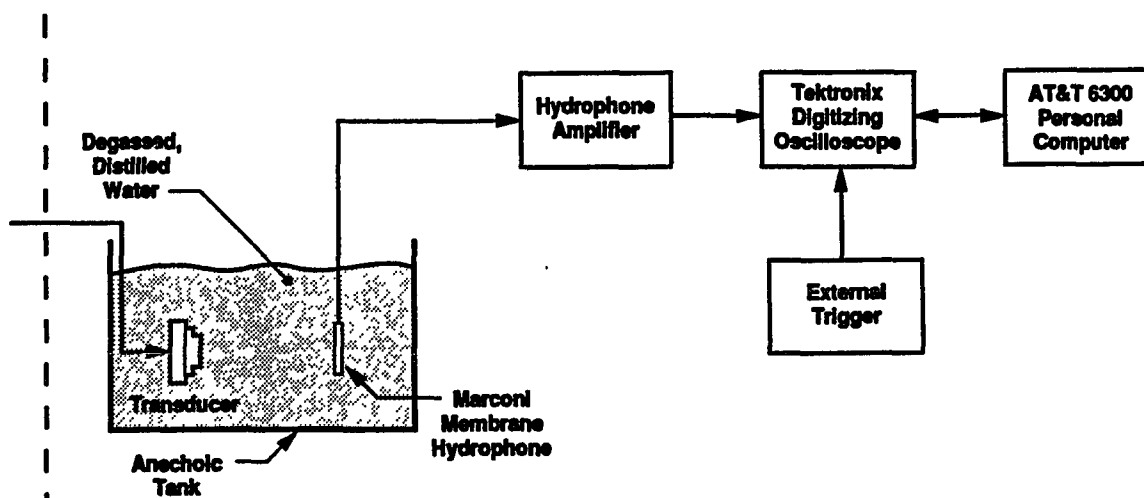


Figure 2.6: Schematic representation of the system employed to measure the nonlinearity of the ultrasound field.

hydrophone response resulting from its own directivity is not significantly decreased for small angles of rotation [11], [172], [181]. The measurement of the harmonics is then performed with the system shown schematically in Figure 2.6. The hydrophone is a PVDF bilaminar shielded membrane hydrophone (Marconi Research Center, Type Y-34-3598) with an active element of 0.5 *mm* diameter. The calibration technique and an accuracy assessment used by the National Physical Laboratory in calibrating the membrane hydrophones are described in a recent report [187]. The end-of-cable, open-circuit sensitivity of the hydrophone is shown in Figure 2.7. Measurements of the second harmonic at fundamental frequencies higher than 4-5 *MHz* will be affected by the hydrophone frequency response. The rolloff in the hydrophone amplifier response beyond 8-10 *MHz*, however, does compensate for the increased hydrophone sensitivity by approximately 1.5-2 *dB* at 15 *MHz* [101]. The output

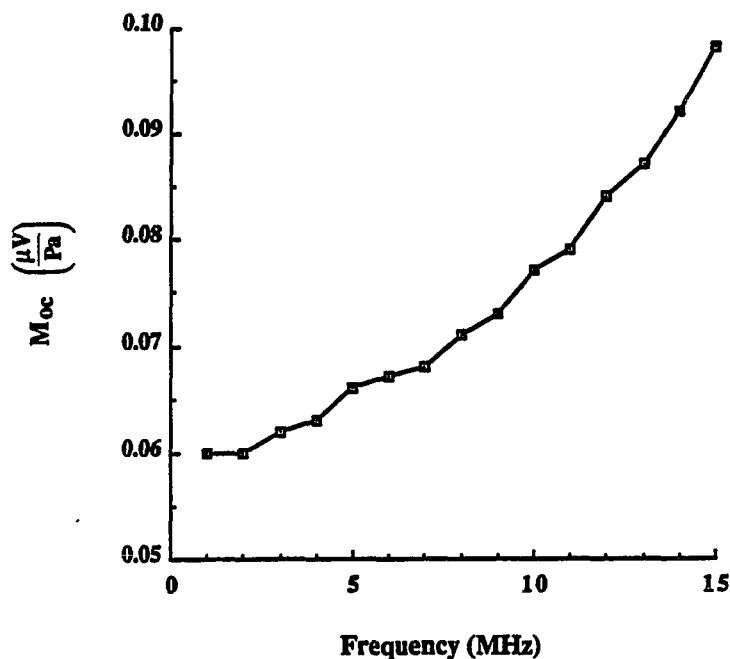


Figure 2.7: End-of-cable, open-circuit sensitivity M_{oc} of the membrane hydrophone used in the measurement of non-linearities in the ultrasound field.

signal of the hydrophone is amplified by a General Electric Company, Model Y-33-9724 amplifier. The input impedance of the amplifier is $50\text{ k}\Omega$, in parallel with a capacitance of 4.8 pF , and an amplifier with a nominal gain of 17 dB from $0.5 - 10\text{ MHz}$. The output of the hydrophone amplifier is the input to the digitizing oscilloscope (Tektronix, Model 2430A) which digitizes and stores a trace. An external source (Berkley Nucleonics, Model 7010) is used to trigger the oscilloscope at a rate of 2 kHz . A $10\text{ }\mu s$ trace is read by the AT&T 6300 personal computer and a spectral analysis is performed using an FFT.

The linearity of the transducer, signal generator, and power amplifier as a function of the drive applied to the transducer is verified for the devices employed in this study by placing a calibrated needle hydrophone probe in the near field of the transducer, displaced laterally from the acoustic axis of propagation [163], [173]. The results of the transducer

characterization described in this section for the devices used in this study are detailed in Appendix B.

2.3 Temperature Measurement Techniques

The temperature increase measurements presented herein are conducted in a water or saline bath maintained at 37 °C by external temperature control (Yellow Springs Instrument Co., Model 72). The increase in the thermal emf at the thermocouple junction resulting from ultrasound absorbed in the tissue is amplified with a dc amplifier, sampled with the Metrabyte DAS-20 data acquisition/controller card, and stored on the PC. To establish the reference, a baseline thermal emf is sampled prior to exposing the tissue to ultrasound. The thermal emf is then multiplied by the Seebeck coefficient to determine the temperature.

The temperature increase in tissue, upon exposure to ultrasound, that is reported in later chapters is measured with type E (chromel-constantan) thermocouples of small diameter [169]. Type E thermocouples are used because of the larger Seebeck coefficient than for other types. For example, the Seebeck coefficient for type J (iron-copper) thermocouples is $52.298 \frac{^{\circ}\text{C}}{\mu\text{V}}$ as opposed to $62.025 \frac{^{\circ}\text{C}}{\mu\text{V}}$ for type E [171]. Typically the thermocouples are constructed from 3 mil (76 μm) diameter, teflon-coated constantan and chromel thermocouple wire. The teflon is stripped from the length of the wires over which the junction is to be formed and the wires are etched in acid to a diameter of 15–25 μm . For temperature and absorption coefficient measurements in soft tissues of low absorption, smaller diameter thermocouple junctions are required [91]. The etched ends of the thermocouple wires are then soldered with an overlap of 200–400 μm .

The acoustic half-power beamwidths (HPBW) for transducers used in the measurements to be presented are greater than 4 *mm*. As a result, the acoustic intensity and, hence, the temperature profile, does not vary in the soft tissue by more than 1% over the thermocouple junction. Since the temperature does not vary significantly over the inhomogeneous region of the thermocouple junction formed by soldering the two wires together, no appreciable error in the measurement of the temperature due to the construction of the junction results [14]. Temperature increase measurements on ultrasonic absorbing fetal femur specimens with dimensions of 0.5 *mm* are given in Chapter 5. In such cases, where the temperature is expected to vary on a scale comparable to the dimensions of the overlap region of the thermocouple junction, significant temperature averaging results. The technique, to be described in Chapter 5, for placing small diameter thermocouples in the tissue precludes constructing the junction with an overlap smaller than approximately 200 μm because of the fragility of the junction. In the above-mentioned case, other errors in the temperature increase measurement are more significant than the averaging effect (see Section 5.3). The error introduced in the temperature measurement by the conduction of heat along the sensor leads has been studied analytically by other investigators [69], [86], [178], [186], and is shown to be less than 0.5% for the small diameter thermocouple wires typically employed in the measurements reported herein.

The thermal emf produced at the thermocouple junction is amplified, filtered, and converted to temperature. Precise measurements of temperatures and absorption coefficients therefore depend on a good amplifier design, as well as the superior construction of the thermocouple, particularly for low absorbing tissues. Low cost, precision amplifiers are readily available and a Fourier analysis of the type of signals to be measured will determine the cut-

off frequency of the necessary low-pass filter. Analytical approximations to the temperature increase with time typically measured in soft tissues exposed to ultrasound were constructed using the infinite, homogeneous, and isotropic Green's function and a Gaussian-shaped heat source to approximate absorptive heating [57]. A cylindrical heat source with a Gaussian taper, to allow for the decrease in the ultrasound field along the wire, was also added to approximate the viscous heating that results from the presence of the thermocouple wire. The resulting analytical approximation to the temperature increase over the first two seconds is shown in Figure 2.8. Curve a approximates a typical trace that would be observed for a soft tissue specimen with an absorption coefficient of 0.03 cm^{-1} at 1 MHz with a thermocouple of diameter $20\text{--}30 \text{ }\mu\text{m}$. Curve b represents the approximation of only the absorptive heating in the tissue, and curve c is the time derivative of curve b. The results of taking the FFT of all three curves are shown in Figures 2.9 (a), and 2.9 (b). An analysis of the the signals shows that 95% of the energy is contained in the frequencies less than 10 Hz , and virtually all of the energy is contained in frequencies less than 30 Hz .

The measured temperature increase in mouse liver exposed to 1 MHz ultrasound at $3 \frac{\text{W}}{\text{cm}^2}$ at 1 MHz and potted in 3% agar is shown in Figure 2.10 [56]. Curve a is the amplified signal after being low-pass filtered with a 30 Hz cutoff frequency. Curve b is the amplified signal filtered with a 10 Hz cutoff frequency. The rise time is slower for curve b as expected. The difference in the curves is primarily a result of the difference in the rise time. The two traces are two different exposures and a portion of the difference may be the result of deviations between exposures, as well as temperature nonuniformities in the experimental environment. The amplified signal filtered with a 100 Hz cutoff frequency is shown in Figure 2.10 (b), where it is observed that there is a significant amount of high frequency noise (relative to

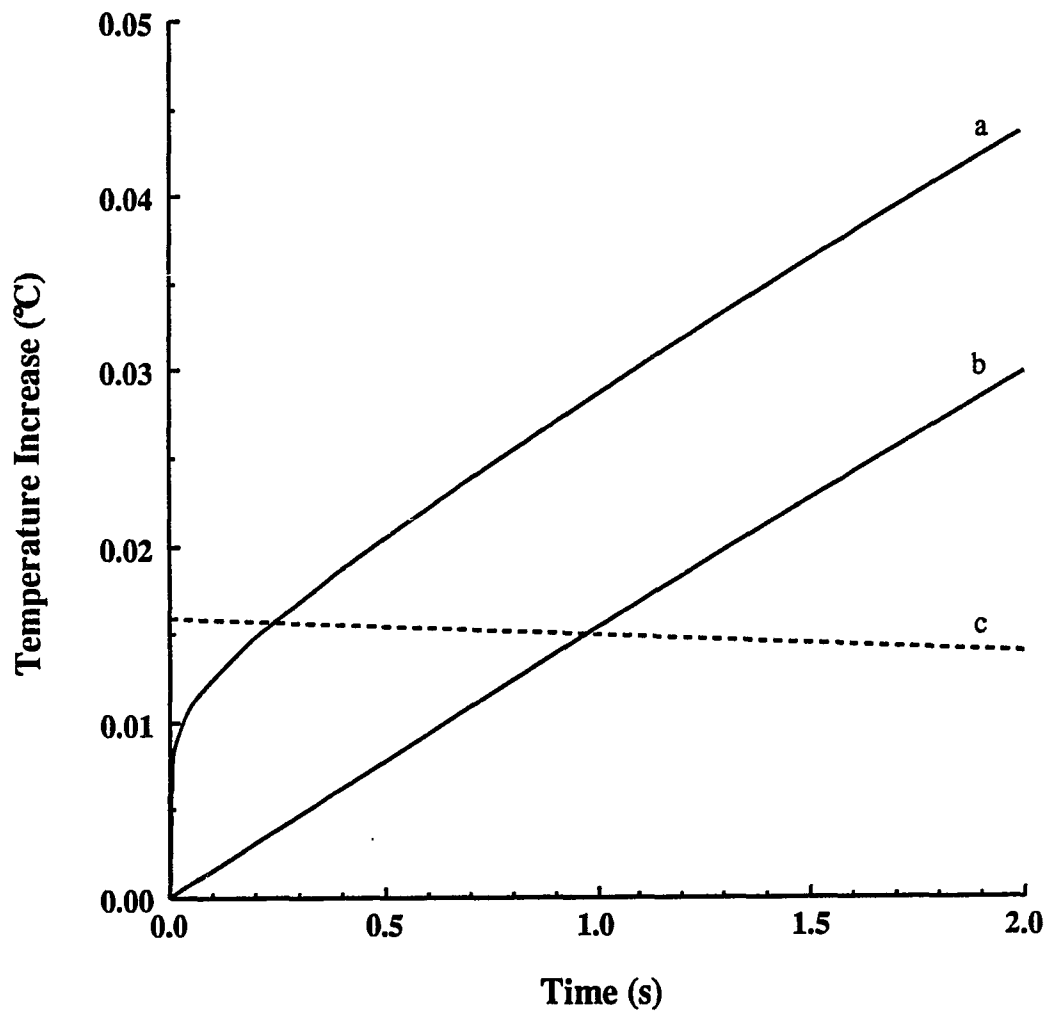
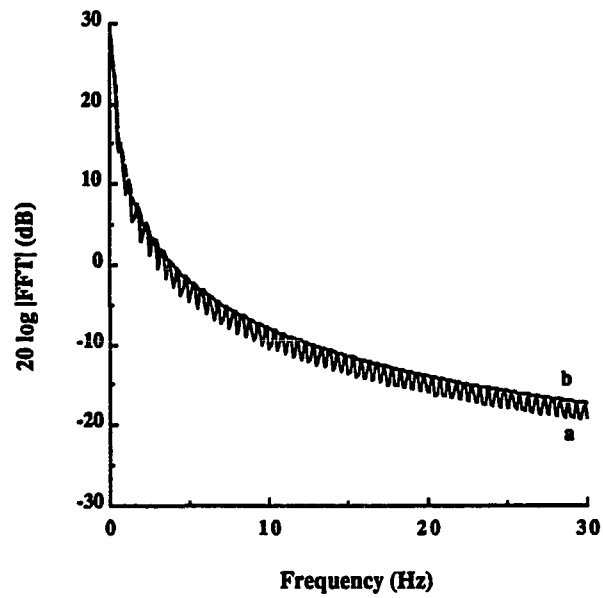
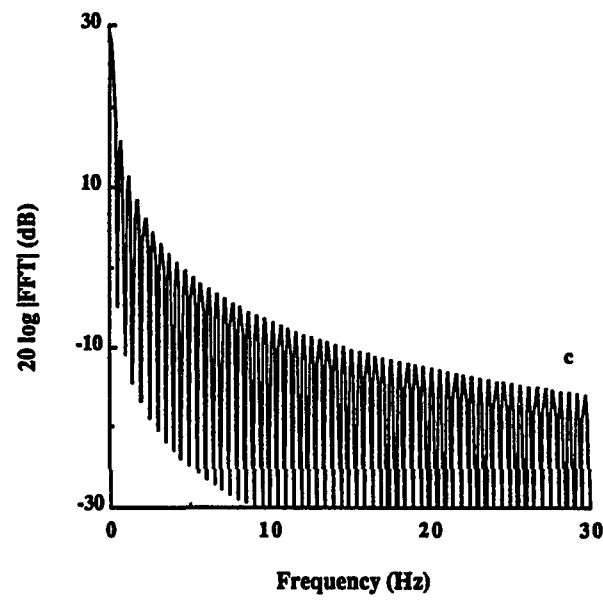


Figure 2.8: Analytical approximations of the temperature increase in tissue; curve a: absorptive heating plus viscous heating from the presence of the thermocouple; curve b: absorptive heating only; curve c: derivative of curve b ($\frac{^{\circ}\text{C}}{\text{s}}$).

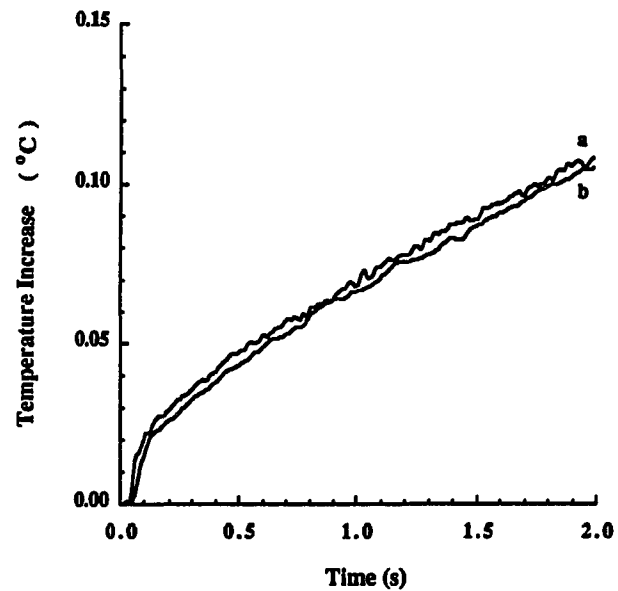


(a)

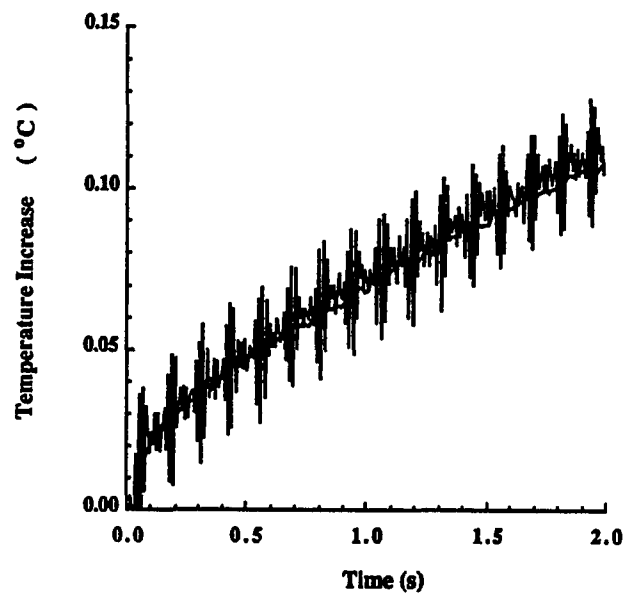


(b)

Figure 2.9: The FFT of curves in Figure 2.8 (a) curves a and b, (b) curve c.



(a)



(b)

Figure 2.10: The measured temperature increase with time in mouse liver potted in 3% agar (a) Thermal emf signal amplified and low-pass filtered with 30 Hz (curve a) and 10 Hz (curve b) and (b) 100 Hz cutoff frequencies.

the expected signal). The 30 Hz low-pass filtered signal is also shown. If the noise is zero mean, and a sufficient number of measurements are taken, the temperature increase and absorption coefficient (proportional to $\frac{\partial T}{\partial t}$) can be determined accurately despite the noise [158]. However, it is typically desired to minimize the number of measurements necessary to determine the temperature increase or its derivative, while achieving an acceptable precision. Low-pass filtering the signal allows the experimenter to judge qualitatively the “goodness” of the measurement and discard the data for which it is clear that some source of noise has introduced a bias. The time derivative at 0.5 s of the least squares quadratic fit to the temperature data between 0.25 s and 0.75 s yields the same result for the data in curves a and b of Figure 2.10 (a) [19].

An amplifier was designed and constructed for making accurate temperature increase measurements. A schematic of the design is shown in Figure 2.11. The first stage is a low noise, precision instrumentation amplifier (Precision Monolithics, AMP-01AX) providing a specified gain of 10^3 or 10^4 , which is set by three 1% metal film resistors and a switch. The second stage of gain is provided by another low noise, precision instrumentation amplifier (Analog Devices, AD522BD) with the gain set by external resistors $R_3 - R_{12}$. A multiple position switch and ten 1% metal film resistors are used to achieve gain settings from 1.5–1000. A low-noise, precision 741 operational amplifier (Precision Monolithics, OP-02EZ), precision reference voltage (Precision Monolithics, REF-02AZ) and a potentiometer provide a low noise variable reference voltage that is input to the noninverting terminal of the second stage, and is used to ensure that the temperature reference signal is within the -10 V to 10 V range of the Metrabyte A/D converter. The thermal emf signal from the thermocouple is transmitted from the measurement tank to the input of the amplifier by a shielded, twisted

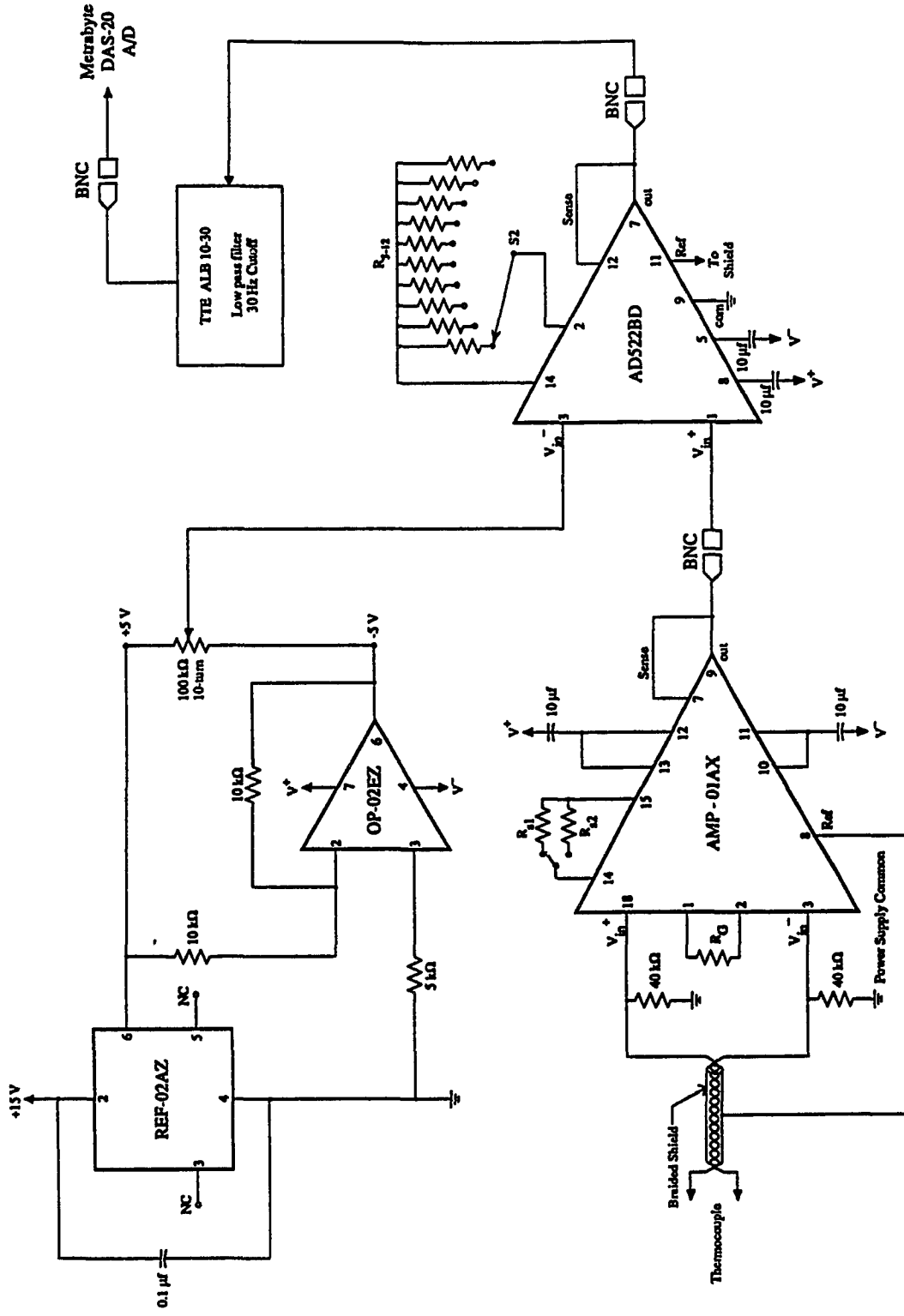


Figure 2.11: Schematic of the dc amplifier used for temperature increase measurements.

pair of leads. The amplifier has low noise and low drift properties and provides high gain. The output signal of the dc amplifier is filtered by a 30 *Hz* cutoff frequency, 10-pole, Butterworth low-pass filter (TTE Inc., ALB10-30). The gain accuracy of the amplifier is better than 3%. It is seen from Figure 2.10 (a) that temperature increases of 50 *m°C* can be measured with a signal-to-noise ratio close to 20 *dB*. Measurements of the amplifier gain using a signal generator operating at 30 *Hz* as the input and reading the voltage at the output of the second stage agreed to within less than 1% of the gain calculated from the manufacturer's gain formula and the measured values of the resistors.

CHAPTER 3

IN UTERO MEASUREMENT OF THE TEMPERATURE ELEVATION IN FETAL MICE EXPOSED TO 1 MEGAHERTZ ULTRASOUND

The teratogenicity of hyperthermia has been documented for a number of mammalian species, including humans [32], [71], [146], [188]. The manifestations of the teratologies are dependent upon the stage of development during which heating occurs and generally results in the production of brain, skeletal, or muscular defects. Heating during the early part of gestation, i.e., during organogenesis, has been shown to result in severe consequences [71], [90], [134], [197]. The possibility of more subtle, as yet undetermined, biological consequences of elevated fetal temperatures is also of concern. The deposition of heat and the resulting temperature increase upon exposure of the fetus to ultrasound are thus of concern in the medical ultrasound community. Although studies of the temperature increase in fetal mice and rats upon exposure to ultrasound have been reported [1], [70], [133], [185], [195], the uterine environment was not preserved, and, in some of them, comparison between the temperature elevation measurements and model calculations was not made.

The study reported in this chapter was undertaken with two factors, considered of greatest importance, for an accurate determination of fetal temperature elevation due to exposure to ultrasound, *viz.*, (1) the preservation of the gravid uterine environment, and (2) the ability to compare temperature elevation measurements with computations based on an improved bioheat transfer model. *In vivo* temperature measurements were made during ultrasound exposure at three different gestational ages. The analytical model comprises a pair of nested rectangular parallelepipeds for which the inner cube increases in dimension and possesses a

different acoustic absorption coefficient for each of the different gestational ages, while the outer cube remains unchanged. Uniform perfusion is assumed throughout the entire region.

3.1 Methods

All animals used in this study are housed in the same quarters. They are maintained on a 14:10 hour light–dark schedule with food (Purina Rat Chow) and water dispensed *ad lib*. Males are housed in close proximity to the females in order to ensure regular 4–5 *day* estrous cycles [199]. Female HSD:ICR (Harlan Sprague–Dawley, Indianapolis, IN) mice 70–100 *days* of age in proestrus or estrus, as determined by vaginal smears, are mated to proven males in the afternoon at a ratio of three females to one male. The following morning the males are removed, and pregnancy is determined by the presence of a vaginal plug or a sperm positive vaginal smear. Pregnant females are kept three to a cage until the day of the temperature elevation measurements.

The temperature sensors are chromel–constantan thermocouples having lap soldered junctions 30–40 μm in diameter and axial dimensions of 300–400 μm . The ends of the chromel and constantan wires are stripped of the Teflon coating and etched with acid to taper the original 75 μm diameter to approximately 15–20 μm at the tip, cleansed with alcohol, and tinned. The individual wires are then retained in a holding device designed for this purpose, the two ends overlapped approximately 300 μm , set in contact, and soldered. The procedure is carried out with the aid of a dissecting microscope. The junction area is then sprayed with a protective coating (Krylon Crystal Clear, Borden, Inc.), designed for electronic equipment, to waterproof the junction and to prevent oxidation.

On the day of the measurement, days 9, 12, or 15 of gestation, the dam is anesthetized by inhalation of methoxyflurane (Metofane, Pittman-Moore). The abdominal area is then shaved and the animal placed in a specially designed holder. A circulator is mounted on the holder to maintain anesthesia during the entire measurement procedure. A midline incision is made through the skin over the abdomen and the skin carefully dissected away leaving the underlying peritoneal tissue intact. This procedure allows visualization of the fetuses without disruption of the gravid uterine environment. The thermocouple probes described above are inserted into three to four randomly selected fetuses with the aid of a 30 gauge hypodermic needle, which is removed after insertion of the thermocouple. The thermocouple wires are then attached with waterproofed set screws to a harness which fits over the animal holder. A photograph of the preparation is shown in Figure 3.1.

The animal holder is placed in the Plexiglas exposure tank with the dam's abdomen facing the transducer, and the muzzle extended out of the medium into the nose cone of the anesthesia circulator. The tank contains degassed mammalian Ringer's solution, maintained at 37°C , and is lined with sound absorbing material to prevent generation of standing waves. The thermocouple wire ends are attached to bus wires leading to the amplifier.

The measurements are carried out in the far field, 25 cm from the face of the transducer. The ultrasound source is a 1 in diameter, 1 MHz, PZT-4, unfocused ceramic transducer with a 95 % power beam width of 1 cm, and a 3 dB beamwidth of 2.0 cm. A hydrophone probe is used to determine the ultrasound beam pattern. A plot of the beam pattern is shown in Appendix B. The exposure intensities were determined in the free field in degassed mammalian Ringer's solution with a thermoelectric probe as a secondary standard that had been calibrated with a steel sphere radiometer primary standard [63].

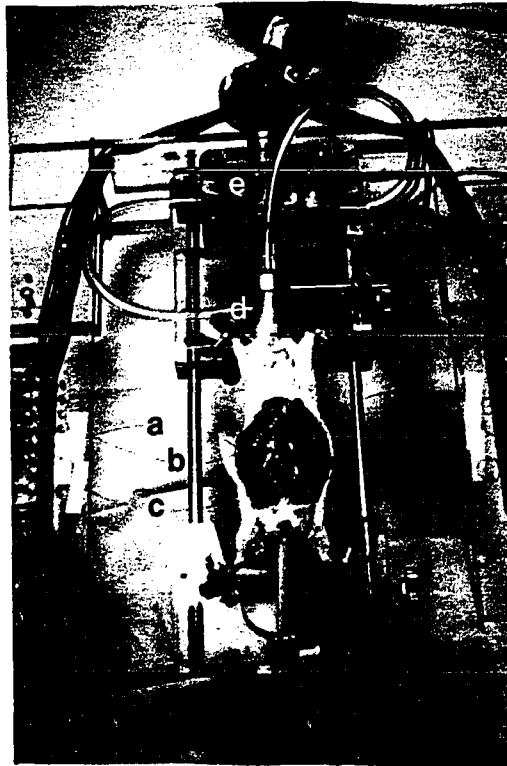


Figure 3.1: Experimental animal preparation showing three thermocouple sensors (a, b, and c), and the nose cone (d) for the anesthesia circulator (e).

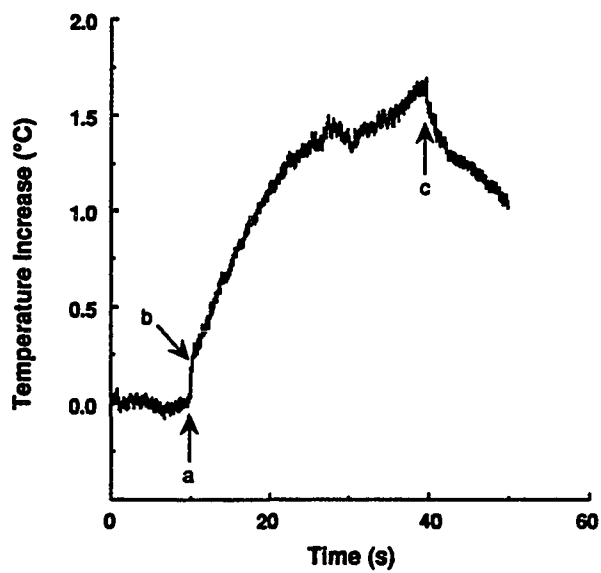
The harmonics in the ultrasound beam at a distance of 25 *cm* from the transducer, generated by nonlinear propagation, are measured with a needle hydrophone probe over the range of spatial-peak, temporal-average (SPTA) exposure intensities 0.5–“10” $\frac{W}{cm^2}$. (The quotation marks around the 10 $\frac{W}{cm^2}$ value indicates that the linear relation established by the calibration procedure, at low acoustic intensities, between the square of the voltage applied to the transducer and the field intensity, was extrapolated to voltages corresponding to 10 $\frac{W}{cm^2}$.) Although the SPTA intensity may deviate from the linear relation by 15% or less, at a distance of 25 *cm* from the transducer [40], the increased heating due to harmonic absorption can be significant [12], [41], [53] [84], [96]. The harmonics in the acoustic field, at the field position selected, were measured with a needle hydrophone probe (NTR Systems, Inc.). The second harmonic was found to be approximately 17 and 14 *dB* below the fundamental at 0.5 and 1 $\frac{W}{cm^2}$, respectively, and approximately 8 *dB* below the fundamental in the 5 – 10 $\frac{W}{cm^2}$ range. The variation in the sensitivity of the needle hydrophone probe with frequency is unknown. Calibrated needle hydrophones received in the Bioacoustics Laboratory from NTR Systems, Inc. have shown deviations from a flat frequency response by as much as 2 – 3 *dB* in the frequency range 1–5 *MHz*. Measurements of the amplitude of the second harmonic relative to the fundamental in the 5–10 $\frac{W}{cm^2}$ intensity range showed only a slight increase, indicating well-developed harmonics [27], [99], [149].

The absorption coefficient was measured in mouse liver over the range of SPTA intensities 1–10 $\frac{W}{cm^2}$ to assess the increase in the heating due to nonlinear absorption. The absorption coefficient at 10 $\frac{W}{cm^2}$ was found to be 2.3 times greater than that at 1 $\frac{W}{cm^2}$. This is consistent with other such reported measurements [12], [39], [53]. Because the volumetric rate of energy deposition in the soft tissue is proportional to the product αI , the intensities were scaled for

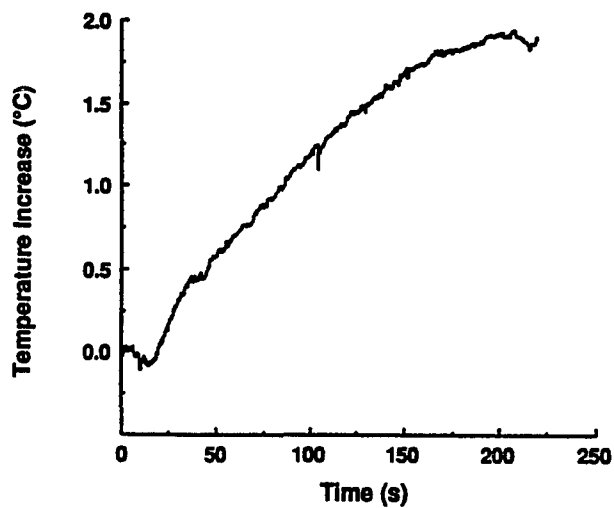
the 5 and 10 $\frac{W}{cm^2}$ irradiations such that αI corresponded to the linear values. For example, measurements of the linear absorption coefficient in mouse liver given in Chapter 4, and reported elsewhere in the literature [141], yield a value of $\alpha = 0.033 \text{ cm}^{-1} \pm 10\%$; hence, $\alpha I = 0.33 \frac{W}{cm^3}$, for $I = 10 \frac{W}{cm^2}$. Then, to obtain the same value of αI for a measured value of $\alpha = 0.059 \text{ cm}^{-1}$ in a nonlinear acoustic field, $I = 5.6 \frac{W}{cm^2}$.

The temperature elevation in the fetus due to ultrasound exposure is estimated by first establishing a thermal emf reference signal over 10 s during which no RF voltage is applied to the transducer, as shown in Figures 3.2(a) and (b). The sound is turned on by applying a predetermined voltage to the transducer after the reference period, for the prescribed exposure time. A 10 s decay period is sampled after the sound exposure is terminated. The thermal emf is amplified by the dc amplifier described in Chapter 2 and digitized by the Metrabyte A/D converter. The temperature elevation is estimated by subtracting the reference voltage from the peak voltage and multiplying the result by the Seebeck coefficient [171]. The exposure system and data acquisition are controlled by an AST Premium 286 personal computer. The measurement system is a modification of that shown in Figure 2.1. A schematic of the modified system is shown in Figure 3.3.

Figures 3.2(a) and (b) are representative data traces of the temperature elevation, measured with the implanted thermocouples, upon exposure of the dam to ultrasound. In the cases shown, the exposures were at an SPTA acoustic intensity of 10 $\frac{W}{cm^2}$ for 30 s and 1 $\frac{W}{cm^2}$ for 200 s for Figures 3.2(a) and (b), respectively. The lower arrow a in Figure 3.2(a) indicates the point at which the exposure is initiated after a 10 s reference signal. Viscous heating is seen to occur initially, as indicated by arrow b, followed by heating due to the absorption of sound in the tissue. The upper arrow c indicates the instant the ultrasound exposure is



(a)



(b)

Figure 3.2: Representative traces of temperature elevation data for (a) 15 *day* fetus exposed to 30 s at $10 \frac{W}{cm^2}$, and (b) 12 *day* fetus exposed for 200 s at $1 \frac{W}{cm^2}$.

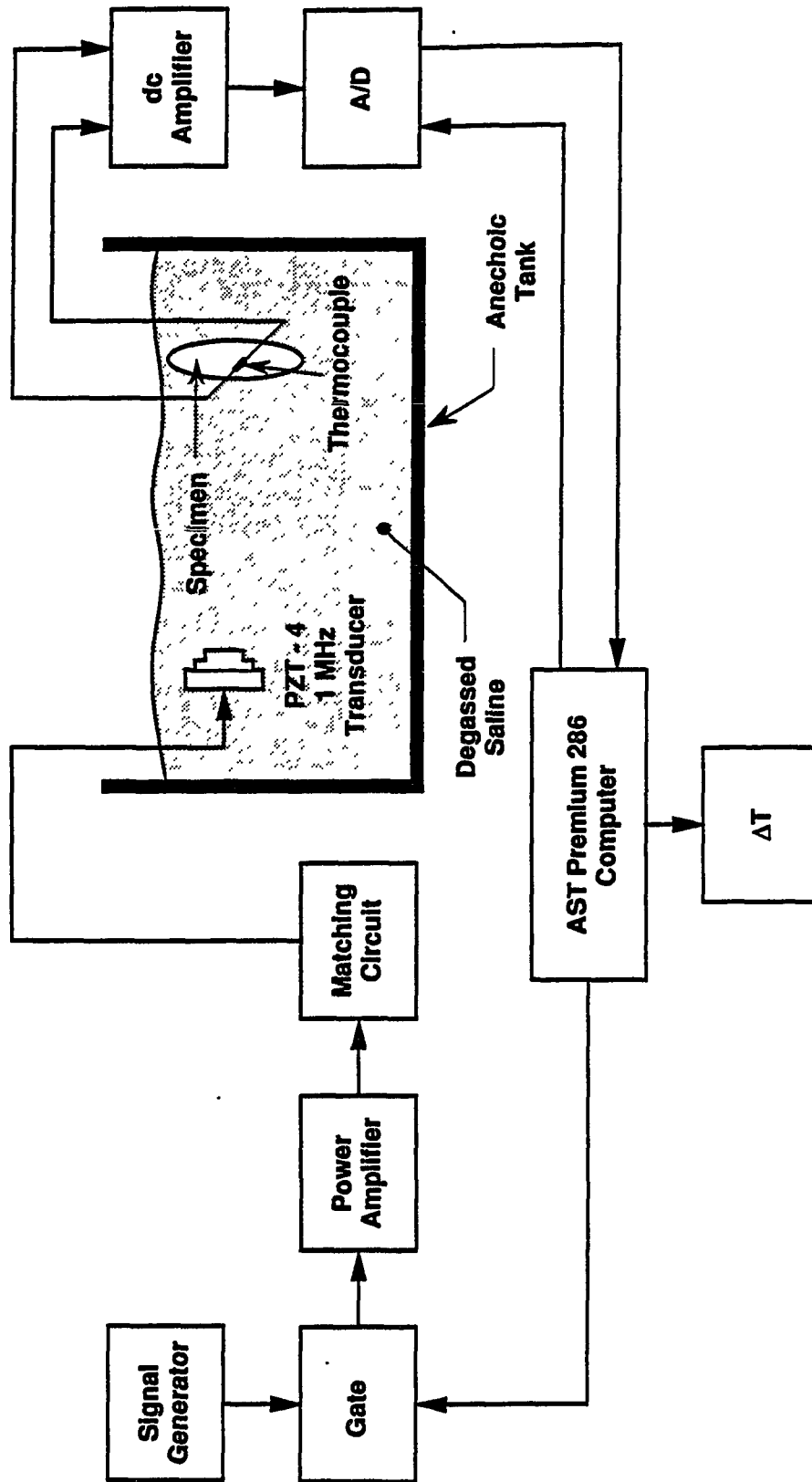


Figure 3.3: Schematic representation of the measurement system.

terminated. Fluctuations in the thermal emf output by the junction sometimes occur during the measurement period that are due to respiration or other movement by the dam. Such movements may change the location of the thermocouple junction relative to the ultrasound beam. Figure 3.2(a) shows an example of such fluctuations which do not affect significantly the determination of the temperature elevation from the measurement.

Following the measurements, the animal and holder are removed from the tank. With the dam still under anesthesia, the abdomen is then opened surgically and the location of the thermocouple junction in each fetus is determined with the aid of a dissecting microscope. The dam is then sacrificed by cervical dislocation.

3.2 Analytical Development

The bioheat equation (1.1) has been employed by others for calculating the temperature increase in soft tissue resulting from exposure to ultrasonic irradiation [75], [120],[138],[154], [155]. A solution to the bioheat equation for an infinite, homogeneous, and isotropic medium can be found by the Green's function method and is given by Eq. (1.6). The infinite, isotropic, homogeneous Green's function given in Equation (1.4) is typically integrated over a sphere or cylinder with uniform heat generation to approximate the temperature elevation resulting from ultrasound exposure. This Green's function is employed in the analysis given below. Although the infinite, homogeneous and isotropic model is simple, it does allow for different heat source functions to be specified in the heating volume V , e.g., specification of the absorption coefficient of the fetus as different from that of the dam. This solution does, however, assume that the blood perfusion is everywhere uniform. Although blood perfusion is known not to be uniform [196], it is a formidable task to find the appropriate Green's

function for Eq. (1.1) for an inhomogeneous region. Alternatively, a numerical method, e.g., a finite element analysis, allows incorporation of nonuniform blood perfusion [10], [110], [113].

An attenuated traveling plane wave is typically assumed for acoustic propagation in soft tissue when computing the temperature increase. The equivalent heat source approximating the heat deposition resulting from ultrasonic absorption is then assumed to be

$$q_{v0}f(\bar{\mathbf{r}})F(t) = 2\alpha I_0 e^{-\alpha z} f(x, y)U(t) \quad (3.1)$$

where α is the ultrasonic absorption coefficient in soft tissue, I_0 is the SPTA intensity, $f(x, y)$ is the beam profile in the plane transverse to the direction of propagation (z direction), and $U(t)$ is the unit step function indicating a *CW* exposure. An unfocused piston ultrasound source was employed in this study. Previous studies have shown that the temperature increase on the axis of propagation, resulting from a piston source with a $\left[\frac{2J_1(ar)}{ar}\right]^2$ transverse beam profile (where $r^2 = x^2 + y^2$, and a is a beamwidth parameter), is not significantly different than a source with a Gaussian distribution [38], [57]. Because a Gaussian function can be treated analytically in performing the spatial integrals in Eq. (1.6), the ultrasound intensity is assumed to vary as [57], [159], [164]

$$I(\bar{\mathbf{r}}) = I_0 e^{-\alpha z} e^{-\frac{x^2 + y^2}{\beta_r}} \quad (3.2)$$

where $\beta_r = \frac{(0.5\text{HPBW})^2}{\ln 2}$ is the beam shape parameter in the radial dimension (HPBW denotes the half-power beamwidth). A Gaussian shape can also be included in the axial direction to approximate a focused beam. Analytical expressions for the acoustic field of transducers that radiate Gaussian beams have been given in the literature [58], [59], [60], and recent work has been published presenting analytical and numerical results of heating from such sources

[202]. The analytical expressions for these beams are significantly more complicated to apply when analytically estimating the heating due to ultrasound exposure than is Eq. (3.2), and not readily amenable to planar source region boundaries. A piecewise linear approximation to the ultrasound beam will also result in analytical expressions for the spatial integrals in Eq. (1.6).

In using the intensity distribution described by Eq. (3.2), it is assumed that the shape of the ultrasound beam is not changed as it propagates through the tissue. Measurements in a homogeneous tissue such as liver suggest this is not the case exactly [160]. If a piecewise constant function of z is used for β_r , analytical simplifications for Eq. (1.6) still result, and allow for some changing of the profile. However, this may imply a better fit between the model and the experimental situation than is actually the case, as discussed in the Section 3.3.

The spatial integrals in Eq. (1.6) can be treated analytically for a separable Gaussian shape intensity profile if the source region is bounded by planar surfaces. Hence, the fetus and dam are modeled with rectangular absorbing volumes as shown in Figure 3.4. Let the source region V be defined by the three regions R_1 , R_2 , and R_3 with heat source functions q_1 , q_2 , and q_3 as

$$R_1 = \begin{cases} x_{1d} < x < x_{2d} \\ y_{1d} < y < y_{2d} \\ z_{1d} < z < z_{2d} \end{cases}$$

$$q_1(x, y, z) = 2\alpha_d I_0 e^{-2\alpha_d(z-z_{1d})} e^{-\frac{x^2+y^2}{\beta_r}}$$

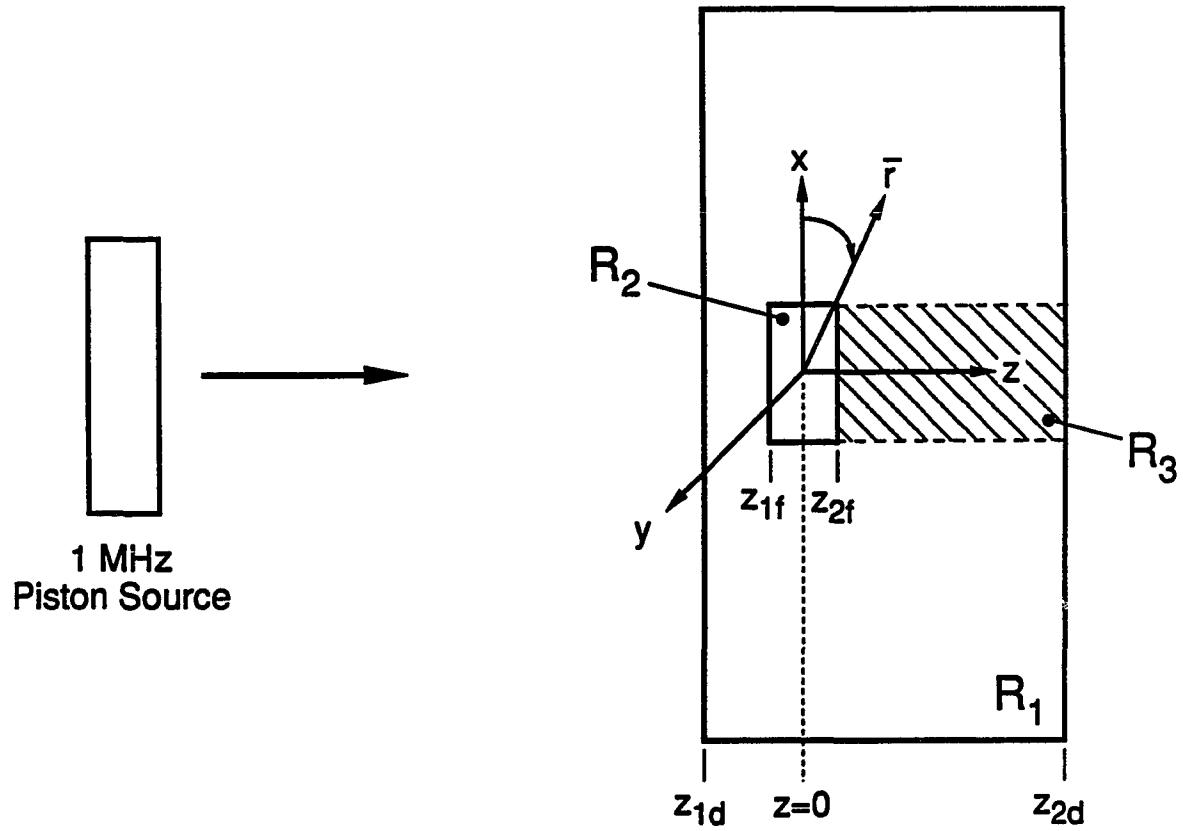


Figure 3.4: Coordinates and heat source volumes used in the analytical treatment of the temperature elevation.

$$R_2 = \begin{cases} x_{1f} < x < x_{2f} \\ y_{1f} < y < y_{2f} \\ z_{1f} < z < z_{2f} \end{cases}$$

$$q_2(x, y, z) = 2\alpha_d I_0 e^{-2\alpha_d(z_{1f}-z_{1d})-2\alpha_f(z-z_{1f})} e^{-\frac{x^2+y^2}{\beta_r}}$$

$$R_3 = \begin{cases} x_{1f} < x < x_{2f} \\ y_{1f} < y < y_{2f} \\ z_{2f} < z < z_{2d} \end{cases}$$

$$q_3(x, y, z) = 2\alpha_d I_0 e^{-2\alpha_d(z_{1f}-z_{1d})-2\alpha_f(z_{2f}-z_{1f})-2\alpha_d(z-z_{2f})} e^{-\frac{x^2+y^2}{\beta_r}}$$

where R_1 is the entire volume of the larger rectangular parallelepiped, R_2 is the volume of the smaller rectangular parallelepiped modeling the fetus, and R_3 is the "shadow" region behind the smaller rectangular parallelepiped. The temperature increase for this heating distribution is then given by

$$\begin{aligned} T(\bar{\mathbf{r}}, t) = & \frac{t}{\rho C_p} \int_0^1 d\xi \left\{ \int_{R_1} d\bar{\mathbf{r}}' q_1(\bar{\mathbf{r}}') G(\bar{\mathbf{r}} - \bar{\mathbf{r}}', t\xi) \right. \\ & - \int_{R_2+R_3} d\bar{\mathbf{r}}' q_1(\bar{\mathbf{r}}') G(\bar{\mathbf{r}} - \bar{\mathbf{r}}', t\xi) \\ & + \int_{R_2} d\bar{\mathbf{r}}' q_2(\bar{\mathbf{r}}') G(\bar{\mathbf{r}} - \bar{\mathbf{r}}', t\xi) \\ & \left. + \int_{R_3} d\bar{\mathbf{r}}' q_3(\bar{\mathbf{r}}') G(\bar{\mathbf{r}} - \bar{\mathbf{r}}', t\xi) \right\} \end{aligned} \quad (3.3)$$

where a unit step ultrasonic exposure has been assumed, and a change of variables $t\xi = t - \theta$ has been introduced in Eq. (1.6). Upon performing the spatial integrals, the temperature increase is given by

$$\begin{aligned}
T(\bar{r}, t) = & \frac{2\alpha_d I_0}{\rho C_p} t e^{2\alpha_d z_{1d}} \\
& \int_0^1 d\xi \left\{ e^{-\frac{t\xi}{\tau}} L(\bar{r}, t\xi, \alpha_d) \right. \\
& \times [M(t\xi, x, x_{1d}) - M(t\xi, x, x_{2d})] \\
& \times [M(t\xi, y, y_{1d}) - M(t\xi, y, y_{2d})] \\
& \times [N(t\xi, \alpha_d, z, z_{1d}) - N(t\xi, \alpha_d, z, z_{2d})] \left. \right\} \\
& + \frac{2\alpha_f I_0}{\rho C_p} t e^{-2\alpha_d(z_{1f}-z_{1d})+2\alpha_f z_{1f}} \\
& \int_0^1 d\xi \left\{ e^{-\frac{t\xi}{\tau}} L(\bar{r}, t\xi, \alpha_f) \right. \\
& \times [M(t\xi, x, x_{1f}) - M(t\xi, x, x_{2f})] \\
& \times [M(t\xi, y, y_{1f}) - M(t\xi, y, y_{2f})] \\
& \times [N(t\xi, \alpha_f, z, z_{1f}) - N(t\xi, \alpha_f, z, z_{2f})] \left. \right\} \\
& + \frac{2\alpha_d I_0}{\rho C_p} t e^{-2\alpha_d(z_{1f}-z_{1d})-2\alpha_f(z_{2f}-z_{1f})+2\alpha_d z_{2f}} \\
& \int_0^1 d\xi \left\{ e^{-\frac{t\xi}{\tau}} L(\bar{r}, t\xi, \alpha_d) \right. \\
& \times [M(t\xi, x, x_{1f}) - M(t\xi, x, x_{2f})] \\
& \times [M(t\xi, y, y_{1f}) - M(t\xi, y, y_{2f})] \\
& \times [N(t\xi, \alpha_d, z, z_{2f}) - N(t\xi, \alpha_d, z, z_{2d})] \left. \right\} \\
& - \frac{2\alpha_d I_0}{\rho C_p} t e^{2\alpha_d z_{1d}} \\
& \int_0^1 d\xi \left\{ e^{-\frac{t\xi}{\tau}} L(\bar{r}, t\xi, \alpha_d) \right. \\
& \times [M(t\xi, x, x_{1f}) - M(t\xi, x, x_{2f})]
\end{aligned}$$

$$\begin{aligned}
& \times [M(t\xi, y, y_{1f}) - M(t\xi, y, y_{2f})] \\
& \times [N(t\xi, \alpha_d, z, z_{1f}) - N(t\xi, \alpha_d, z, z_{2d})] \} \quad (3.4)
\end{aligned}$$

where

$$L(\bar{r}, t\xi, \alpha_i) = \frac{e^{-\left(\frac{x^2+y^2}{\beta_r} + \frac{1}{1+\frac{4\kappa t\xi}{\beta_r}}\right)}}{1 + \frac{4\kappa t\xi}{\beta_r}} e^{-(2\alpha_i z - 4\alpha_i^2 \kappa t\xi)}$$

$$M(t\xi, v, v_{mn}) = \frac{1}{2} \operatorname{erf} \left[\frac{1}{\sqrt{4\kappa t\xi}} \left(1 + \frac{4\kappa t\xi}{\beta_r}\right)^{\frac{1}{2}} \left(\frac{1}{1 + \frac{4\kappa t\xi}{\beta_r}} v - v_{mn}\right) \right]$$

$$N(t\xi, \alpha_i, z, z_{mn}) = \frac{1}{2} \operatorname{erf} \left[\frac{1}{\sqrt{4\kappa t\xi}} (z - 4\alpha_i \kappa t\xi - z_{mn}) \right]$$

The differences between this particular method of modeling the ultrasound beam and absorbing region over solutions given by other investigators include the shape of the beam, incorporation of plane wave attenuation in the intensity function, and allowance for a different absorption coefficient in the fetus than that for the surrounding tissues of the dam [1], [155]. The source region has been approximated with rectangular parallelepipeds as opposed to spherical or cylindrical regions to enable analytical integration of the volume integrals for the described heat source [1], [155].

3.3 Results and Discussion

The measured values of fetal temperature increase for each of the five ultrasound doses employed are shown in Table 3.1. The dose is defined as the product of the SPTA intensity and exposure duration $I_e t$. The intensity given in Table 3.1 is denoted as the SPTA effective intensity I_e to indicate that the effects of heating due to nonlinear absorption have been

Table 3.1: Measured and Computed (in parentheses) Temperature Elevation ($^{\circ}C$)

$I_e t$ ($\frac{J}{cm^2}$)	I_e ($\frac{W}{cm^2}$)	Exposure Duration (s)	Perfusion Constant τ (s)	Day of Gestation		
				9	12	15
200	0.5	400	2000	2.0 ± 0.7 (1.4)	2.1 ± 0.6 (1.3)	1.5 ± 0.5 (1.3)
200	1	200	2000	1.9 ± 0.4 (1.9)	2.4 ± 0.7 (1.9)	2.2 ± 0.8 (1.8)
300	2.5	120	500	2.9 ± 1.2 (3.2)	3.1 ± 0.8 (3.0)	2.0 ± 0.9 (3.0)
300	10	30	100	3.4 ± 1.3 (3.6)	3.2 ± 1.0 (3.4)	2.1 ± 0.7 (3.5)
450	5	90	100	4.0 ± 1.2 (3.8)	3.9 ± 0.8 (3.6)	2.8 ± 0.6 (3.6)

taken into account by scaling the intensity as described in Section 3.1. Each datum point is the average of measurements made in at least 10 different specimens. Values obtained from measurements in the disk (area of placental attachment) and placement of the junction in the gestational sac but not in the fetus were also included. These areas are integral components of the fetoplacental unit and will have a bearing on the well being of the fetus. In addition, it is assumed, based on the measured data, that the temperature elevation at these points will not differ measurably from points in the fetus. Computed values of the temperature elevation are also given in parentheses.

The data indicate that the temperature increase is related approximately linearly to the dose, It . If the source terms q_1 , q_2 , and q_3 are substituted into Eq. (3.3), it is observed that

$$T(\bar{r}, t) \propto It v(\bar{r}, t, \alpha_i, \tau, R_i) \quad (3.5)$$

where the R_i are the source regions. Then v is a function of time as well as other quantities. The perfusion constant τ is expected to be a function of temperature, hence, will also be time dependent. Thus, the linear relation observed between the energy flux It and the temperature elevation is not necessarily expected.

The temperature elevation in some cases was of the same magnitude, or higher than those previously shown to cause teratological effects in mice [71]. The table also shows that the temperature elevation is nearly equal in the 9 and 12 *day* fetuses, but less in most instances in the 15 *day* fetuses, as compared to the 9 and 12 *day* cases. This suggests that the earlier gestation fetuses are prone to temperature increases of greater magnitude from ultrasound exposure. The lower temperature increase in the 15 *day* fetuses is not presently understood. It is believed that absorption increases with fetal development because of the decreasing water content and increasing collagen and globular protein content as tissues develop, as well as bone development [56], [92], [95], which would lead one to expect greater heating. It is possible that the smaller size of the early gestation fetuses relative to the beam and the increased fetal and maternal vascularizations in later gestation fetuses play a significant role that is not presently understood.

The mouse is an suitable animal model for this study despite maternal size differences because the mouse and the human have the same type of placentation, *viz.*, hemochorial [119], [180]. Although vascularization increases during placental development, the uterine blood flow rate reaches a maximum on day 3 of pregnancy in the mouse [22] and on day

14–15 in the human [200]. Approximately 20% of the incoming uterine blood flows to the myometrium and endometrium and the other 80% to the area of placental attachment [174]. The blood flow volume increases due to the increase in the size of the placenta and uterus during gestation, particularly in the latter half of gestation. The blood flow per unit weight, however, remains constant [174].

The fetus is dependent on conduction to adjoining maternal tissues to remove heat, which is then carried off by maternal blood flow [77], [145]. The mechanics of circulation in this case are not conducive to rapid perfusion and thus heat removal. Briefly, placental blood enters from the uterine arteries under high pressure in jetlike spurts and flows into the intervillous spaces. Blood flow in the intervillous space is slowed significantly forming pools to allow time for exchange of nutrients and waste products from the chorionic villi. This blood is then forced into the uterine venous system by new incoming arterial blood [28], [200]. The continually increasing fetal temperature during the ultrasound exposures used in this study is an indication that heat is not rapidly removed as would be the case for well-perfused tissues.

The computed temperature increases are also shown in Table 3.1 (in parentheses) and can be compared to the measured values. The size of the rectangular parallelepiped employed to approximate the dam is $5 \times 4 \times 2 \text{ cm}$ ($x_{1d} = -2.5, x_{2d} = 2.5; y_{1d} = -2, y_{2d} = 2; z_{1d} = -0.5, z_{2d} = 1.5$), and the absorption coefficient is taken to be 0.035 cm^{-1} . The size of the rectangular parallelepipeds approximating the fetuses are $5 \times 3 \times 3 \text{ mm}$ ($x_{1f} = -0.25, x_{2f} = 0.25; y_{1f} = -0.15, y_{2f} = 0.15; z_{1f} = -0.15, z_{2f} = 0.15$), $8 \times 5 \times 5 \text{ mm}$, and $15 \times 9 \times 9 \text{ mm}$ for the 9, 12, and 15 *day* fetuses, respectively. The absorption coefficient for the three gestational ages are taken, respectively, to be 0.018, 0.023, and 0.028 cm^{-1} . This corresponds

to a linear function of gestational age, where on day 19 (birth) the absorption coefficient for this function would be 0.035 cm^{-1} , a reported value for the absorption coefficient in liver [141]. The perfusion constant τ was chosen to be different for the various exposure times and intensities in order to obtain agreement between the measured and computed temperature increases. Immediate increases in the blood flow following the initiation of the exposure might be expected at the higher intensities and shorter exposure times as a result of the rapid temperature increase. Hence, a high perfusion rate ($\tau = 100 \text{ s}$) is chosen [182]. At the longer exposure times and lesser intensities where the rate of temperature increase is slower, a lesser perfusion rate ($\tau = 2000 \text{ s}$) is used. A moderate rate of perfusion ($\tau = 500 \text{ s}$) is chosen for the intermediate exposure time and intensity. In all cases, the rate of perfusion could be expected to be a function of the temperature and the rate of temperature increase, and hence time. Such details, however, are presently not available. The effect of perfusion on the temperature elevation is shown in Table 3.2 for the parameters of the 15 *day* fetuses used in the computations. At short exposure times even a high perfusion rate ($\tau = 100 \text{ s}$) affects the total temperature elevation only slightly, whereas for longer exposure times the rate of perfusion affects the temperature increase significantly, as would be expected.

The computed elevation is nearly equal to or greater than the measured increases at the higher doses. However, at the lower doses, and for the younger gestational ages, the computed temperature elevation is lower than or comparable to the measured values. The comparison between the measured temperature elevation and model calculations, while being reasonable, emphasize that exposure criteria based on such calculations should be conservative. It is clear that the model from which the computed results are obtained is overly simple relative to the actual experimental physiological situation. A more realistic model would include better

Table 3.2: Computed Temperature Elevation For Different Perfusion Constants ($^{\circ}C$)

I_{SPTA} ($\frac{W}{cm^2}$)	Exposure Duration (s)	It ($\frac{W_s}{cm^2}$)	τ (s)					
			100	200	500	1000	2000	∞
0.5	400	200	0.5	0.8	1.1	1.2	1.3	1.4
1	200	200	0.2	1.3	1.6	1.7	1.8	1.9
2.5	120	300	2.0	2.6	3.0	3.1	3.2	3.3
10	30	300	3.5	3.8	3.9	4.0	4.0	4.0
5	90	450	3.6	4.3	4.9	5.1	5.2	5.3

determination and modeling of the ultrasound beam as it propagates and impinges on the fetus. Nonuniform blood flow and reasonable approximations of absorption coefficients and perfusion rates also need to be included. It should be noted that the absorption coefficient, which affects the calculations primarily as a scale factor outside the integral in Eq. (3.4), and the perfusion time constant τ , can be chosen to fit approximately most experimental data obtained in a manner such as that of this study. An attempt was made, however, to present reasonable arguments for the values of absorption coefficients and perfusion constants assumed for the model calculations.

CHAPTER 4

AN ANALYSIS FOR A MORE ACCURATE DETERMINATION OF THE
ULTRASONIC ABSORPTION COEFFICIENT IN SOFT TISSUE

This chapter comprises an analytical study of the effects of heat conduction resulting from finite beamwidths and sample sizes in the measurement of the ultrasonic absorption coefficient in soft tissues. The measurement of the absorption coefficient in fetal tissues is typically more difficult than for adult tissues because of low absorption and small dimensions of the tissue at earlier stages of gestation. If a small animal, e.g., a mouse, is used for experimental verification of a proposed thermal model, a knowledge of the absorption coefficient is required [1], and the error in the determination of the absorption coefficient is of concern because of the small sample size and low absorption of the tissue [189].

The rate of heat production per unit volume $q_v(\bar{r}, t)$, as given in Eq. (1.1), can be related to the absorption coefficient in soft tissue if the shear viscosity is taken to be zero, as given by Nyborg [153]. The relationship given by Nyborg includes the plane wave result

$$q_v(\bar{r}, t) = 2\alpha I(\bar{r})F(t) \quad (4.1)$$

where α is the absorption coefficient, I is the intensity, and $F(t)$ is a time-dependent function included here to indicate a *CW* or pulsed exposure, but is also valid for more complex ultrasound fields as well. Let q'_v be the instantaneous rate per unit volume at which heat is produced in the tissue by energy absorbed from the ultrasound field, and $q_v = \langle q'_v \rangle$ be its temporal average. The types of exposures typically of concern in experimental research and clinical applications of ultrasound are continuous wave (*CW*) and pulsed fields. The time average of q'_v is then taken over a single cycle of the field for *CW* exposures and over the

length of a single pulse, i.e., the time over which the ultrasound is on during a single period, for pulsed exposures. The rate of ultrasound energy absorbed in a unit volume of the tissue for any ultrasound field is given by [153]

$$-\nabla \cdot \langle p\bar{v} \rangle = -\nabla \cdot \bar{I} \quad (4.2)$$

where p is the pressure, \bar{v} is the particle velocity, and \bar{I} is the energy flow vector or intensity. The rate of ultrasound energy absorbed per unit volume in the tissue must also be $\langle q'_v \rangle$, the rate of heat production, so that

$$q_v = \langle q'_v \rangle = -\nabla \cdot \bar{I} \quad (4.3)$$

Upon employing Eq. (4.3), the heat source function q_v in a relaxing medium with zero shear viscosity is given by Nyborg [153] for a general ultrasound field as

$$q_v = \langle q'_v \rangle = \alpha \frac{p_0^2}{\rho c_0} \quad (4.4)$$

where p_0 is the pressure amplitude, and c_0 is the small amplitude speed of sound. The intensity for a plane wave field is $I = \frac{1}{2} \frac{p_0^2}{\rho c_0}$. The volumetric rate of heat production for a traveling plane wave in an absorbing soft tissue medium is then

$$q_v(\bar{r}, t) = 2\alpha I_0 f(\bar{r}) F(t) \quad (4.5)$$

where I_0 is a reference intensity, taken here to be the spatial-peak intensity for single beam ultrasound fields, and $f(\bar{r})$ is the spatial variation of the field. The absorption coefficient in soft tissue can be readily related to the rate of temperature increase by noting that the heat equation for negligible heat conduction becomes

$$\left. \frac{\partial T}{\partial t} \right|_{t \rightarrow 0} = \frac{q_{v0} f(\bar{r}) F(t)}{\rho C_p} = Q_0 f(\bar{r}) F(t) = \frac{2\alpha I_0 f(\bar{r}) F(t)}{\rho C_p} \quad (4.6)$$

where q_{v0} is the magnitude of the volumetric rate of energy deposition, ρ is the density, and C_p is the specific heat.

Two methods, *viz.*, the transient thermoelectric method (TTM) [64] and the pulse decay method (PDM) [159], [162], are currently employed to measure the absorption coefficient, α , in soft tissue. Both techniques seek to determine the absorption coefficient from [86], [87]

$$\rho C_p \frac{\partial T_{nc}}{\partial t} = 2\alpha I = 2\alpha I_0 e^{-2\alpha d} \quad (4.7)$$

where the density ρ , the specific heat C_p , and the spatial-peak intensity I , at the tissue depth of interest d are assumed known, and $\frac{\partial T_{nc}}{\partial t}$ is the measured rate of increase of temperature with no heat conduction. The intensity at the site of temperature observation is determined from the free-field intensity, I_0 , by correcting for attenuation, which is taken here as approximately equal to the absorption [160]. Since the conduction term in the heat equation is zero only when the heat source is uniform and infinite in extent, which is not usually the case, it is necessary to determine analytically the error in the estimate of the absorption coefficient that is calculated employing this assumption. The error can then be minimized in the measurements. The absorption coefficient is determined by exposing the tissue to ultrasound and making temperature measurements with embedded thermocouples to evaluate $\frac{\partial T_{nc}}{\partial t}$. The measurements are performed in a large isotonic saline bath, described in Chapter 2, which serves as the uniform-temperature, acoustic-coupling medium [85].

The contribution to $\frac{dT}{dt}$, the time rate of change of the temperature determined from the measurements, from the absorption of shear waves in the soft tissues is typically neglected. An asymptotic analysis of the scattering of a Gaussian beam from a fluid-solid interface has shown that to zeroth order, a beam at normal incidence is transmitted in the tissue entirely as a longitudinal wave [102], [170]. Further, a plane wave analysis shows the conversion of

the incident longitudinal wave to a shear wave at the fluid–tissue interface to be small [9]. The small amount of acoustic energy converted to a shear wave at the water–tissue interface is absorbed within fractions of a wavelength of the boundary. Reported values of shear attenuation in soft tissues are 10^4 times as large as those of longitudinal attenuation [81], [142]. Thus, the resulting equivalent heat source is very localized and contributes negligibly to the derivative $\frac{\partial T_{nc}}{\partial t}$ at the 0.5–1.5 s of interest in the TTM [76].

The subscript on T_{nc} indicates that the derivative of the measured temperature increase resulting from ultrasonic exposure is to be evaluated when heat conduction is negligible. In the TTM the derivative is evaluated at short times such that the effect of heat conduction on the measured temperature–increase data can be neglected. The temperature derivative is determined indirectly in the PDM by assuming an analytical form for the temperature decay resulting from a short ultrasound pulse and by fitting the measured data to the assumed analytical expression. The curve fit then yields $\frac{\partial T_{nc}}{\partial t}$ [159].

Each technique has advantages and limitations. The existence of an error in evaluating the derivative of the temperature, which arises from viscous heating due to the relative motion of the embedded thermocouple and the tissue, is well–known [86], [91]. The TTM attempts to minimize this artifact by evaluating the temperature derivative at a time sufficiently long such that the contribution of the viscous heating to the derivative is negligible. This necessitates using small thermocouples and large acoustic beamwidths to provide a temporal window during which the viscous artifact is minimal, while heat conduction remains negligible. The PDM avoids having to determine this temporal window in estimating the temperature derivative for those situations in which assumptions concerning the acoustic beam profile, tissue boundaries, and homogeneity of the heat conducting medium are met

experimentally. Although infinite transverse tissue dimensions are assumed for the PDM, as it is currently applied, finite dimensions for rectangular and cylindrical tissue boundaries can be included in the analytical expressions for heat conduction, when heating with a Gaussian transverse beam profile. The PDM is, however, more difficult to implement than the TTM. For example, the beam shape must be accurately plotted and the curve fit to a Gaussian function for each measurement in the process of accurately determining the acoustic intensity. Because the experimental temperature history is curve fit to an analytical form of the temperature increase, which must include the boundary effects of the finite source region, the thermocouple junction must be accurately positioned in the tissue. In addition, since the derivative of the unit step exposure temperature history is taken to obtain the impulse response needed in the analytical procedure, a low noise signal are required to reduce numerical differentiation noise in the processed data. These difficulties can be surmounted, though considerable care and effort are required. Thus, for those frequencies and beamwidths for which the accuracies of the two methods are comparable, the TTM may be a more desirable technique.

A difference in reported values of absorption between the PDM and TTM has indicated a need for analysis and improvement in the measurement techniques [141]. Specifically, absorption coefficient measurements reported on liver employing the PDM were 14% higher than those employing the TTM at low megahertz frequencies, with greater differences at higher frequencies. A theoretical and experimental investigation of absorption coefficient measurements using the PDM has been reported [141], [164]. Error estimates were presented and guidelines given for making accurate estimates of the absorption coefficient with this technique. However, no comparable study of the TTM has been reported. The primary sources

of error in applying the TTM to determine the absorption coefficient are heat conduction toward or away from the temperature sensor and the viscous heating artifact associated with the temperature sensor. A previous study of the heat conduction error resulting from the finite transverse half-power beamwidth (HPBW) of the acoustic beam and the viscous heating artifact due to the presence of the embedded thermocouple yielded guidelines for selecting the most appropriate size of thermocouple and specifications for the HPBW when applying the TTM [91]. The modeling of acoustic wave propagation, however, did not account for attenuation of the plane wave propagating in the tissue, and heat conduction to the tissue-coupling medium boundary was not investigated. In addition, the time derivative of the temperature was evaluated only at 0.5 s, and the error resulting from heat conduction was not quantified [91].

The purpose of this chapter is to quantify analytically the errors resulting from heat conduction for a prescribed acoustic beamwidth and specified tissue dimensions, when using the TTM to measure the ultrasonic absorption coefficient in soft tissue. Experimental guidelines for minimizing errors due to finite beamwidth and tissue dimensions, absorption, and viscous heating result from the analysis. An expression is defined for the relative error at any given time after the initiation of a unit step ultrasonic exposure. The relative error is the difference between the result obtained in the ideal situation with no heat conduction as represented by Eq. (4.7) and the result obtained using the model of the experimental situation, which includes heat conduction due to finite beamwidths, finite tissue dimensions, and absorption. Results are presented for various beamwidths, specimen dimensions, and absorption coefficients.

The analysis provides fundamental limits on the accuracy of a measurement of the absorption coefficient employing the TTM, within the limitations of the model. For example, measurements of the absorption coefficient for tissues of small dimensions have been reported where uncertainties concerning the accuracy of the measurement remain because of the effect of heat conduction on the temperature derivative at the time of evaluation [35], [189]. The results presented in this chapter provide the fundamental limit on the accuracy of the measurements imposed by finite beamwidth and sample dimensions. A further example of the utility of this analysis is in reducing the error introduced in the derivative of the temperature by the viscous heating from the presence of the thermocouple. As the TTM is currently applied [64], [85], and as described in the original papers by Fry and Fry [86], [87], it is prescribed that the time derivative of the temperature be evaluated at 0.5 s following the initiation of a unit step ultrasonic exposure. As shown in Section 4.2, for sufficiently large tissue dimensions and beamwidths, the time derivative of the temperature can be evaluated at times later than 0.5 s without significantly increasing the error due to heat conduction, while decreasing the error resulting from the viscous heating artifact. This is particularly useful for low absorbing tissues. Finally, by quantifying the error associated with heat conduction, which results from the finite beam dimensions, the beamwidths for which the PDM can provide greater accuracy are determined. The narrowing of the acoustic beam for single, focused radiators is particularly important at higher frequencies.

The thermal properties of the tissue and water coupling medium are assumed uniform as in previous studies [91], [159], [162]. The use of this model for the thermal properties of the water-tissue medium has been verified experimentally [91], [93], [141], [159], [162], [175]. A focused acoustic field is modeled as a circularly symmetric Gaussian beam [132], [159],

and includes plane wave attenuation in the tissue. Linear wave propagation is assumed. Planar boundaries are assumed for the tissue, i.e., the tissue possesses rectangular geometry. The Gaussian beam acoustic profile, together with assumed planar boundaries, allow the temperature for an arbitrary irradiation time envelope to be expressed in terms of a single integral. The error is then defined and investigated as a function of time, acoustic beamwidth, sample dimensions, and absorption.

4.1 Theory

A schematic representation of the TTM measurement configuration is shown in Figure 4.1. A soft tissue specimen with ultrasonic absorption coefficient α , specific heat C_p , and thermal diffusivity κ is irradiated with a focused ultrasound source. A thermocouple probe of small diameter, embedded at a depth d in the tissue, is the temperature sensor. The tissue is assumed to have planar boundaries with a surface facing the ultrasonic source and oriented normal to the acoustic axis of propagation as shown in Figure 4.1. The position vector \bar{r} is used to denote the site of the temperature observation, relative to the center of the focal region, as determined in the free field. The experimental environment is modeled for heat conduction as an infinite, isotropic, homogeneous medium, with a zero temperature increase at infinity, and zero initial conditions. A diffusion length $l = \sqrt{4\kappa t}$ may be defined that is indicative of the spatial extent of the heating due to a localized heat source at a given time t . For a time of 2 s and a thermal diffusivity characteristic of water, $\kappa = 1.5 \times 10^{-3} \frac{\text{cm}^2}{\text{s}}$, the diffusion length is 0.11 cm. The dimensions of the water bath in which the absorption coefficient measurements are performed is typically more than two orders of magnitude greater than this; hence, the medium may be considered infinite. The thermal diffusivity of

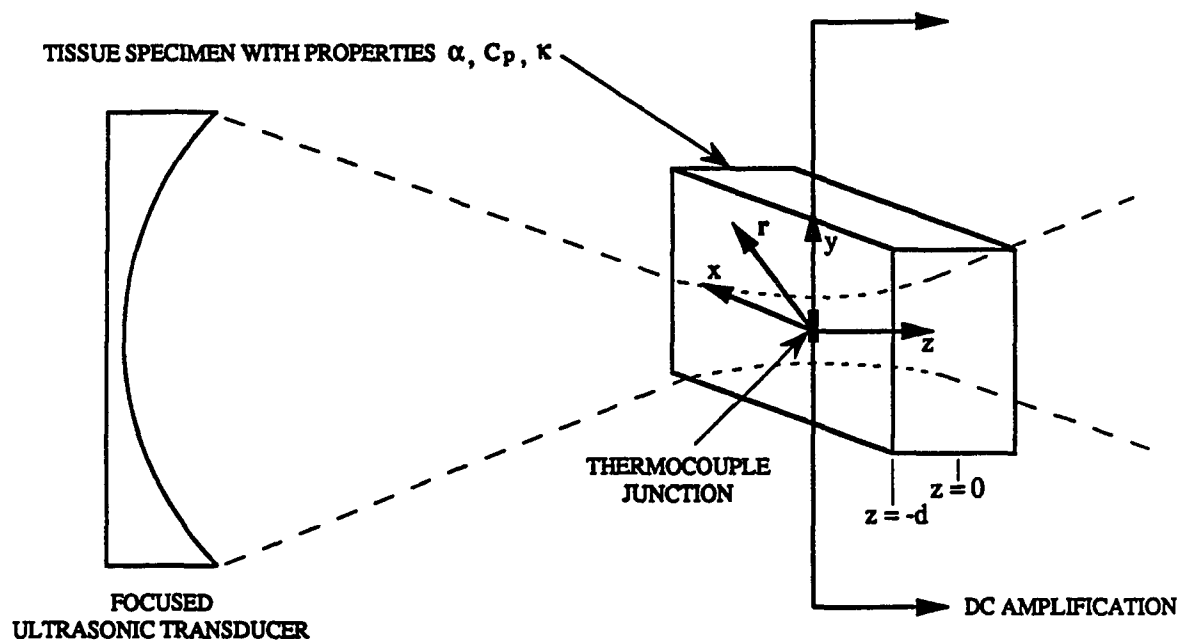


Figure 4.1: Schematic representation of the experimental procedure, conducted in a large, isotonic saline bath. The temperature is observed at $z = 0$.

many soft tissues is approximately that of water [182], such that the entire medium may be considered homogeneous. Exceptions, however, are skin and fat with thermal diffusivities of approximately $1 \times 10^{-3} \frac{cm^2}{s}$. A solution to the heat equation for two media of differing thermal properties is given in Section 4.4, from which the errors resulting from heat conduction in applying the TTM to measure the absorption coefficient in these tissues can be determined. The errors for skin and fat will be less than that for other soft tissues under identical measurement conditions because of the smaller thermal diffusivity of these tissues.

The temperature $T(\bar{\mathbf{r}}, t)$, at any point of observation $\bar{\mathbf{r}}$ and time t , is given by the solution of the inhomogeneous heat equation

$$\frac{\partial T}{\partial t} - \kappa \nabla^2 T = Q(\bar{\mathbf{r}}, t) \quad (4.8)$$

The source term $Q(\bar{\mathbf{r}}, t)$ in Eq. (4.8) is given by

$$Q(\bar{\mathbf{r}}, t) = Q_0 f(\bar{\mathbf{r}}) F(t) = \frac{2\alpha}{\rho C_p} I(\bar{\mathbf{r}}) F(t) \quad (4.9)$$

for a traveling plane wave in an absorptive medium [153], where $I(\bar{\mathbf{r}})$ is the intensity as a function of position, and $F(t)$ is employed to denote a *CW* or pulsed exposure. The temperature increase resulting from ultrasonic absorption, as well as the absolute temperature, are governed by the heat equation, though, only the temperature increase is important for present purposes. Thus, $T(\bar{\mathbf{r}}, t)$ in Eq. (4.8) is the temperature increase above the ambient temperature in the bath. A solution to Eq. (4.8) can be obtained for the assumed model by the method of Green's functions. The temperature at position $\bar{\mathbf{r}}$ and time t is given by

$$T(\bar{\mathbf{r}}, t) = Q_0 \int_0^t d\theta F(\theta) \int_V d\bar{\mathbf{r}}' I(\bar{\mathbf{r}}') G(\bar{\mathbf{r}} - \bar{\mathbf{r}}', t - \theta) \quad (4.10)$$

where

$$G(\bar{\mathbf{r}} - \bar{\mathbf{r}}', t - \theta) = \frac{e^{-\frac{|\bar{\mathbf{r}} - \bar{\mathbf{r}}'|^2}{4\kappa(t-\theta)}}}{[4\pi\kappa(t-\theta)]^{\frac{3}{2}}}$$

is the Green's function for an infinite, isotropic, homogeneous medium, and the volume integration is performed over the region of the absorbing soft tissue [36], [156].

The linear, focused acoustic beam is modeled with a Gaussian dependence in both the transverse and axial directions. The error for a Gaussian beam is compared to a $\left[\frac{2J_1(ar)}{ar}\right]^2$ (henceforth referred to as uniform-displacement, circular-aperture (UDCA)) beam shape transverse to the direction of propagation in Section 4.3. The Gaussian shape in the axial

direction has been shown to be a reasonable first-order approximation for medium and highly focused beams in the focal region [132], [159], [162], [175]. A piecewise linear approximation to the axial beam variation will also result in an analytical expression for the temperature increase due to absorption; however, a Gaussian shape is adequate for a first-order approximation. The shape of the theoretical transverse profile for a focused, cylindrically symmetric radiator at the center of the radius of curvature, as well as the transverse profile for an unfocused radiator in the far field, are given by a UDCA profile. Although the axial variation of the beam radiated by a planar source differs considerably from a Gaussian function over the entire field, a Gaussian shape is still a useful approximation at the near-field – far-field transition region, for dimensions typically of concern in the TTM. Hence, the analysis presented is useful for unfocused as well as for focused sources.

The intensity distribution in a dissipationless medium is taken to be

$$I(\bar{r}) = I(r, z) = I_0 e^{-\frac{r^2}{\beta_r} - \frac{z^2}{\beta_z}} \quad (4.11)$$

where $r^2 = x^2 + y^2$, β_r and β_z are the beamwidth parameters in the transverse and axial dimensions, respectively, and I_0 is the spatial peak intensity at $(r, z) = (0, 0)$. The beamwidth parameters β_r and β_z are related to the radial and axial HPBWs by $\beta_i = \frac{(\frac{1}{2}HPBW)^2}{\ln 2}$, where i denotes either the radial or axial dimension. The axial half-power beamwidth, which for clarity will be referred to as the half-power beamlength (HPBL), is approximately ten times greater than the radial HPBW for medium and highly focused beams, and a factor of ten will be used in the analysis [85]. The intensity distribution for a traveling plane wave in a

tissue specimen with absorption coefficient α and boundary through which the ultrasound enters at $z = -d$ is considered to be

$$I(\bar{r}) = I(r, z) = I_0 e^{-2\alpha(z+d)} e^{-\frac{r^2}{\beta_r} - \frac{z^2}{\beta_z}} \quad (4.12)$$

The exponential decay in the intensity is assumed to result primarily from absorption [160]. In using the functional form of Eq. (4.11) multiplied by a decaying exponential term as the intensity distribution in the tissue, as given in Eq. (4.12), it has been assumed that propagation in the tissue does not significantly affect the shape of the acoustic beam. This assumption may be somewhat tenuous for very thick specimens [160], though the results will show that only the intensity distribution over a few millimeters into the tissue is of consequence. By substituting the Gaussian beam shape of Eq. (4.12) into Eq. (4.10), and introducing the limits of integration for the planar boundaries, the temperature increase is given by

$$T(\bar{r}, t) = \frac{2\alpha I_0}{\rho C_p} \int_0^t d\theta F(\theta) \int_{-d}^{z_2} dz' \int_{-y_1}^{y_2} dy' \int_{-x_1}^{x_2} dx' e^{-2\alpha(z'+d)} e^{-\frac{x'^2+y'^2}{\beta_r} - \frac{z'^2}{\beta_z}} \\ \times \frac{e^{-\left(\frac{(x-x')^2+(y-y')^2+(z-z')^2}{4\kappa(t-\theta)}\right)}}{(4\pi\kappa(t-\theta))^{\frac{3}{2}}} \quad (4.13)$$

After performing the volume integration, the temperature increase at any point $\bar{r} = (x, y, z)$ and time t is given by

$$T(\bar{r}, t) = \frac{2\alpha I_0}{\rho C_p} e^{-2\alpha d} v(\bar{r}, t, \beta_r, \beta_z, \alpha) \quad (4.14)$$

where

$$v(\bar{r}, t, \beta_r, \beta_z, \alpha) = \int_0^t d\theta F(\theta) \frac{e^{-\left(\frac{r^2}{\beta_r} \frac{1}{1 + \frac{4\kappa(t-\theta)}{\beta_r}}\right)}}{1 + \frac{4\kappa(t-\theta)}{\beta_r}} \\ \times \frac{e^{-\left(\frac{z^2}{\beta_z} \frac{1}{1 + \frac{4\kappa(t-\theta)}{\beta_z}} + \frac{2\alpha z - 4\alpha^2 \kappa(t-\theta)}{1 + \frac{4\kappa(t-\theta)}{\beta_z}}\right)}}{\left(1 + \frac{4\kappa(t-\theta)}{\beta_z}\right)^{\frac{1}{2}}}$$

$$\begin{aligned}
& \times \frac{1}{2} \left\{ \operatorname{erf} \left[\frac{1}{\sqrt{4\kappa(t-\theta)}} \left(1 + \frac{4\kappa(t-\theta)}{\beta_r} \right)^{\frac{1}{2}} \left(\frac{1}{1 + \frac{4\kappa(t-\theta)}{\beta_r}} x + x_1 \right) \right] \right. \\
& \left. - \operatorname{erf} \left[\frac{1}{\sqrt{4\kappa(t-\theta)}} \left(1 + \frac{4\kappa(t-\theta)}{\beta_r} \right)^{\frac{1}{2}} \left(\frac{1}{1 + \frac{4\kappa(t-\theta)}{\beta_r}} x - x_2 \right) \right] \right\} \\
& \times \frac{1}{2} \left\{ \operatorname{erf} \left[\frac{1}{\sqrt{4\kappa(t-\theta)}} \left(1 + \frac{4\kappa(t-\theta)}{\beta_r} \right)^{\frac{1}{2}} \left(\frac{1}{1 + \frac{4\kappa(t-\theta)}{\beta_r}} y + y_1 \right) \right] \right. \\
& \left. - \operatorname{erf} \left[\frac{1}{\sqrt{4\kappa(t-\theta)}} \left(1 + \frac{4\kappa(t-\theta)}{\beta_r} \right)^{\frac{1}{2}} \left(\frac{1}{1 + \frac{4\kappa(t-\theta)}{\beta_r}} y - y_2 \right) \right] \right\} \\
& \times \frac{1}{2} \left\{ \operatorname{erf} \left[\frac{1}{\sqrt{4\kappa(t-\theta)}} \left(1 + \frac{4\kappa(t-\theta)}{\beta_z} \right)^{\frac{1}{2}} \left(\frac{z - 4\alpha\kappa(t-\theta)}{1 + \frac{4\kappa(t-\theta)}{\beta_z}} + d \right) \right] \right. \\
& \left. - \operatorname{erf} \left[\frac{1}{\sqrt{4\kappa(t-\theta)}} \left(1 + \frac{4\kappa(t-\theta)}{\beta_z} \right)^{\frac{1}{2}} \left(\frac{z - 4\alpha\kappa(t-\theta)}{1 + \frac{4\kappa(t-\theta)}{\beta_z}} - z_2 \right) \right] \right\} \quad (4.15)
\end{aligned}$$

and erf denotes the error function [2].

The results for the PDM can be obtained from Eq. (4.14) by neglecting the exponential decrease of the intensity, letting the boundaries go to infinity, and observing the temperature at $r = 0$, yielding [159]

$$T(0, t) = \frac{2\alpha I_0}{\rho C_p} \int_0^t d\theta F(\theta) \frac{1}{1 + \frac{4\kappa(t-\theta)}{\beta_r}} \frac{1}{\left(1 + \frac{4\kappa(t-\theta)}{\beta_z} \right)^{\frac{1}{2}}} \quad (4.16)$$

By letting $\beta_z \rightarrow \infty$, i.e., assuming an axially uniform beam, Eq. (4.16) can be integrated analytically for a short ultrasonic pulse $F(t) = U(t) - U(t - t_0)$, where $U(t)$ is the unit step function, to yield

$$T(0, t) = \frac{2\alpha I_0}{\rho C_p} \frac{\beta_r}{4\kappa} \left[\ln \left(1 - \frac{\frac{4\kappa t_0}{\beta_r}}{1 + \frac{4\kappa t}{\beta_r}} \right)^{-1} \right] \quad (4.17)$$

Upon expanding Eq. (4.17) in a Taylor series and keeping only the leading-order term, the temperature is given by

$$T(0, t) = \frac{2\alpha I_0}{\rho C_p} t_0 \frac{1}{1 + \frac{4\kappa t}{\beta_r}} \quad (4.18)$$

which is the result previously obtained for the PDM assuming a thermally impulsive source, i.e., $F(t) = \delta(t)$ [159]. As seen from the preceding development, the ultrasound heating source can be considered thermally impulsive if

$$\frac{4\kappa t_0}{\beta_r} \frac{1}{1 + \frac{4\kappa t}{\beta_r}} \ll 1 \quad (4.19)$$

The first 1 s of data, following the initiation of the ultrasound exposure, is typically ignored in implementing the PDM, to allow the temperature artifact from the viscous heating of tissue surrounding the embedded thermocouple to become negligible. Then, Eq. (4.19) is satisfied, for experimental purposes, if the length of the ultrasound pulse is of the order of 100 ms or less for any HPBW. For example, a 1 mm HPBW, $\kappa = 1.5 \times 10^{-3} \frac{\text{cm}^2}{\text{s}}$, $t = 1 \text{ s}$, and $t_0 = 100 \text{ ms}$, yield $\frac{\frac{4\kappa t_0}{\beta_r}}{1 + \frac{4\kappa t}{\beta_r}} = 0.062$. Recent implementations of the PDM in determining the absorption coefficient have utilized the integral-differential relationship between the impulse and unit step responses for the heat equation [141], [164]. In practice, the temperature history is measured for a unit step exposure and the impulse response obtained by differentiating the measured data. The usefulness of this procedure is in producing sufficient temperature increases that can be accurately measured, without generating significant harmonic components in the acoustic field due to nonlinear propagation. A lesser intensity can be used to produce a measurable temperature increase with a unit step ultrasonic exposure than with a short pulse exposure approximating a delta function.

The error in measuring the absorption coefficient using the TTM, which results from heat conduction due to the finite acoustic beam and tissue boundaries, can be investigated by defining the relative error

$$E(\bar{r}, t, \beta_r, \beta_z, \alpha) = \left(\frac{\frac{\partial T_{nc}}{\partial t} - \frac{\partial T(\bar{r}, t)}{\partial t}}{\frac{\partial T_{nc}}{\partial t}} \right) \times 100\% \quad (4.20)$$

where T_{nc} is the temperature increase in the absence of heat conduction as given by Eq. (4.7), and $T(\bar{r}, t)$ includes heat conduction and is given by Eq. (4.14) with $F(t) = U(t)$ (in Eq. (4.15)). Equations (4.7) and (4.14) can be used to simplify Eq. (4.20) to yield

$$E(\bar{r}, t, \beta_r, \beta_z, \alpha) = \left(1 - \frac{\partial v}{\partial t}\right) \times 100\% \quad (4.21)$$

The limits on E as t goes to zero and infinity can be found by using the relation between the impulse and unit step responses for $\frac{\partial v}{\partial t}$ [190]. In the case of a halfspace with the water-tissue interface at $z = -d$, $\frac{\partial v}{\partial t}$ is given by

$$\begin{aligned} \frac{\partial v}{\partial t} = & \frac{e^{-\left(\frac{r^2}{\beta_r} \frac{1}{1 + \frac{4\kappa t}{\beta_r}}\right)} e^{-\left(\frac{z^2}{\beta_z} \frac{1}{1 + \frac{4\kappa t}{\beta_z}} + \frac{2\alpha z - 4\alpha^2 \kappa t}{1 + \frac{4\kappa t}{\beta_z}}\right)}}{1 + \frac{4\kappa t}{\beta_r} \left(1 + \frac{4\kappa t}{\beta_z}\right)^{\frac{1}{2}}} \\ & \times \frac{1}{2} \left\{ \operatorname{erf} \left[\frac{1}{\sqrt{4\kappa t}} \left(1 + \frac{4\kappa t}{\beta_z}\right)^{\frac{1}{2}} \left(\frac{z - 4\alpha\kappa t}{1 + \frac{4\kappa t}{\beta_z}} + d\right)\right] + 1 \right\} \end{aligned} \quad (4.22)$$

The limits on E as $t \rightarrow 0$ and $t \rightarrow \infty$ are then

$$\begin{aligned} \lim_{t \rightarrow 0} E = & \left[1 - \frac{1}{2} e^{-\frac{r^2}{\beta_r} - \frac{z^2}{\beta_z} - 2\alpha z} \right. \\ & \left. \times \lim_{t \rightarrow 0} \left\{ \operatorname{erf} \left[\frac{1}{\sqrt{4\kappa t}} \left(1 + \frac{4\kappa t}{\beta_z}\right)^{\frac{1}{2}} \left(\frac{z - 4\alpha\kappa t}{1 + \frac{4\kappa t}{\beta_z}} + d\right)\right] + 1 \right\} \right] \times 100\% \end{aligned} \quad (4.23)$$

and

$$\lim_{t \rightarrow \infty} E = 100\% \quad (4.24)$$

At the water-tissue interface the limit on the error function in Eq. (4.23) goes to zero, and

$$\lim_{t \rightarrow 0} E = \left(1 - \frac{1}{2} e^{-\frac{r^2}{\beta_r} - \frac{d^2}{\beta_z} + 2\alpha d}\right) \times 100\% \quad (4.25)$$

For $z < -d$, the relative error in Eq. (4.23) goes rapidly to 100% as z decreases, and for $z > -d$, E goes rapidly to

$$\left(1 - e^{-\frac{r^2}{\beta_r} - \frac{z^2}{\beta_z} - 2\alpha z}\right) \times 100\% \quad (4.26)$$

as $t \rightarrow 0$.

The infinite, isotropic, homogeneous modeling of the thermal properties of the water-tissue medium assumed in the derivation of Eq. (4.14) neglected heat conduction along the thermocouple wire and loss of heat due to convection at the water-tissue interface. The additional heat conduction due to conduction along the thermocouple wire and to convective loss at the water-tissue interface will result in a lower rate of temperature increase, determined from the measurements, in the tissue at the focal point of the ultrasonic beam than predicted by Eq. (4.14). An increase in the relative error defined in Eq. (4.20) will result from these additional components of heat conduction away from the thermocouple junction. However, as discussed in Section 4.2, the heat conduction along the thermocouple wire is negligible for a typical experimental procedure, and convective heat removal at the water-tissue interface can be avoided by “potting” the tissue specimen in a tissue equivalent medium [34], [56].

4.2 Results and Discussion

The integral-differential relation between the impulse and unit step responses shown in Appendix A can be used to determine $\frac{\partial v}{\partial t}$ without performing the time integration. The error expression of Eq. (4.20) can then be evaluated as a function of spatial coordinates, time, beamwidth, beamlength, tissue specimen dimensions, and absorption. The axial HPBL is assumed to be ten times the radial HPBW, i.e., $\beta_z = 100 \beta_r$ for the results presented in this section [85], [159], [162]. The relative error for a Gaussian beam profile as given by Eq. (4.11) for an infinite source region is compared with measured results in mouse and horse liver from Goss et al. [91], and beef liver from Parker [159] in Figure 4.2. Since the reported values of the absorption coefficient in liver vary from 0.023 cm^{-1} to greater than

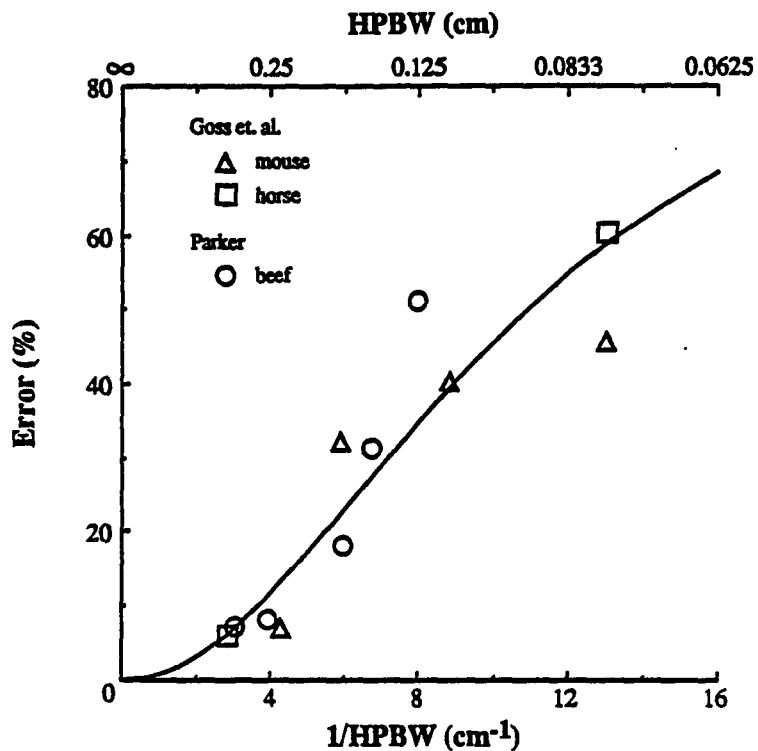


Figure 4.2: The relative error versus reciprocal HPBW and HPBW at 0.5 s following the initiation of the ultrasonic exposure. Comparison of a Gaussian profile (solid line) and experimental results in liver from Goss et al. [91] and Parker [159] (symbols).

0.04 cm^{-1} at 1 MHz [94], [159], the data from both references are normalized such that the experimental point corresponding to the largest experimental HPBW in both cases falls on the computed error curve. As can be seen, the analytical results compare favorably with the experimental values.

The effect of the HPBW on the relative error is shown in Figure 4.3 at $t = 0.5, 1.0,$ and 1.5 s. The heating volume has been taken to be infinite, and the exponential decay of the intensity in the tissue neglected; hence, the intensity distribution of Eq. (4.11) is used. The site of temperature observation is $(x, y, z) = (0, 0, 0)$. As expected, the relative error goes to zero at each of the times shown as the HPBW approaches infinity. For a

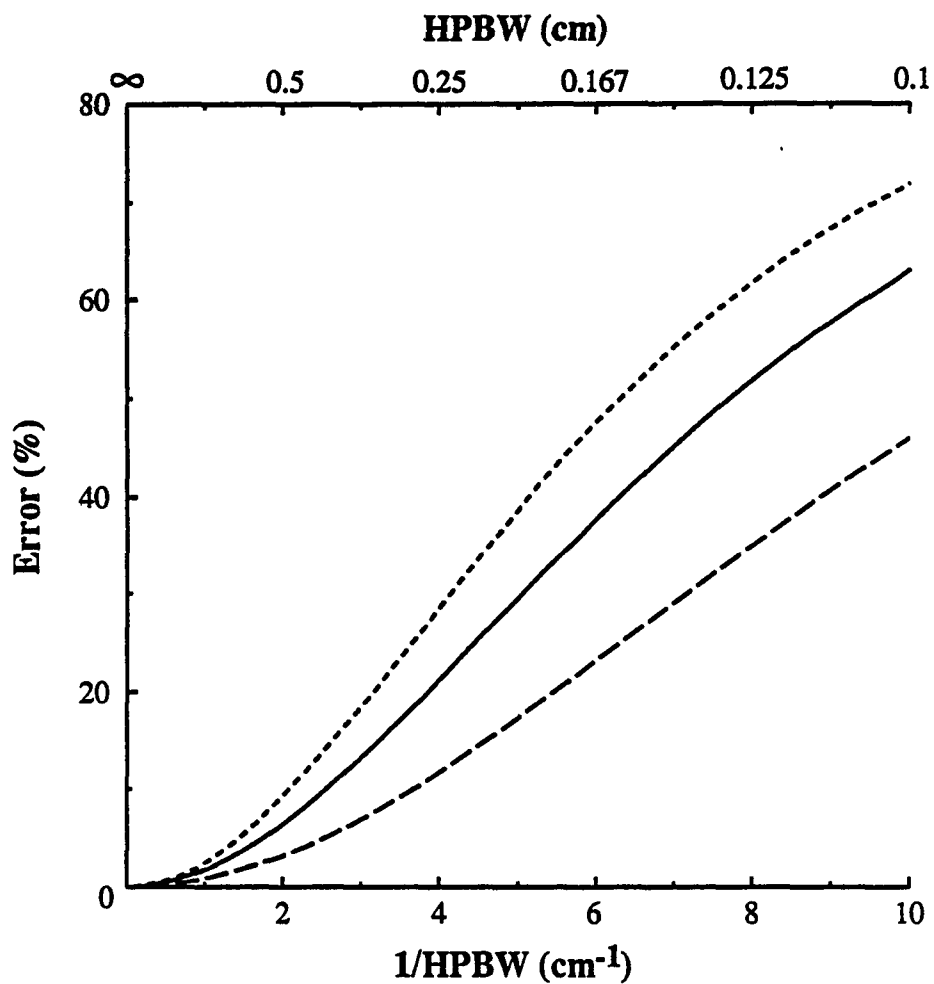


Figure 4.3: Relative error versus reciprocal HPBW and HPBW for an absorbing volume of infinite extent at 0.5 (long dashed line), 1.0 (solid), and 1.5 (short dash) s following the initiation of exposure.

typical experimental procedure employing a medium focused acoustic beam with a 5 mm HPBW, the relative errors are 3.2%, 6.3%, and 9.1%, at 0.5, 1.0, and 1.5 s, respectively. The coefficient of variation (standard deviation expressed as a percentage of the mean) for absorption coefficient measurements using the TTM typically ranges from 10–30% [94]. Although the defined relative error which results from heat conduction can generally be kept smaller than the standard deviation of the measurements, in some instances, the errors resulting from heat conduction can add a significant bias to the estimate. For example, a 1.5 mm HPBW acoustic field will result in an estimate for the absorption coefficient that is approximately 20% smaller than the value determined for negligible heat conduction, or a thermocouple junction at a depth of only 0.5 mm will similarly bias the estimate by more than 10%. Heat conduction along the thermocouple also biases the measurement, but for typical experimental procedures employing 13–25 μm constantan–chromel thermocouples, this bias can be made less than 0.5% [86], [186]. It has been common practice to attempt to minimize the error due to heat conduction by employing large acoustic HPBWs and evaluating the time derivative of the temperature at 0.5 s. However, for those experimental situations for which the thermal model used herein is appropriate, e.g., a thermally homogeneous tissue such as liver, the analysis may be used to correct for heat conduction.

It is advantageous to heat for a time longer than 0.5 s before evaluating the derivative $\frac{\partial T}{\partial t}$, for low-absorbing tissues, in order to minimize the error from the viscous heating associated with the thermocouple in the estimate of the absorption coefficient. For a tissue specimen of sufficient dimension that no significant heat flow has occurred due to finite boundaries, at 1 or 1.5 s, a broader HPBW can result in the same percent error at 1.5 s as with a narrow HPBW at 0.5 s. For example, $E = 3.2\%$ at 0.5 s for an HPBW of 5 mm, while $E = 2.5\%$

at 1.5 s for an HPBW of 1 cm. If the heat distribution resulting from the viscous heating is approximated transverse to the wire as a uniform cylinder with a radius equal to that of the thermocouple wire diameter, and along the wire axis as a Gaussian function, with a halfwidth equal to the acoustic HPBW, the time derivative of this portion of the total temperature increase at $(x, y, z) = (0, 0, 0)$ is given by

$$\frac{\partial T_v}{\partial t} = \frac{q_0 I_0}{\rho C_p} \left(1 - e^{-\frac{r_w^2}{4\kappa t}} \right) \frac{1}{\left(1 + \frac{4\kappa t}{\beta r} \right)^{\frac{1}{2}}} \quad (4.27)$$

where r_w is the wire radius, and $q_0 I_0$ is the equivalent heat generation rate per unit volume. The heat source is assumed to be in an infinite, isotropic, homogeneous medium with $\kappa = 1.5 \times 10^{-3} \frac{\text{cm}^2}{\text{s}}$. Taking the ratio of Eq. (4.27) and the derivative of Eq. (4.16) yields an approximation to the error introduced in the rate of the temperature increase, determined from the measurements, by the presence of the thermocouple. For low absorbing tissues such as testis, which has an absorption coefficient of 0.017 cm^{-1} at 1 MHz [93], the ratio $\frac{q_0}{2\alpha}$ can be large. However, by evaluating the temperature derivative at longer times, the error due to viscous heating can be significantly reduced. For example, employing a thermocouple with a 13 μm diameter, and taking $\frac{q_0}{2\alpha} = 1700$ [86], the error in the estimate of the absorption coefficient can be reduced from 24% to 8% by evaluating the temperature derivative at 1.5 s as opposed to 0.5 s.

Although the absorbing volume for the relative error shown in Figure 4.3 is infinite, the same conclusion can be reached even for very small absorbing volumes. The relative error versus reciprocal HPBW is shown at 0.5, 1.0, and 1.5 s in Figure 4.4 for the Gaussian heating distribution given in Eq. (4.11) integrated over a cube of dimension $3 \times 3 \times 3 \text{ mm}^3$. The relative error for a 5 mm HPBW at 0.5 s is 3.2%, while the relative error for a 1 cm HPBW

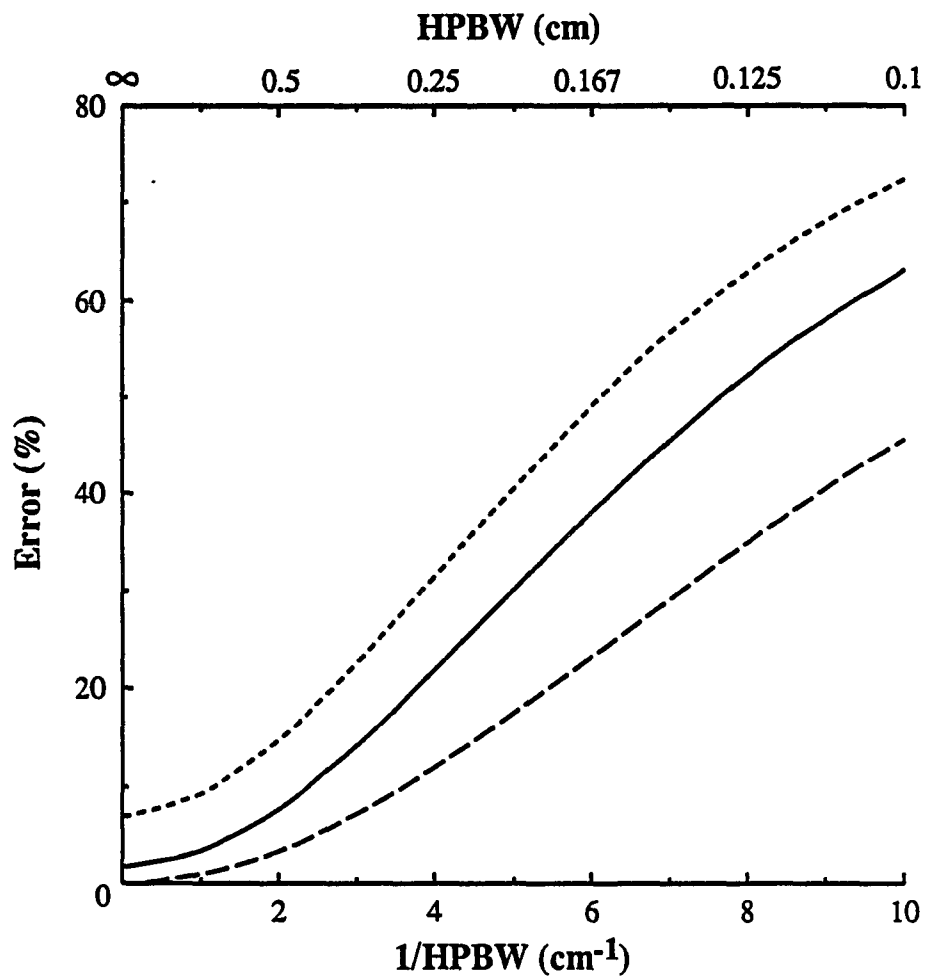


Figure 4.4: Relative error versus reciprocal HPBW and HPBW for a $3 \times 3 \times 3 \text{ mm}^3$ absorbing cube in an infinite medium at 0.5 (long dashed line), 1.0 (solid), and 1.5 (short dash) s following initiation of ultrasonic exposure.

at 1.0 s is 3.4%. It is seen by comparing Figures 4.3 and 4.4 that as the HPBW becomes smaller, the heat conduction at the boundary is small compared to heat conduction resulting from the small HPBW for the times shown.

The relative error as a function of time for several values of tissue thicknesses and HPBWs is shown in Figure 4.5. The temperature is observed at the center of the specimen thickness. The dimensions transverse to the acoustic axis of propagation, i.e., the x and y directions, are taken to be infinite, and a Gaussian heating distribution as given in Eq. (4.11) has been assumed. At 0.5 s there is negligible difference between the finite and infinite specimen thicknesses. The contribution of the finite beamwidth to the relative error is more significant (at 0.5 s) than that from the finite size of the tissue specimen. At longer times, the portion of the relative error due to the finite sample size becomes very significant. For example, note the 2 mm specimen thickness results. However, a wide HPBW of 1 cm results in a relative error of approximately 5% at 1.5 s even for a 3 mm thick specimen.

There are experimental situations when it is necessary to measure the absorption coefficient of tissue specimens with dimensions of only a few millimeters [35], [189]. The relative error as a function of time for several sizes of cubes and several values of HPBW, is shown in Figure 4.6. The Gaussian function of Eq. (4.11) has been employed for the heating distribution, and the site of temperature observation is the center of the cube for the finite dimensional cases, and the origin for the infinite dimensional case. The relative error at 0.5 s for a $3 \times 3 \times 3 \text{ mm}^3$ cube is essentially identical to that for an infinite heating volume. The relative error for a wider HPBW of 1 cm at 1.0 s is 3.4% for a $3 \times 3 \times 3 \text{ mm}^3$ cube and is less than 3.2% for a $4 \times 4 \times 4 \text{ mm}^3$ cube even at 1.5 s. It is clear that the TTM can be employed to measure the absorption coefficient of tissue specimens of small dimensions.

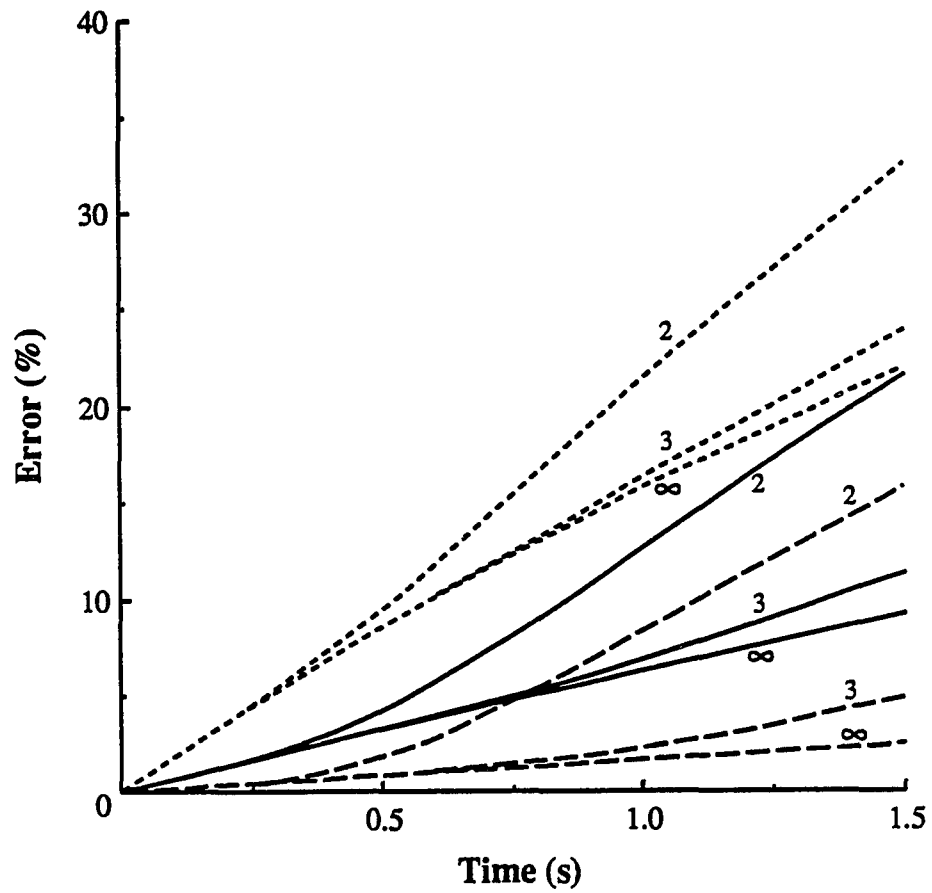


Figure 4.5: Relative error versus exposure time for 2, 3, and ∞ mm thicknesses of the absorbing medium at HPBW's of 3 (short dashed lines), 5 (solid), and 10 (long dash) mm.

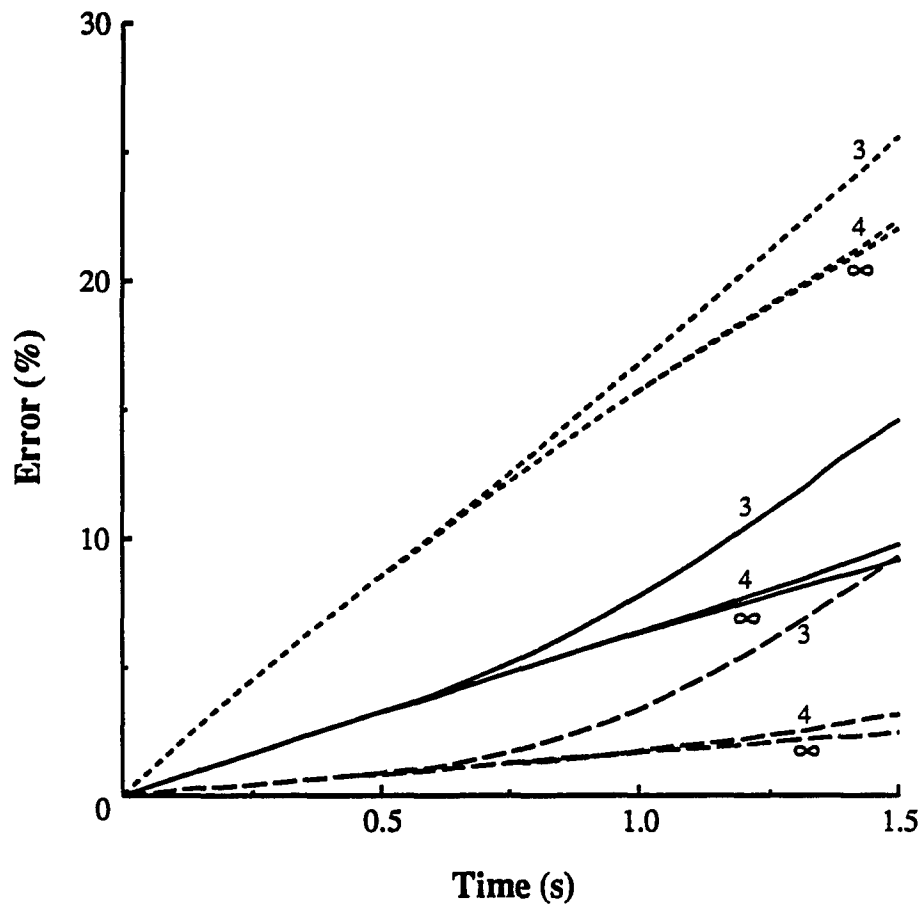


Figure 4.6: Relative error versus exposure time for $3 \times 3 \times 3 \text{ mm}^3$, $4 \times 4 \times 4 \text{ mm}^3$, and infinite volumes of absorbing media for 3 (short dashed lines), 5 (solid), and 10 (long dash) mm HPBW.

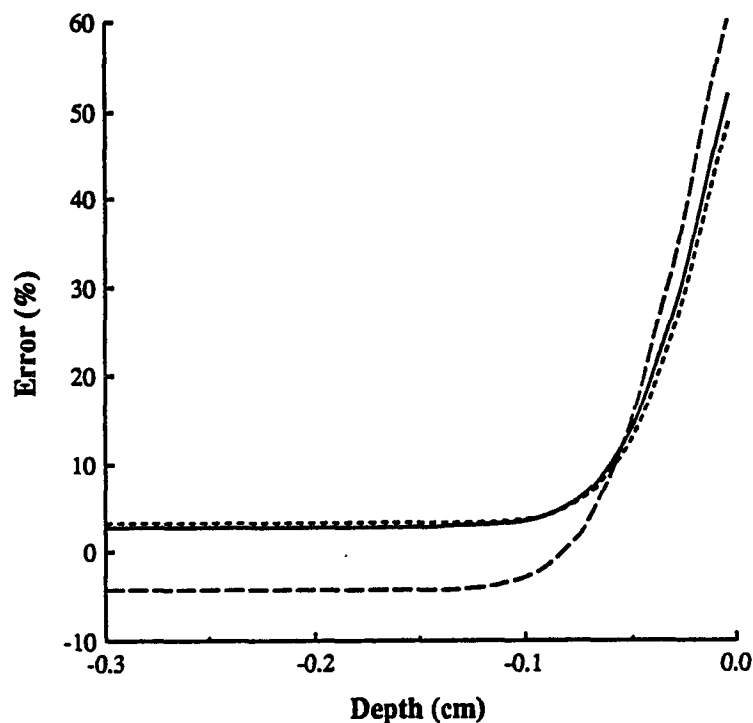


Figure 4.7: Relative error versus depth of observation for an absorbing halfspace with a Gaussian heating distribution exponentially decaying from the interface for $\alpha = 0$ (short dashed line), 1.0 (solid), and $\alpha = 5.0$ (long dash), error at 0.5 s for a 5 mm HPBW.

The PDM, however, may not be useful in such cases because the tissue boundaries will have an effect on the measured temperature increase. It is then necessary to consider the tissue boundaries in deriving an analytical form for the temperature. The shape of small tissue specimens may not, in general, lend themselves easily to boundaries for which an analytical form for the temperature can be found, in particular, rectangular or cylindrical geometries. Thus a significant error may result in using such assumptions in the determination of the absorption coefficient using the PDM.

The relative error at 0.5 s as a function of the thermocouple depth for several values of absorption α and a 5 mm HPBW is shown in Figure 4.7, for the heating distribution of Eq.

(4.12) integrated over the half space $z > -d$. The site of temperature observation is the origin, and the beginning of the halfspace is the depth. The relative error does not exhibit a rapid increase for increasing thermocouple depth as might be expected for the case of $\alpha \neq 0$, because in the ideal case of negligible heat conduction given by Eq. (4.7), the exponential decay of the intensity is assumed. Hence, the $e^{-2\alpha d}$ factor in Eq. (4.14) has been normalized from the expression for E . The z dependence of $\frac{\partial v}{\partial t}$ at 0.5 s, as given by Eq. (4.22), then causes E to be less in the absorbing than in the nonabsorbing case at depths for which the boundary has no effect. Physically, for large absorption coefficients, the observation point at $z = 0$ is on the tail of a heat distribution exponentially decreasing with depth. Hence, the temperature increase with time, at $z = 0$, results from absorption and heat flow from the region $-d < z < 0$. As a result, the relative error can even be negative upon normalizing the $e^{-2\alpha d}$ factor from the expression for E .

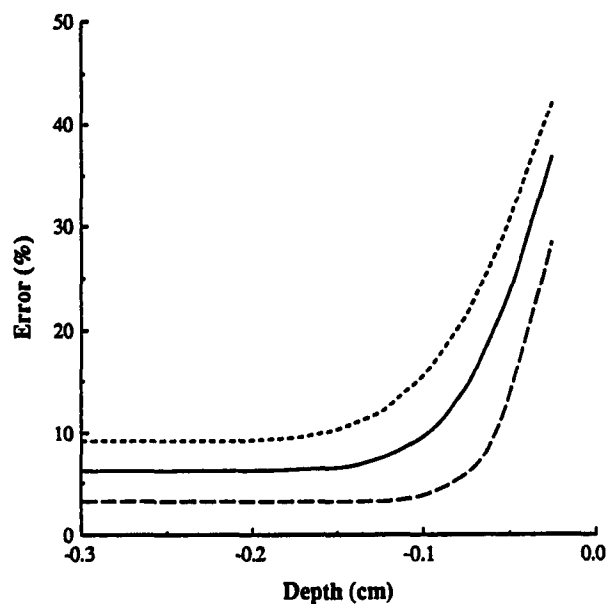
Absorption is important in contributing to the error if the depth at which the thermocouple is placed is not known precisely. It has been assumed in deriving Eq. (4.14) that the embedded thermocouple is located at the beam maximum, i.e., $z = 0$, as determined in the free field, and that the depth in the tissue at which the junction is located is known precisely. As seen in Eq. (4.22), $\frac{\partial v}{\partial t}$ has an $e^{-\left(\frac{2\alpha z}{1 + \frac{2\alpha t}{\beta z}}\right)}$ dependence, where $z > -d$ is the location of the thermocouple junction. Essentially, this factor represents an error in the calculated intensity resulting from the error in the position. This factor becomes particularly important at higher frequencies where the absorption coefficient is larger. For example, at 8 MHz the absorption coefficient for liver is approximately 0.5 cm^{-1} [141]. For an HPBW of 5 mm, an absorption coefficient of 0.5 cm^{-1} and a positioning error of 1 mm, i.e., $z = +1 \text{ mm}$, the exponential factor contributes 9% to the error at 0.5 s following the initiation of exposure.

The exponential factor $\exp\left\{-\frac{z^2}{\beta_z} \frac{1}{1+\frac{4\kappa t}{\beta_z}}\right\}$ in $\frac{\partial v}{\partial t}$ contributes negligibly to this error for the given values of HPBW and z .

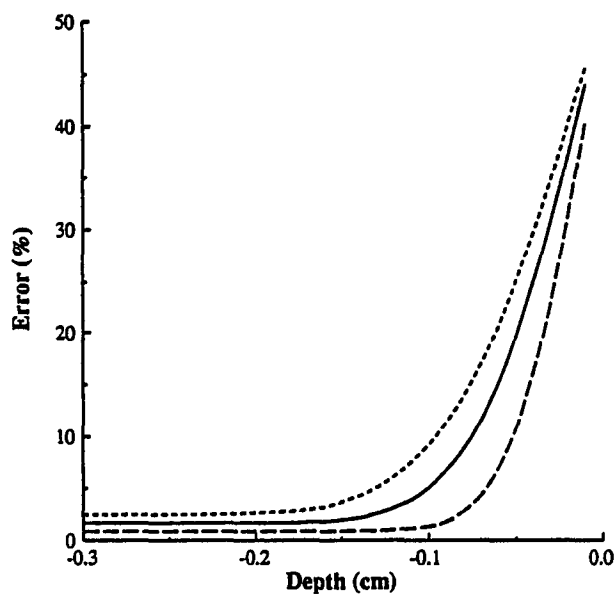
The relative error as a function of thermocouple depth in the tissue at 0.5, 1.0, and 1.5 s, with $\alpha = 0$, is shown in Figures 4.8(a) and 4.8(b) for 5 mm and 1 cm HPBWs, respectively.

At $t = 0.5$ s, no significant heat conduction results from the halfspace boundary for thermocouples placed 1 mm or deeper in both cases. The asymptotic value of the error with increasing depth is determined by the beamwidth as can be seen by comparing Figures 4.8(a) and 4.8(b) with the appropriate HPBWs in Figure 4.3. If the critical depth is defined as the depth at which heat conduction toward the boundary is negligible, at $t = 0.5, 1.0,$ and 1.5 s, the critical depth is approximately 1.0, 1.5, and 1.75 mm, respectively. It is advantageous to place the thermocouple deeper than the critical depth because of the rapid rise in the relative error for more shallow depths, as seen in Figures 4.8(a) and 4.8(b).

The thermocouple junction is centered on the acoustic beam when measuring the absorption coefficient using the TTM. The center of the beam is found by stepping the thermocouple junction transversely across the beam and recording the temperature increase that results from a short ultrasonic pulse. The resulting set of points is then fit to a second- or fourth-order polynomial and the thermocouple junction is positioned at the maximum of the fitted curve. Errors in finding the beam maximum by this procedure can result from noise and from sampling increments that are too large. The relative error as a function of time for 3 mm and 5 mm HPBWs for several displacements from the beam maximum is shown in Figures 4.9(a) and (b), computed using the Gaussian heating distribution of Eq. (4.11) integrated over an infinite absorbing region. As with an axial error in the estimate of the position, a radial positioning error essentially results in an error in the estimate of the intensity for the times

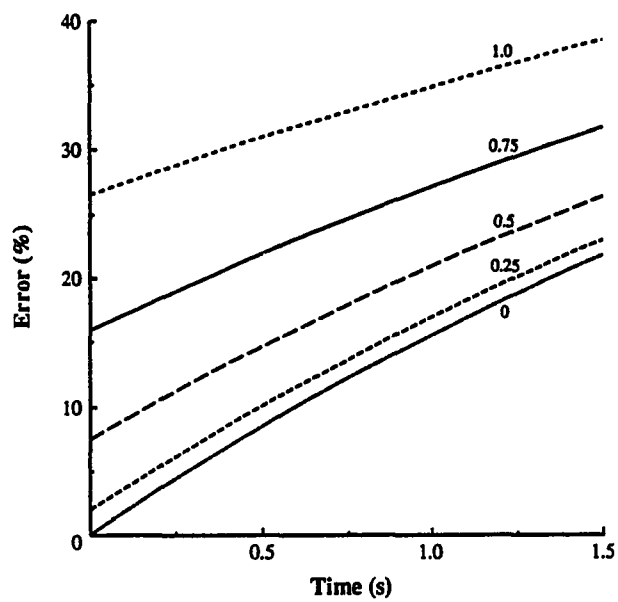


(a)

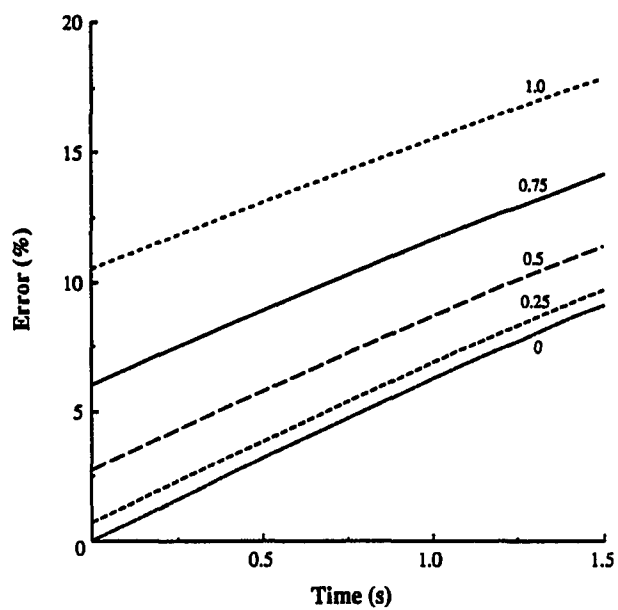


(b)

Figure 4.8: Relative error versus depth of observation for an absorbing halfspace for a Gaussian heating distribution and no exponential decay for (a) a 5 mm HPBW at 0.5 (long dashed line), 1.0 (solid), and 1.5 (short dash) s following the initiation of exposure; (b) same as (a) with a 1 cm HPBW.



(a)



(b)

Figure 4.9: Relative error versus exposure time for observation points displaced radially (in *mm*) from the acoustic beam maximum for (a) 3 *mm* and (b) 5 *mm* HPBWs.

Table 4.1: Measured Absorption Coefficients in Soft Tissue

Tissue	measured absorption coefficient (cm^{-1})
mouse liver	0.033, 0.034, 0.035
pig kidney cortex	0.029, 0.033

of interest. In general, the thermocouple junction can be precisely positioned at the center of the acoustic beam profile. Figures 4.9(a) and (b) emphasize that precision is necessary in finding the beam maximum for narrow HPBW's.

Absorption coefficient measurements at 1 *MHz* obtained by the author in the course of other work are shown in Table 4.1. The mouse liver absorption coefficients were measured in three different animals on different days, and the pig kidney measurements were on the same animal but different sites in the tissue. The HPBW of the transducer was 5 *mm*. Although the number of measurements is few, the results illustrate that the measurement to measurement deviation in a specific tissue can be kept small if the guidelines concerning thermocouple depth and ultrasound beamwidth are followed. The results in liver compare well with those of Lyons et al. [141]. Although the values of absorption in kidney are lower than those measured by Benkeser et al. [17], they compare well with those of Goss et al. [94].

4.3 Comparison of Gaussian and UDCA Beams

A Gaussian approximation to the theoretical UDCA intensity profile for a focused radiator at the focal point has been employed in Section 4.1. This approximation resulted in a simple analytical expression for $\frac{\partial T}{\partial t}$ for a rectangular absorbing region. The ease in handling the Gaussian approximation analytically makes it more desirable to use for the intensity profile of a focused transducer than the UDCA profile. However, to use the results for the Gaussian beam approximation presented in Section 4.2 for the focused and unfocused radiators typically encountered in experimental measurements, it is first necessary to compare the relative error for a Gaussian beam to that for a UDCA beam. Methods for fabricating transducers that radiate Gaussian beams have been reported in the literature [31], [58], [109], [143]. However, practical considerations such as expense, frequency, and required intensity levels prevent the use of these devices in some instances where it is desired to measure the absorption coefficient employing the TTM. A solution to the wave equation within the parabolic approximation has been given for a Gaussian amplitude source [58], [60]. This solution provides a more complete description of the shape of the beam as it propagates; however, the mathematical expressions are more complicated than what is required for the analysis of the TTM.

The relative error between the cases of no heat conduction and heat conduction for each heat distribution is defined in Section 4.2. The relative error for a circularly symmetric, axially uniform beam in an infinite, thermally homogeneous and isotropic medium can be compared for Gaussian and UDCA beams by solving Eq. (4.8) with the appropriate source functions. In this case, the ultrasound beam is considered to heat the entire region. Equation

(4.8) is again solved by the Green's function method. The temperature as a function of the radial coordinate r and time t for a heat distribution $Q(\bar{r}, t) = Q_0 f(\bar{r}) F(t)$ is given by

$$T(r, t) = Q_0 \int_0^t F(\theta) d\theta \int_0^\infty r' dr' f(r') G(r, r', t - \theta) \quad (4.28)$$

where

$$G(r, r', t - \theta) = \frac{e^{-\frac{r^2 + r'^2}{4\kappa(t-\theta)}}}{2\kappa(t-\theta)} I_0 \left(\frac{rr'}{2\kappa(t-\theta)} \right)$$

is the two-dimensional cylindrically symmetric Green's function, and I_0 is the modified Bessel function of order zero [2]. The difference in the relative error is given by

$$\delta E = |E_J - E_G| = \left| \frac{\partial v_J}{\partial t} - \frac{\partial v_G}{\partial t} \right| \times 100\% \quad (4.29)$$

where the J and G subscripts indicate the temperature distribution is to be solved with the UDCA and Gaussian intensity profiles, respectively. Using the integral-differential relation between the impulse and unit step responses, the derivatives $\frac{\partial v_J}{\partial t}$ and $\frac{\partial v_G}{\partial t}$ for $F(t) = U(t)$ are then

$$\frac{\partial v_J(r, t)}{\partial t} = \int_0^\infty r' dr' \left[\frac{2J_1(ar')}{ar'} \right]^2 \frac{e^{-\frac{r^2 + r'^2}{4\kappa t}}}{2\kappa t} I_0 \left(\frac{rr'}{2\kappa t} \right) \quad (4.30)$$

and

$$\frac{\partial v_G(r, t)}{\partial t} = \int_0^\infty r' dr' e^{-\frac{r'^2}{\beta_r}} \frac{e^{-\frac{r^2 + r'^2}{4\kappa t}}}{2\kappa t} I_0 \left(\frac{rr'}{2\kappa t} \right) \quad (4.31)$$

where a and β_r are the beam parameters for UDCA and the Gaussian profiles, respectively. If the temperature is observed at the origin, i.e., $r = 0$, the Gaussian function can be integrated analytically to yield

$$\frac{\partial v_G(0, t)}{\partial t} = \frac{1}{1 + \frac{4\kappa t}{\beta_r}} \quad (4.32)$$

The two beam profile functions are compared in Figure 4.10 for identical HPBW's of 3 mm. The difference in the relative error $\delta E(t)$ is shown in Figure 4.11 for 1, 3, 5, and

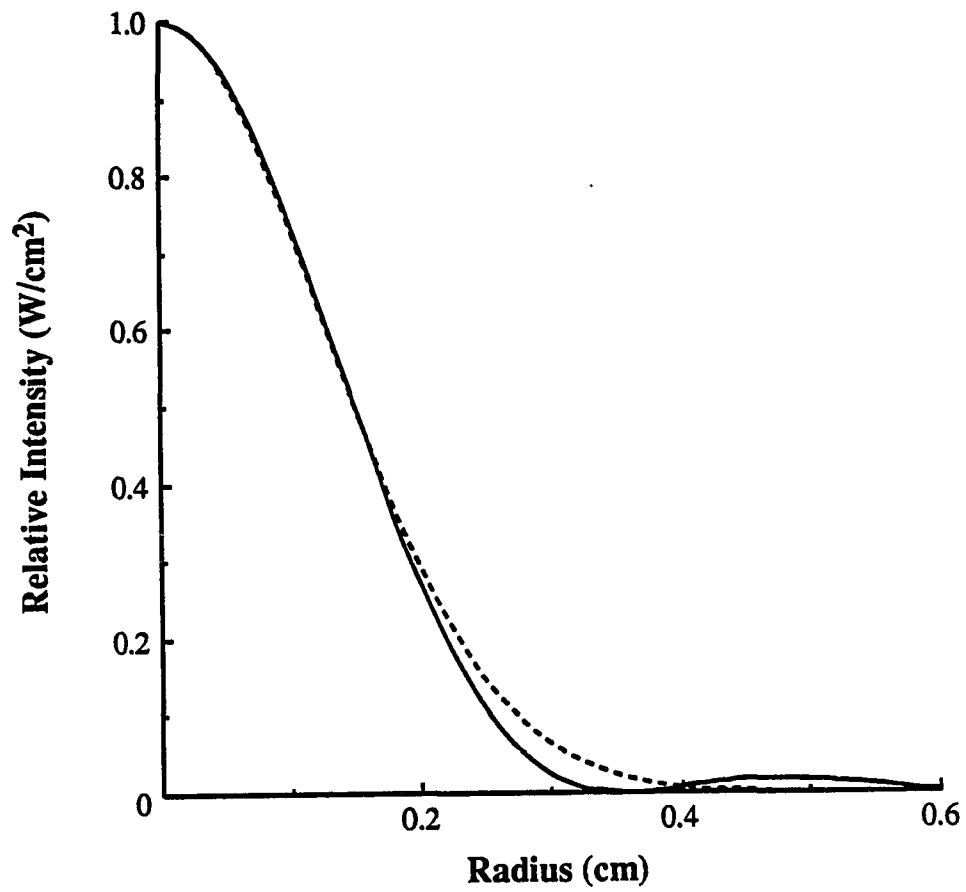


Figure 4.10: Comparison of Gaussian (dashed line) and $\left[\frac{2J_1(ar)}{ar}\right]^2$ (solid) beams for identical HPBW's of 3 mm.

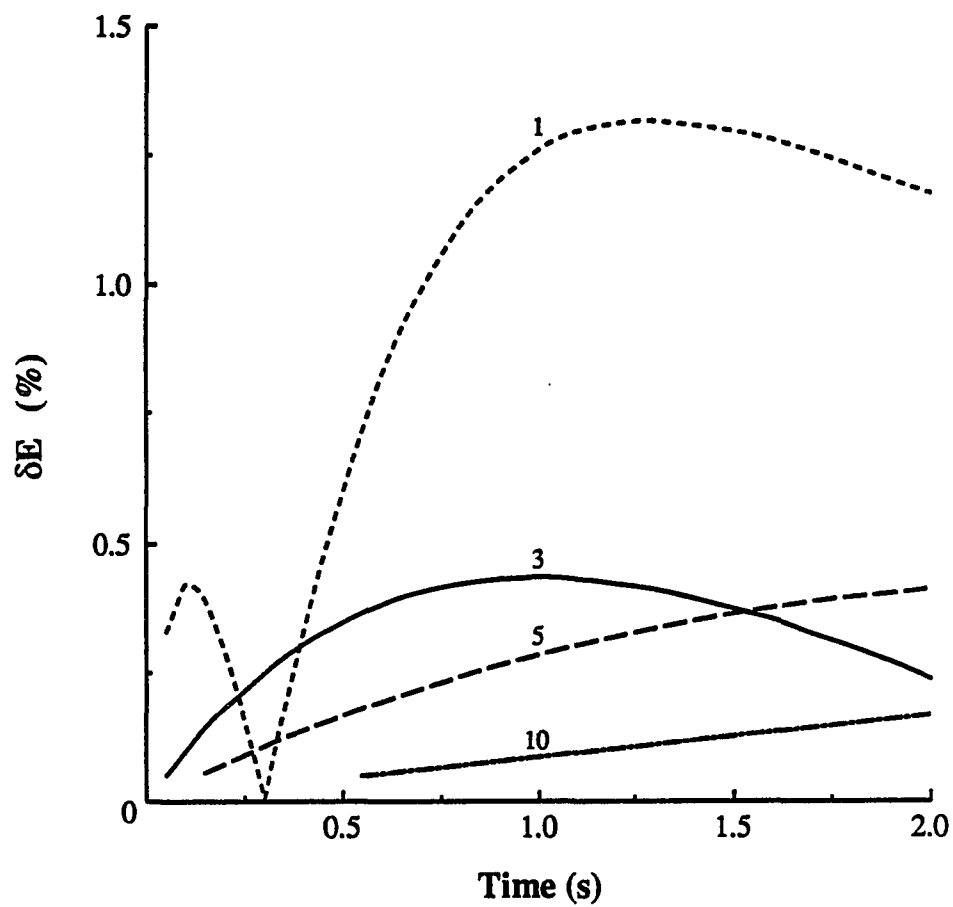


Figure 4.11: δE versus exposure time for 1, 3, 5, and 10 mm HPBWs.

10 mm HPBW intensity profiles. The behavior of δE with time is the same in all four curves, with the exception of the time scale, though, only the first two seconds following the initiation of the ultrasonic exposure are shown here. The main features of δE as a function of time occur within the first two seconds of exposure for a 1 mm HPBW. Initially, $\frac{\partial v_I}{\partial t} > \frac{\partial v_G}{\partial t}$, reaching a maximum of $\delta E = 0.43\%$ at 0.1 s following the initiation of the ultrasonic exposure. The difference in the relative error goes to zero and then increases again with $\frac{\partial v_I}{\partial t} < \frac{\partial v_G}{\partial t}$, reaching a maximum of 1.3%. At longer times, the steady state is approached and $\delta E \rightarrow 0$ as $t \rightarrow \infty$. The second maximum for the 3, 5, and 10 mm HPBWs is not reached in the first two seconds following the initiation of exposure, and $\delta E(t)$ remains less than 0.5% over this time interval. Thus, for beamwidths of concern in using the TTM to measure the ultrasonic absorption coefficient, a Gaussian beam is a good approximation to a UDCA profile for identical HPBWs.

4.4 Results for Tissues with a Thermal Diffusivity Different from Water

Skin and fat have thermal diffusivities significantly different from that of other soft tissues. Whereas most soft tissues have a thermal diffusivity near that of water, $\kappa = 1.5 \times 10^{-3} \frac{\text{cm}^2}{\text{s}}$, skin and fat have a thermal diffusivity of approximately $\kappa = 1.0 \times 10^{-3} \frac{\text{cm}^2}{\text{s}}$. The critical depth to implant the thermocouple junction can then be expected to be less in skin and fat than that for other soft tissues when evaluating the temperature derivative at identical times. Or the temperature derivative can be evaluated at later times than other soft tissues for the same depth of implantation of the thermocouple. The relative error E as a function of HPBW will also be less in the case of smaller κ when evaluating $\frac{\partial T}{\partial t}$ at a specific time. A quantitative knowledge of the relative error for varying parameters allows the measurement

procedures to be designed to obtain the best precision and accuracy. The heat conduction problem for two media of differing thermal properties must then be solved. The thermal diffusivity in acoustically absorbing oils is also typically different from that of water, and a solution to the two media problem will provide insight and guidance in measuring the absorption coefficient. In addition, an analytical solution similar to that in Section 4.1 for the two media problem can be used for further experimental verification of the theory. The relative error as a function of HPBW was found to compare well with experimental results published by Goss et al. [91] and Parker [159], as shown in Figure 4.2. Further experimental work investigating the critical depth and variation of the relative error with sample thickness and time would provide additional support for the theory. Oils are typically easier to work with than soft tissues. An appropriate cell can be constructed with the thermocouple depth precisely known. For further comparison of the experiments with the theory, the two media problem must then be solved.

The temperature increase in an absorbing halfspace with a thermal diffusivity different from that of the surrounding water coupling medium can be solved by the Green's function method as was done for the homogeneous medium in Section 4.1. The Green's function for this problem can be found by seeking solutions in the two separate media and then matching the boundary and source conditions. The inhomogeneity is in only one direction for the halfspace problem, and only the one-dimensional problem need be solved. The equations for which a solution is sought are

$$\frac{\partial G}{\partial t} = \kappa_1 \frac{\partial^2 G}{\partial z^2} \quad z < -d \quad (4.33)$$

$$\frac{\partial G}{\partial t} = \kappa_2 \frac{\partial^2 G}{\partial z^2} + \delta(z - z')F(t) \quad z > -d$$

where the boundary is located at $z = -d$ ($d > 0$). The boundary conditions and initial values are given by

$$\begin{aligned} G &= 0 & z &\rightarrow \pm\infty \\ \kappa_1 \frac{\partial G}{\partial z} &= \kappa_2 \frac{\partial G}{\partial z} & z &= z_1 \end{aligned} \quad (4.34)$$

$$G = 0 \quad t = 0$$

and the source conditions implied by the delta function are

$$G(z, z'_+) = G(z, z'_-) \quad (4.35)$$

$$\frac{\partial G}{\partial z} \Big|_{z'_+} - \frac{\partial G}{\partial z} \Big|_{z'_-} = -\frac{F(t)}{\kappa_2}$$

where the point source is located at $z = z'$. The solution to Eq. (4.33), subject to the boundary conditions and initial values given by Eq. (4.34), can be found using the Laplace transform [54]. The Green's function for the observation point at $z > -d$ is then given by

$$\begin{aligned} G(\bar{r}, \bar{r}', t - \theta) &= \frac{e^{-\frac{(x-x')^2 + (y-y')^2}{4\kappa_2(t-\theta)}}}{[4\pi\kappa_2(t-\theta)]^{\frac{3}{2}}} \\ &\times \left\{ \frac{\eta - 1}{\eta + 1} e^{-\frac{(z+z'+2d)^2}{4\kappa_2(t-\theta)}} + e^{-\frac{(z-x')^2}{4\kappa_2(t-\theta)}} \right\} \end{aligned} \quad (4.36)$$

where $\eta = \frac{K_2}{K_1} \sqrt{\frac{\kappa_1}{\kappa_2}}$, K is the thermal conductivity, and the x and y dependences have been reintroduced to yield a three-dimensional Green's function. If the heat source is given by the decaying Gaussian intensity distribution as in Eq. (4.12), the temperature increase in the absorbing medium for a CW ultrasonic exposure is then

$$T(\bar{r}, t) = \frac{2\alpha_2 I_0}{\rho_2 C_{p2}} t \int_0^1 d\xi \int_{-d}^{\infty} dz' \int_{-\infty}^{\infty} dy' \int_{-\infty}^{\infty} dx' e^{-2\alpha_2(z'+d)} e^{-\frac{\xi^2 + y'^2}{\beta_r} - \frac{z'^2}{\beta_z}}$$

$$\begin{aligned}
& \times \frac{e^{-\frac{(x-x')^2+(y-y')^2}{4\kappa_2 t\xi}}}{[4\pi\kappa_2 t\xi]^{\frac{3}{2}}} \\
& \times \left\{ \frac{\eta-1}{\eta+1} e^{-\frac{(z+z'+2d)^2}{4\kappa_2 t\xi}} + e^{-\frac{(z-z')^2}{4\kappa_2 t\xi}} \right\} \quad (4.37)
\end{aligned}$$

for $z > -d$, where a change of variables $t\xi = t - \tau$ has been introduced. Since Medium 2 is assumed to be an absorbing halfspace, the integration in the $\pm x$ and $\pm y$ directions is to positive and negative infinity and in the positive z direction is to positive infinity. If a solution is needed at times for which the finite sample dimensions are of concern, the three media problem must be solved. The above solution, however, is useful for evaluating the accuracy of the TTM in tissues and oils having thermal diffusivities different from water by a factor of two or three, and sample dimensions of the order of several millimeters. Upon performing the spatial integrations, the temperature elevation in the absorbing medium is

$$\begin{aligned}
T(\bar{r}, t) = & \frac{2\alpha_2 I_0}{\rho C_p} e^{-2\alpha_2 d t} \int_0^1 d\xi \frac{\exp\left[-\frac{x^2+y^2}{\beta_r} \frac{1}{1+\frac{4\kappa_2 t\xi}{\beta_r}}\right]}{\left(1+\frac{4\kappa_2 t\xi}{\beta_r}\right)\left(1+\frac{4\kappa_2 t\xi}{\beta_z}\right)^{\frac{1}{2}}} \\
& \times \frac{1}{2} \exp\left[-\frac{z^2}{\beta_z} \frac{1}{1+\frac{4\kappa_2 t\xi}{\beta_z}} + \frac{2\alpha_2 z - 4\alpha_2^2 \kappa_2 t\xi}{1+\frac{4\kappa_2 t\xi}{\beta_z}}\right] \\
& \times [1 + \operatorname{erf} A] \\
& + \frac{1}{2} \frac{\eta-1}{\eta+1} \exp\left[-\frac{(2d+z)^2}{\beta_z} \frac{1}{1+\frac{4\kappa_2 t\xi}{\beta_z}}\right. \\
& \left. - \frac{2\alpha_2(2d+z) + 4\alpha_2^2 \kappa_2 t\xi}{1+\frac{4\kappa_2 t\xi}{\beta_z}}\right] \\
& \times [1 - \operatorname{erf} B] \quad (4.38)
\end{aligned}$$

where

$$A = \frac{1}{\sqrt{4\kappa_2 t\xi}} \left(1 + \frac{4\kappa_2 t\xi}{\beta_z}\right)^{\frac{1}{2}} \left(\frac{z - 4\alpha_2 \kappa_2 t\xi}{1 + \frac{4\kappa_2 t\xi}{\beta_z}} + d\right)$$

$$B = \frac{1}{\sqrt{4\kappa_2 t \xi}} \left(1 + \frac{4\kappa_2 t \xi}{\beta_z} \right)^{\frac{1}{2}} \left(\frac{2d + z + 4\alpha_2 \kappa_2 t \xi}{1 + \frac{4\kappa_2 t \xi}{\beta_z}} - d \right)$$

Tissue specimens with dimensions of several millimeters are typically available such that the boundaries in the x , y , and positive z directions can be assumed to be infinite for the times of interest. In addition, the solution to the two media problem is sufficient for the purpose of comparison between the theory and further experiments. Cells of absorbing oil can also be constructed sufficiently large to fit the infinite boundary conditions in the $\pm x, y$ and $+z$ directions for the times of interest in the TTM. An alternative to using an absorbing oil for further experimental verification of the analysis is an absorbing rubber such as polymethylmethacrylate [175].

4.5 Summary

It is clear that heat conduction can contribute a significant error to the measurement of the ultrasonic absorption coefficient when using the TTM. The temperature increase in a soft tissue specimen irradiated by a traveling plane wave has been derived in this chapter for the purpose of evaluating fundamental limits of the TTM, and for serving as a guide for improving the accuracy of the measurement of the ultrasonic absorption coefficient using the TTM. The infinite, isotropic, homogeneous modeling of the heat conducting medium, introduced earlier, has been employed. The acoustic beam profile has been approximated with a Gaussian function transverse to and along the axis of propagation. A relative error that represents the difference between the case of negligible heat conduction and that of the assumed model for the experimental environment has been defined. The relative error

has been studied for varying spatial coordinates, time, radial and axial beamwidths, and absorption.

The analysis demonstrates that HPBW's of the order of 1 cm result in a significantly lesser error than more highly focused beams. A wider HPBW has the advantage that the time derivative of the temperature can be evaluated at times longer than 0.5 s, e.g., 1.0 or 1.5 s, for an error due to heat conduction less than 5% in most practical cases. The contribution of the thermocouple related viscous heating to the temperature derivative is then reduced, thereby improving the estimate of the absorption coefficient. The effect of absorption on the accuracy of the measurement was found to be important only when the actual depth of the thermocouple junction differed from the assumed position, and then was significant only for large absorption coefficients. The depth at which the thermocouple junction should be located, such that heat conduction at the water-tissue interface is negligible, was found to be a function of time. The critical depths at 0.5 and 1.5 s were found to be 1 and 1.75 mm, respectively.

The error in the TTM measurement increases as the frequency is increased because of the decrease in the HPBW of the acoustic beam for single, focused, radiating elements. Larger HPBW's at higher frequencies entail longer focal distances over which nonlinear distortions in the acoustic wave may result. It is possible to generate ultrasound beams with HPBW's of the order of 5 mm at frequencies from 3 to 7 MHz. Beam profiles with 5 mm HPBW's at 3, 5, and 7 MHz are shown in Appendix B. Measurements of the harmonic content of the wave with a hydrophone have shown that at 7 MHz an intensity of $1 \frac{W}{cm^2}$ can be generated with a second harmonic component that is greater than 10 dB below the fundamental. The error in the TTM measurement due to heat conduction can be kept under 10% for HPBW's greater

than 3 *mm*. However, for the narrow HPBWs typically encountered at higher frequencies and at high intensities, the PDM measurement can be expected to yield more accurate results than the TTM [141].

Linear wave propagation has been assumed in the analysis; however, it is possible to make extensions to include the error contributed by harmonic absorption in a nonlinear acoustic field to the measurement of the “linear” absorption coefficient at a given frequency [41]. Some medical ultrasound devices produce highly nonlinear acoustic fields as measured in water [61], [62], and some evidence for the production of nonlinear fields in tissue also exists [194]. A nonlinear absorption coefficient, which is a function of the shock parameter σ [20], [27], [53], [99], [149], [179], is then also important [41], [84], [96], [150]. The analysis presented in this chapter is applicable in such cases for estimating the error resulting from heat conduction and for providing guidelines for the experimental procedure. The only condition that must be met is that a Gaussian function, or sum of Gaussian functions, suffice to describe the heat source.

CHAPTER 5

ULTRASONIC ABSORPTION IN FETAL BONE

Although the values of the absorption coefficient for many tissues have been reported, including some attenuation values for bone [97], [98], [124], little is known about the acoustic absorption in fetal bone and its variation with fetal development. Thus good estimates of the temperature increase in the fetal bone and in the surrounding tissue during exposure to ultrasound cannot be made. The anisotropic, heterogeneous nature of bone is known to make the measurement of the elastic constants difficult [106], [118], [203], [204]. The measurement of attenuation and absorption in bone is likewise difficult. The absorption is likely to be a function of the type of wave as well as direction of propagation. Also, knowledge of acoustic intensity values at the site of temperature measurement needed to calculate the absorption is inadequate [64]. Calculation of absorption from the temperature-increase data also requires knowledge of the heat capacity C_p [64], at the site of interest, which is not available for fetal bone.

In this chapter, acoustic wave propagation in anisotropic elastic solids is reviewed and difficulties in measuring the elastic constants and attenuation and absorption in solid materials are enumerated. In the absence of detailed knowledge of absorption in fetal bone, as a function of the type of wave and propagation direction, the measurable temperature increase resulting from exposure of the specimen to ultrasound becomes the useful quantity for assessing thermal effects. The temperature increase in human fetal femurs exposed, *in vitro*, to 1 MHz, continuous-wave (CW) ultrasound is presented. The transient thermoelectric method, originally developed for measuring the absorption coefficient in soft tissues and

liquids is employed to measure the temperature increase [86] [87]. The specimens studied represent the range of gestational ages from 59–108 *days*. The temperature increase measured over an extended period of time, as well as the time derivative of the temperature at 0.2 *s* following the initiation of a unit step acoustic exposure are presented. The time necessary for the temperature to increase by 1°C is considered a useful parameter and is presented for described exposure conditions [6]. Estimates of the error in the temperature measurement associated with the method of insertion of the thermocouple are also given.

5.1 Acoustic Waves in Solids

The necessary equations to describe the elastodynamic state of a body are Newton's law (the force equation), a description of the deformation of the body, and a constitutive relation. Newton's law may be written for a volume element V , bounded by a surface S , in the linear theory as [3]

$$\int_S \bar{\mathbf{t}} dS + \int_V \rho \bar{\mathbf{f}} dV = \int_V \rho \frac{\partial^2 \bar{\mathbf{u}}}{\partial t^2} \quad (5.1)$$

The general nonlinear statement of Eq. (5.1) must have $\frac{\partial}{\partial t}$ replaced by the total differential $\frac{D}{Dt}$. The vector $\bar{\mathbf{t}}$ represents a distribution of surface traction forces over S , $\bar{\mathbf{f}}$ is the body force per unit mass to which the volume element is subjected, and $\bar{\mathbf{u}}$ is the element displacement vector. The Cauchy stress formula can be used to relate the traction force to the second rank stress tensor $\bar{\bar{\mathbf{T}}}$ [48]

$$t_i = T_{ij}n_j \quad (5.2)$$

where n_j is the unit normal to the surface in the j direction, and the Einstein summation convention is followed. Applying the divergence theorem to Eq. (5.1) results in the Cauchy equation of motion

$$\partial_j T_{ji} + \rho f_i = \rho \frac{\partial^2 u_i}{\partial t^2} \quad (5.3)$$

where ∂_j denotes partial differentiation with respect to the j spatial variable. The deformation of the body is described by the second rank strain tensor

$$S_{ij} = \frac{1}{2} (\partial_j u_i + \partial_i u_j) \quad (5.4)$$

An interchange of i and j leaves the right-hand side unchanged; hence, the strain tensor is symmetric. The final equation describing the elastodynamic state of a body is the constitutive equation relating the stress and strain, which for a Voight solid is given by [144]

$$T_{ij} = c_{ijkl} S_{kl} + \eta_{ijkl} \frac{\partial S_{kl}}{\partial t} \quad (5.5)$$

where c_{ijkl} and η_{ijkl} are the stiffness and viscosity tensors, respectively. Symmetry arguments can be invoked to reduce the 81 components of c_{ijkl} and η_{ijkl} to 21 independent components. An analogous development of the equations of motion can be given for liquids [165].

In the absence of body torques, it can be shown that the stress tensor $\bar{\bar{\mathbf{T}}}$ is symmetric. As a consequence of the symmetry of $\bar{\bar{\mathbf{T}}}$, $\bar{\bar{\mathbf{S}}}$, and $\bar{\bar{\mathbf{c}}}$, a reduced notation can be introduced and is given by Auld [8], [9]. The stress and strain tensors are then represented by a six-component vector, and the stiffness tensor can be represented by a 6×6 symmetric matrix. The three elastodynamic equations for a lossless medium then read [9]

$$\nabla \cdot \bar{\bar{\mathbf{T}}} + \rho \bar{\mathbf{f}} = \rho \frac{\partial^2 \bar{\mathbf{u}}}{\partial t^2} \quad (5.6)$$

$$\bar{\bar{\mathbf{S}}} = \frac{1}{2} \nabla_{,s} \bar{\mathbf{u}} \quad (5.7)$$

$$\bar{\bar{\mathbf{T}}} = \bar{\bar{\mathbf{c}}} : \bar{\bar{\mathbf{S}}} \quad (5.8)$$

The operators ∇ and $\nabla_{,s}$ are defined by Auld for Cartesian, cylindrical, and spherical coordinates [8], [9].

The boundary conditions for two solids that are in firm contact, i.e., no slippage at the interface, are given for the velocity and stress by

$$\begin{aligned} (\bar{\bar{\mathbf{T}}}_1 - \bar{\bar{\mathbf{T}}}_2) \cdot \hat{\mathbf{n}} &= 0 \\ \bar{\mathbf{v}}_1 - \bar{\mathbf{v}}_2 &= 0 \end{aligned} \quad (5.9)$$

The normal component of force, as well as the velocity, must be continuous across the interface. Equation (5.9) applies for a stationary boundary; however, in elastic wave propagation the boundary actually moves. This motion is neglected in the linearized theory.

The power flow for elastic waves can be derived in a manner similar to Poynting's theorem in electromagnetism as [9]

$$\bar{\mathbf{P}} \cdot \hat{\mathbf{n}} = -\bar{\mathbf{v}} \cdot \bar{\bar{\mathbf{T}}} \cdot \hat{\mathbf{n}} \quad (5.10)$$

and is the power flow density in the $\hat{\mathbf{n}}$ direction. The negative sign is a result of the sign convention used for the force exerted by Medium 1 on Medium 2, and the power flow is from Medium 1 to Medium 2.

The acoustic wave equation can be derived from Eqs. (5.3) – (5.5), or from Eqs. (5.6) – (5.8). Upon differentiating Eqs. (5.6) and (5.7) with respect to time, writing $\frac{d\bar{\mathbf{u}}}{dt} = \bar{\mathbf{v}}$, and

using the constitutive relation for a lossless medium, two coupled equations for velocity and strain result

$$\begin{aligned} \nabla \cdot \bar{\bar{c}} : \frac{\partial \bar{\bar{S}}}{\partial t} + \rho \frac{\partial \bar{f}}{\partial t} &= \rho \frac{\partial^2 \bar{v}}{\partial t^2} \\ \frac{\partial \bar{\bar{S}}}{\partial t} &= \nabla_s \bar{v} \end{aligned} \quad (5.11)$$

where the double dot product denoted by $:$ is given by Auld [9]. Eliminating $\bar{\bar{S}}$ from the two equations results in the wave equation for the velocity vector

$$\nabla \cdot \bar{\bar{c}} : \nabla_s \bar{v} - \rho \frac{\partial^2 \bar{v}}{\partial t^2} = -\rho \frac{\partial \bar{f}}{\partial t} \quad (5.12)$$

The complexity of wave propagation in anisotropic solids can be illustrated by investigating plane wave solutions. The dispersion relation for plane waves is found by making the substitution $\bar{v}(\bar{r}, t) = \bar{v} e^{j\omega t - jk\hat{l} \cdot \bar{r}}$ in Eq. (5.12), where the vector \hat{l} is given by $\hat{l} = l_x \hat{x} + l_y \hat{y} + l_z \hat{z}$ and k is the propagation constant. The resulting equation for the velocity vector is

$$\left[\frac{k^2}{\omega^2} \Gamma_{ij} - \delta_{ij} \rho \right] v_j = 0 \quad (5.13)$$

where

$$\Gamma_{ij} = \begin{bmatrix} \Gamma_{11} & \Gamma_{12} & \Gamma_{13} \\ \Gamma_{12} & \Gamma_{22} & \Gamma_{23} \\ \Gamma_{13} & \Gamma_{23} & \Gamma_{33} \end{bmatrix}$$

$$\begin{bmatrix} \Gamma_{11} \\ \Gamma_{22} \\ \Gamma_{33} \\ \Gamma_{12} \\ \Gamma_{13} \\ \Gamma_{23} \end{bmatrix} = \begin{bmatrix} c_{11} & c_{66} & c_{55} & 2c_{56} & 2c_{15} & 2c_{16} \\ c_{66} & c_{22} & c_{44} & 2c_{24} & 2c_{46} & 2c_{26} \\ c_{55} & c_{44} & c_{33} & 2c_{34} & 2c_{35} & 2c_{45} \\ c_{16} & c_{26} & c_{45} & c_{46} + c_{25} & c_{14} + c_{56} & c_{12} + c_{66} \\ c_{15} & c_{46} & c_{35} & c_{45} + c_{36} & c_{13} + c_{55} & c_{14} + c_{56} \\ c_{56} & c_{24} & c_{34} & c_{44} + c_{23} & c_{36} + c_{45} & c_{25} + c_{46} \end{bmatrix} \begin{bmatrix} l_x^2 \\ l_y^2 \\ l_z^2 \\ l_y l_x \\ l_x l_y \\ l_x l_y \end{bmatrix}$$

and δ_{ij} is the Kronecker delta. The nontrivial solution to Eq. (5.13) must have

$$\left| \frac{k^2}{\omega^2} \Gamma_{ij} - \delta_{ij} \rho \right| = 0 \quad (5.14)$$

which is the dispersion relation. Equation (5.13) is commonly referred to in the literature as Christoffel's equation, and Γ_{ij} as the Christoffel matrix. However, Green first worked on the theory of plane wave propagation in anisotropic media in 1839 while pursuing the mechanical theory of light.

The dispersion relation, Eq. (5.14), results in a third-order polynomial in $(\frac{k}{\omega})^2$. The positive and negative roots of the three solutions correspond to positive- and negative-going plane waves of three different types. Because the Christoffel matrix is Hermitian, the eigenvalues $(\frac{k}{\omega})^2$ are real. For all but the most simple cases, the solutions of Eq. (5.14) must be obtained numerically. Once the eigenvalues are obtained, the corresponding eigenvectors can be found from Eq. (5.13), which, in general, also requires a numerical solution. Equation (5.14) defines a surface in k -space at a fixed frequency that gives $\frac{k}{\omega}$ as a function of its direction $\bar{\mathbf{I}}$. This surface is referred to as the slowness surface because $\frac{k}{\omega} = \frac{1}{v_p}$ is the inverse of the phase velocity. Several examples of the slowness surface for a number of crystal types and crystal planes are given by Auld [9].

In general, the particle velocity vector will be neither orthogonal nor parallel to the propagation vector for plane wave propagation. Thus, except for isotropic crystals, there are no pure shear or pure longitudinal modes of propagation for an arbitrary direction. It should be noted that shear and longitudinal modes are entirely plane wave concepts and are not applicable to other types of waves, *viz.*, cylindrical and spherical. There are, however, particular directions and planes in an anisotropic crystal in which a pure longitudinal or shear wave will propagate. For example, a pure longitudinal mode can propagate if [29]

$$\bar{\mathbf{v}} \times \bar{\mathbf{l}} = 0 \quad (5.15)$$

i.e.,

$$l_y v_z - l_z v_y = 0$$

$$l_x v_z - l_z v_x = 0$$

$$l_x v_y - l_y v_x = 0$$

Equation (5.15) represents only two independent equations. A third independent equation can be found by noting that Eq. (5.13) can be written as

$$\left[\frac{k^2}{\omega^2} \Gamma_{ij} - \delta_{ij} \rho \right] \frac{v_j}{|\bar{\mathbf{v}}|} = 0 \quad (5.16)$$

where the v_{ij} are the direction cosines of the velocity vector. Since $\bar{\mathbf{v}}$ and $\bar{\mathbf{l}}$ are parallel in the directions for which a pure longitudinal mode can exist

$$\left[\frac{k^2}{\omega^2} \Gamma_{ij} - \delta_{ij} \rho \right] l_j = 0 \quad (5.17)$$

The v_i in Eq. (5.15) can then be replaced by the l_i . Upon using Eq. (5.15) with Eq. (5.17), three equations for the pure longitudinal mode directions, given by l_x , l_y , and l_z in terms of

the elastic constants of the medium, result. The polarization vectors and phase velocities for pure mode directions have been derived in terms of the elastic stiffness constants for several different crystal types [9], [29], [33], [47].

A dynamic method for determining the elastic stiffness constants of a material is to measure the velocity in several directions in the bulk material [203], [204]. The propagation velocity is measured using plane wave techniques along a known direction in the crystal and then related to the constants of the elastic stiffness tensor. The number of independent constants of the stiffness tensor fixes the number of independent measurements that are necessary. Another method that has been used in the 100 *MHz* to 1 *GHz* frequency range, to determine the elastic stiffness constants of solid materials, is the line focus beam acoustic microscope [121], [122]. This method has also been used to acoustically characterize dental material [123].

The attenuation of the acoustic wave as it propagates through the solid is an important consideration. Numerous experimental and theoretical studies of attenuation in both crystalline and polycrystalline materials appear in the literature [13], [108], [157]. The constitutive relation given by Eq. (5.5), which includes viscous damping effects, applies to a Voigt solid and is valid only if the frequency of the acoustic wave is well below that of any relaxation frequencies in the material; the acoustic loss per wavelength in the material is therefore small. The two processes involved in viscous damping are the thermoelastic and the Akhieser mechanisms. Thermoelastic attenuation is the result of irreversible heat flow from compressed regions to rarefacted regions and occurs only for longitudinal waves since shear motions produce deformations of unit volume elements and not size changes. Akhieser damping results from interactions between the equilibrium phonon distribution in the ma-

terial and the passing, coherent acoustic wave. The attenuation that results from these mechanisms is proportional to the square of the frequency.

Typical experimental studies for determining the viscoelastic portion of the complex stiffness matrix involve measurement of attenuation via insertion loss or optical measurement in the solid for well-characterized modes and direction of propagation. A theoretical analysis then enables the viscosity tensor to be determined. For example, the viscosity tensor has been determined for lithium niobate, which has six independent constants, from twelve different measurements (six independent) of attenuation [13]. A perturbation formula for the propagation vector for uniform plane wave fields then allows the viscosity tensor to be determined from the attenuation measurements [8]. It should be noted that the modes and directions of propagation in this study were well-known and this knowledge is inherently necessary for designing the experimental procedure and determining the viscosity tensor. The results showed the attenuation of lithium niobate to fit a square law behavior to within the experimental accuracy of the measurements.

Other types of attenuation, which are not a viscous effect, occur in solids with a resulting variety of attenuation versus frequency behaviors [21], [107], [144]. In these cases the simple constitutive relation of Eq. (5.5) is not sufficient to describe the loss properties of the material. This may be the case for attenuation and absorption in bone. Not only is little known of acoustic wave propagation in bone, it is possible that it does not behave as a Voigt solid since the attenuation measurements that have been reported in the literature show it to be highly attenuating [97], [98]. The result is that the constitutive relation of Eq. (5.5) may not be adequate for describing the loss properties of bone, and the methods for characterizing the loss in a Voigt solid are not applicable.

Previous studies have shown that cortical bone is anisotropic and piezoelectric with pseudohexagonal crystalline properties [117], [118], [125], [203], [204], [205]. In these studies the six independent coefficients of the elastic stiffness tensor were determined from sonic velocity measurements with specified orientations to the long bone axis of human and bovine femurs. Plane wave techniques were used, and a knowledge of the crystalline structure of the bone was presumed. The dispersion of the ultrasonic velocity in a human femur has also been studied using these techniques [206]. Disagreement, however, over the precise anisotropy of bone and the applicability of the above techniques used to determine the elastic stiffness coefficients remains [128], [129]. Other studies have reported ultrasound measurements of the elastic modulus in trabecular bone [7] and the distribution of ultrasound velocities over a human tibia [114]. The anisotropic nature of dental tissues has also been studied using critical angle reflection techniques [130]. It has been shown, however, that a critical angle reflection technique does not generally allow for the determination of the elastic constants because pure mode propagation must be assumed [106]. It has been shown above that this is the case only for certain directions of propagation in the crystal.

Attenuation studies based on insertion loss measurements in bone have also been reported in the literature [83], [89], [124], and a compilation of these studies is given by Goss et al. [97], [98]. Approximate values of attenuation for the "longitudinal" and "shear" waves in cortical bone are $4 \frac{dB}{cm-MHz}$ and $7.5 \frac{dB}{cm-MHz}$, respectively [89]. However, none of the experimental studies of attenuation reported to date have properly taken into account the different modes of propagation in an anisotropic crystal. The attenuation can be expected to be a function of the direction as well as of the mode of propagation [13].

It is clear that the anisotropic and inhomogeneous nature of bone makes the determination of the elastic and loss properties of the tissue difficult. All previous studies have been performed in adult bone where samples are of sufficient size to apply plane wave measurement techniques in the low megahertz frequency range used in medical ultrasound. These specimens can be cut and machined to obtain planar faces at specified orientations to the crystallographic axes. The problem is more complex for fetal bone because of the size and shape. The diameter of the human fetal femur is approximately 0.5–4.0 *mm* for gestational ages of 60–150 *days*. Fetal bone is not only too small to cut and machine, but also too soft. Thus, determining the elastic and loss properties of fetal bone in a manner as might be obtained in adult bone may not be possible.

Finally, determining the heat deposition in the bone resulting from power loss from the acoustic wave requires a knowledge of the acoustic velocity \bar{v} and the stress tensor $\bar{\mathbf{T}}$ in the material. The equivalent heat source is then given by the negative of the divergence of the real power flow [45], i.e.,

$$q_v(\bar{\mathbf{r}}) = -\frac{1}{2} \nabla \cdot \Re e [\bar{\mathbf{v}} \cdot \bar{\mathbf{T}}] \quad (5.18)$$

The scattering of an incident ultrasonic wave from a fluid to an anisotropic cylinder is a formidable problem. Solutions for scattering of plane and cylindrical waves incident from a fluid on a fluid cylinder appear in the literature [44], [73], [140], [148], [191]. Studies of the scattering of plane and cylindrical waves incident from a fluid on an isotropic elastic cylinder have also been reported [72], [78], [79], [126], [136], [192], [193]. Studies of both plane wave scattering from an elastic halfspace and from an elastic cylinder that include attenuation in the elastic medium have been reported as well [51], [78]. However, no solutions for scattering

of plane or cylindrical waves incident on a lossless or absorbing anisotropic elastic cylinder are known.

Thus, not only are the elastic stiffness and loss properties of fetal bone as a function of gestational age unknown, so too are the solutions to the particular scattering problem. Hence, the heating in the fetal bone resulting from ultrasound exposure cannot presently be determined by computation. The equivalent heat source, which results from ultrasonic absorption, is thus unavailable by indirect methods for studies of heat transfer in the bone and the surrounding tissue. The temperature elevation resulting from ultrasonic exposure in the fetal bone, however, can be measured directly. In Section 5.4, the measured temperature increase in human fetal femurs irradiated *in vitro* with unfocused ultrasound at 1 *MHz* is presented. Measurements of the temperature elevation in the skulls of mice irradiated with focused ultrasound at 3.6 *MHz* have also recently been reported [38].

5.2 Methods

The fetal femur specimens are obtained from the Central Laboratory for Human Embryology, University of Washington, Seattle, WA. The specimens are frozen and packed in dry ice, shipped via overnight mail, and stored at $-70^{\circ}F$ prior to the measurement procedures. The fetal femurs are exposed to 1 *MHz*, *CW* ultrasound, and the transient thermoelectric method is employed to obtain the thermal history [64]. All soft tissue attached to the bone is removed. A constantan–chromel thermocouple junction of diameter 25 to 40 μm , lap soldered to yield an axial dimension of approximately 300 μm , is the temperature sensor. The thermocouple is positioned midway along the length of the femur in the diaphysis with the aid of a 30 *gauge* hypodermic needle, o.d. 0.31 *mm*. The needle is readily inserted by

pushing for the earlier gestational age specimens (59-78 days), but it is necessary to drill a hole with a # 80 drill bit (0.33 mm diameter) to enable insertion in the harder bone of later gestational age specimens. The thermocouple junction is positioned in the specimen with the aid of a dissecting microscope. The specimen, with the junction in position, is then submerged in physiological Hank's solution to allow fluid to fill the space created by the insertion process. The specimen is held in a special supporting device, which does not interfere with the incident ultrasound field, and is potted in 3 % Bacto-agar (Difco Laboratories). The agar is heated and dissolved at 78 °C and is poured as a liquid into the supporting device with the specimen in place at 38 °C to 40 °C. The liquid solidifies at 35 °C, and remains solid at 37 °C, the temperature of the bath in which the measurements are conducted. The agar has negligible acoustic absorption and a sound speed nearly that of water [34]. The agar potting minimizes the removal of heat by convection to the ultrasound transmission fluid. The dimensions of the agar potting are 3 × 5 × 8 cm, with the 5 × 8 cm plane lying in the plane of the *xy* axis, and normal to the direction of the incident ultrasonic field, as shown in Figure 5.1. The femur cross section is approximately elliptical, and the specimen is oriented with the major axis parallel to the direction of the incident field.

The supporting device, containing the potted specimen, is positioned in a gently stirred bath of degassed mammalian Ringer's solution maintained at 37 °C during the measurement procedures. The specimen is irradiated with ultrasound and the change in the thermal emf, developed by virtue of the temperature increase at the thermocouple junction relative to the "cold junctions" outside the acoustic beam, is amplified, digitized, and stored for later analysis. A schematic representation of the preparation and measurement procedure is shown in Figure 5.1. The acoustic beam is centered on the thermocouple junction in the

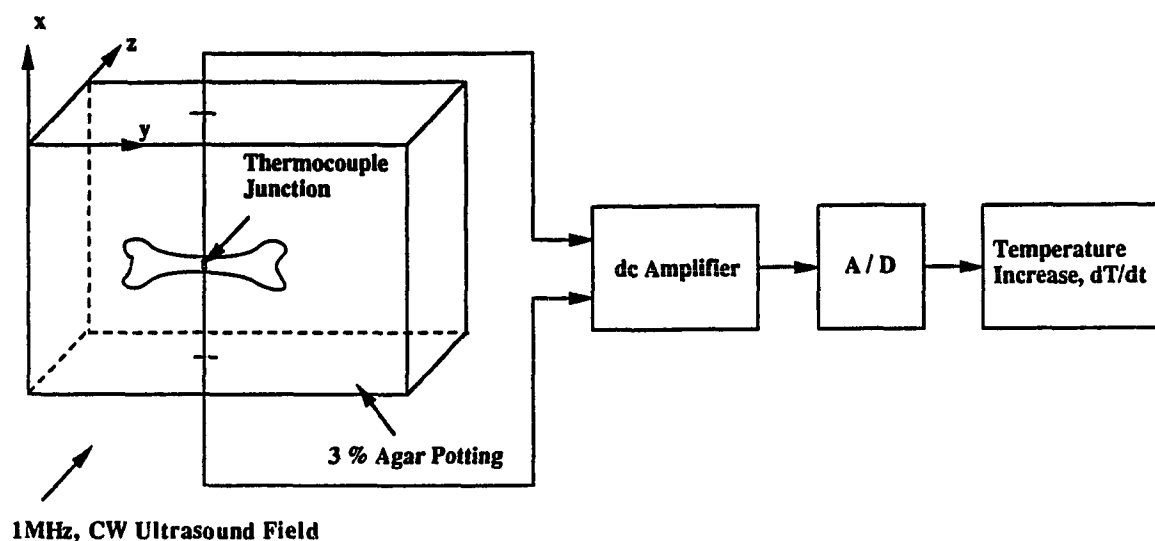


Figure 5.1: Schematic representation of the experimental procedure.

bone specimen by irradiating the specimen with short ultrasound pulses, typically 200 msec, and observing the resulting temperature spike. The beam is then stepped across the bone specimen. The beam is axisymmetric so that plotting along the x and y directions only is necessary (see Figure 5.1). A typical beam plot is shown in Figure 5.2. An example of the measured temperature increase versus time trace is shown in Figure 5.3. The reference temperature, which is assumed to be the temperature of the bath, i.e., 37 °C, is established by sampling the thermal emf prior to the initiation of the ultrasound exposure. The ultrasound is then turned on while sampling of the thermal emf continues. A short cooling period is also sampled, after the ultrasound exposure has been terminated.

The exposure intensities are determined in the free field in degassed mammalian Ringer's solution with a thermoelectric probe that is calibrated against a steel sphere radiometer as

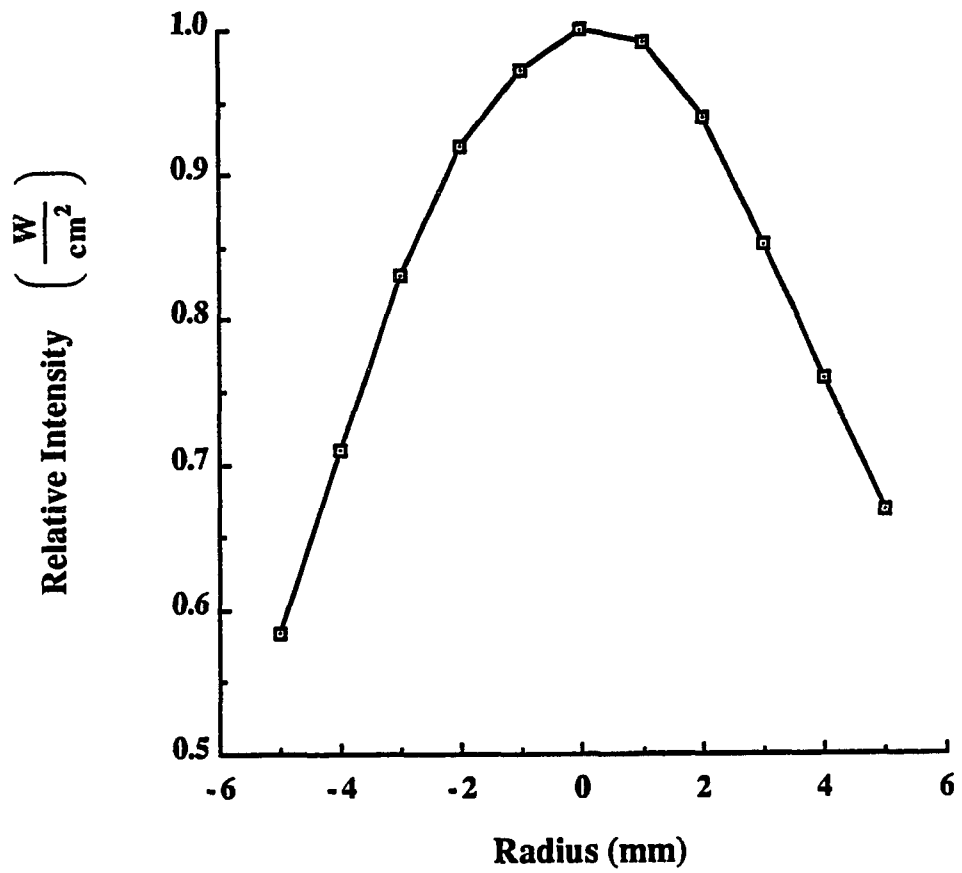


Figure 5.2: Ultrasound beam profile in a 78 *day* femur along the *y* direction (see Figure 5.1) plotted with an implanted thermocouple.

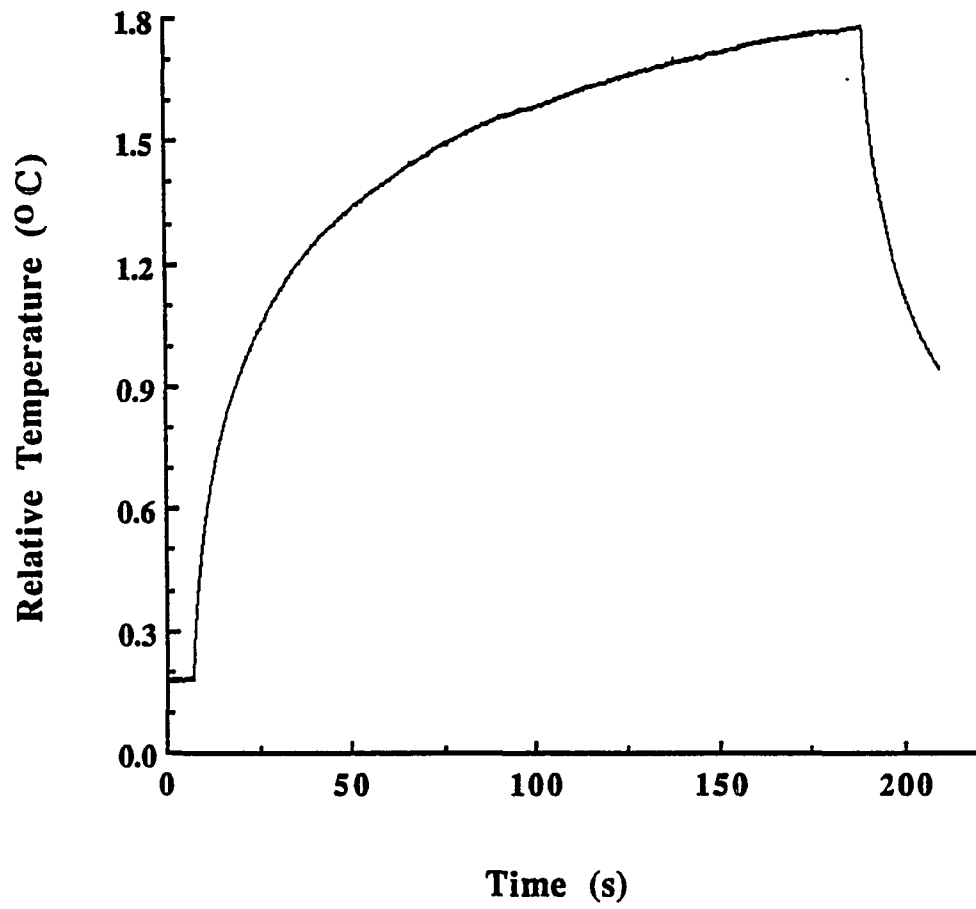


Figure 5.3: Measured temperature increase versus time for a 91 *day* specimen irradiated at $0.5 \frac{W}{cm^2}$.

discussed in Chapter 2 [63]. The specimens are irradiated with *CW* ultrasound at the beam maximum; hence, the intensities given are spatial-peak, temporal-average (SPTA). However, it is easily shown that it is also the SPTA intensity that is important in assessing the temperature elevation upon exposure to the pulsed ultrasound fields typically encountered in clinical fetal imaging.

Although the temperature increase with time in the femur specimens does not follow precisely a simple exponential curve, this mathematical form will suffice for the present argument. Assume that the temperature increase as a function of time in the specimen for a *CW* (unit step) exposure is given by

$$T_{CW} = T_{\infty} \left(1 - e^{-\frac{t}{\tau}}\right) \quad (5.19)$$

where T_{∞} is the steady state temperature as $t \rightarrow \infty$, and τ is the time constant. The behavior of the assumed form as $t \rightarrow 0$ and as $t \rightarrow \infty$ is what would be measured. The thermal impulse response $T_{\delta}(t)$ is

$$\frac{dT_{CW}}{dt} = T_{\delta}(t) = \frac{T_{\infty}}{\tau} e^{-\frac{t}{\tau}} \quad (5.20)$$

Typical clinical imaging devices use a pulse of the order of $1 \mu s$ and pulse repetition frequencies (PRF) approximately $1 kHz$. Such a pulse train can be described by

$$F(t) = \sum_{n=0}^{\infty} u(t - nt_{PRF}) - u(t - nt_{PRF} - t_{PW}) \quad (5.21)$$

where t_{PW} is the pulse width in seconds, and t_{PRF} is the reciprocal of the PRF. Although the sum in Eq. (5.21) extends to infinity when the ultrasound will clearly be turned off, it is unimportant because the time integration would extend only over the period of the exposure if the time dependence given by Eq. (5.21) were put in the solution for the temperature

increase given by Eq. (4.10). A significant simplification for the temperature elevation then results by using Eq. (5.21) to describe the ultrasound pulse train. Proceeding with the standard linear systems theory development, the temperature elevation resulting from the pulsed ultrasound field is

$$T_p(t) = \left(\frac{dT_{cw}}{dt} \right) * F(t) = T_s(t) * F(t) \quad (5.22)$$

where the asterisk denotes the convolution operation. An analytical form for $T_p(t)$ is most easily obtained through the use of the Laplace transform. The convolution becomes a multiplication in the transform domain, and $\tilde{T}_p(s) = \tilde{T}_s(s) \tilde{F}(s)$, where the tilde denotes the Laplace transform of the function, and s is the transform variable. The Laplace transform of a periodic function is given by [176]

$$\tilde{F}(s) = \frac{1}{1 - e^{-Ps}} \tilde{F}_1(s) \quad (5.23)$$

where P is the period, in this case t_{PRF} , and $\tilde{F}_1(s)$ is the transform of a single period of Eq. (5.21)

$$\tilde{F}_1(s) = \frac{1}{s} \frac{1 - e^{-st_{PW}}}{1 - e^{-st_{PRF}}} \quad (5.24)$$

The Laplace transform of the temperature increase resulting from the pulsed exposure is

$$\tilde{T}_p(s) = \frac{T_\infty}{\tau} \frac{1}{s + \frac{1}{\tau}} \frac{1}{s} \frac{1 - e^{-st_{PW}}}{1 - e^{-st_{PRF}}} \quad (5.25)$$

The inverse transform of Eq. (5.25) can be obtained from the inversion integral and residue theorem as [50]

$$T_p(t) = T_\infty \left(\frac{t_{PW}}{t_{PRF}} - \frac{1 - e^{-\frac{t_{PW}}{\tau}}}{1 - e^{-\frac{t_{PRF}}{\tau}}} e^{-\frac{t}{\tau}} \right) \quad (5.26)$$

The pulse width t_{PW} and pulse repetition period t_{PRF} are several orders of magnitude greater than the thermal response time constant τ , even for very small specimens and/or beam sizes; hence,

$$\frac{1 - e^{-\frac{t_{PW}}{\tau}}}{1 - e^{-\frac{t_{PRF}}{\tau}}} \approx \frac{t_{PW}}{t_{PRF}} = t_{PW} \times PRF \quad (5.27)$$

The temperature elevation is then

$$T_p(t) \approx T_\infty \times t_{PW} \times PRF (1 - e^{-\frac{t}{\tau}}) \quad (5.28)$$

It is necessary to relate T_∞ to the time-average heat source $\langle q'_v \rangle$, where the brackets denote the time average. In the case of an exposure in a relaxing medium with zero shear viscosity, $\langle q'_v \rangle = \frac{\alpha p_0^2}{\rho c_0}$, where α is the absorption coefficient, p_0 is the pressure amplitude, ρ is the density, and c_0 is the infinitesimal amplitude speed of sound [43], [153]. Then

$$T_\infty = \frac{\langle q'_v \rangle}{\rho C_p} \phi = \frac{\alpha}{\rho C_p} \frac{p_0^2}{\rho c_0} \phi \quad (5.29)$$

where ϕ (s) is a unit strength quantity to give T_∞ the correct dimensions. This quantity is necessary because of the mathematical form assumed in Eq. (5.19) for the temperature increase

$$T(\bar{r}_0, t) = \frac{q_{v0}}{\rho C_p} t \int_0^1 d\xi F(t - t\xi) \int_V d\bar{r}' f(\bar{r}') G(\bar{r}_0 - \bar{r}', t\xi) \approx T_\infty (1 - e^{-\frac{t}{\tau}}) \quad (5.30)$$

For plane waves, the square of the pressure divided by ρc_0 integrated over the period of the waveform is the temporal average intensity [16], [42]. The period for a *CW* exposure is simply the reciprocal of the frequency, and $\frac{p_0^2}{2\rho c_0} = I_{SPTA}$. The temperature increase for a *CW* exposure would then be

$$T_{CW} = \frac{2\alpha}{\rho C_p} \phi I_{SPTA} (1 - e^{-\frac{t}{\tau}}) \quad (5.31)$$

The time average is taken over the length of one pulse for a pulsed exposure when determining the equivalent heat source $\langle q'_v \rangle$ and is the spatial-peak, pulse-average (SPPA) intensity. The temperature increase resulting from the pulsed ultrasound exposure is then

$$T_p = \frac{2\alpha}{\rho C_p} \phi \times I_{SPPA} \times t_{PW} \times PRF (1 - e^{-\frac{t}{\tau}}) \quad (5.32)$$

The product $I_{SPPA} \times t_{PW} \times PRF$ is defined for medical ultrasound fields as I_{SPTA} [100]. Upon substituting this into Eq. (5.32), the temperature elevation resulting from a pulsed exposure would then be the same as that measured for a *CW* exposure for the identical I_{SPTA} . The sphere radiometer has been used as a calibration for the I_{SPTA} of pulsed ultrasound fields [40], [84]. The time constant of the deflection of the suspended sphere is orders of magnitude greater than the ultrasound pulse width t_{PW} and the reciprocal of the PRF t_{PRF} . The above mathematical development can be used to justify this calibration procedure as well.

Three implicit assumptions were made above which deserve further discussion. First, the simple exponential rise assumed for the temperature increase upon exposure to *CW* ultrasound can be improved to include other exponential terms, e.g.,

$$T(t) = T_\infty \left(\sum_{n=1}^{\infty} a_n e^{-\frac{t}{\tau_n}} \right) \quad (5.33)$$

The pulsed response would then be

$$T_p = T_\infty \times t_{PW} \times PRF \sum_{n=1}^{\infty} a_n (1 - e^{-\frac{t}{\tau_n}}) \quad (5.34)$$

where only those time constants τ_n for all $\frac{t_{PW}}{\tau_n}, \frac{t_{PRF}}{\tau_n} \ll 1$ are included in the above summation. Equation (5.34) is then the same result as Eq. (5.32) as far as the temperature elevation at a particular I_{SPTA} for a pulsed ultrasound field is concerned. It has also been assumed that the absorption coefficient given in Eq. (5.29) is the same for diagnostic ultrasound as that for

a *CW* ultrasound field. This is not always the case. It is well-documented that some medical diagnostic instruments produce a highly nonlinear acoustic field at the focus [62], [161], [194] and that the absorption in such fields can be significantly greater than that in a "linear" acoustic field of the same intensity but with insignificant harmonic development [37], [41], [53], [84], [96]. This consideration cannot be neglected when interpreting the results of the next section. Finally, Eq. (5.29) applies to absorption in soft tissue, i.e., a fluid medium, since a medium with zero shear viscosity must be assumed to deduce Eq. (5.29) for $\langle q_v \rangle$. It will be seen from the results in the next section that the temperature increase in fetal bone upon exposure to ultrasound is linearly related to the incident intensity as determined in the free field. Hence, the above results should apply to bone as well, *viz.*, that the temperature increase is proportional to I_{SPTA} independent of the type of exposure, i.e., *CW* or pulsed.

5.3 Estimation of the Error in the Temperature Increase Measurements

The implantation of the thermocouple in the bone requires that a hole be introduced to allow for insertion of the hypodermic needle and "threading" of the thermocouple wire through the bone. The hole that results from this process is approximately 0.3 *mm* in diameter. In the case of soft tissue it is presumed that the tissue relaxes back around the thermocouple wire and junction, but the tissue is actually removed from the bone by the insertion process. The hole that remains is filled with very low absorbing physiological Hank's solution. Hence, a portion of the heat source, i.e., the highly absorbing bone, is removed from the source region. The removal of part of the heat source will result in a lesser measured temperature upon exposure of the specimen to ultrasound than if no hole had been introduced in the bone. The resulting difference between the temperature that is measured

and the temperature that would result if no hole were present can be expected to be small for the later gestational ages, for which the diameter of the bone is approximately ten times that of the hole. However, the diameter of the bone is roughly two or three times that of the hole in the earlier gestational ages, and a significant error resulting from the removal of highly absorbing tissue might be expected. An error in the rate of temperature increase is also expected for the earlier and later gestational ages. It is necessary, for interpreting the results of the measurements, to obtain a reasonable approximation of these errors.

An approximation to the error introduced in the measurement by the insertion of the thermocouple is obtained in a manner similar to that used in Chapter 4 for determining the error due to heat conduction resulting from finite beams and sample dimensions. The heat flow problem for fetal bone is more complex than that in soft tissue, because of the differing thermal diffusivity of the bone specimen and the surrounding 3% agar medium and water bath. A two- or three-dimensional finite element analysis would yield an accurate result for the error if the equivalent heat source, as well as the thermal diffusivity, are well known in the bone. However, the heat source function in the bone is likely to change with gestational age because of the changing ultrasound properties and dimensions, hence, a changing intensity distribution. Also the thermal diffusivity is expected to vary. The soft tissue value is approximately $\kappa = 1.5 \times 10^{-3} \frac{\text{cm}^2}{\text{s}}$ and the values for adult cortical and cancellous bones are $\kappa = 8.43 \times 10^{-3} \frac{\text{cm}^2}{\text{s}}$ and $\kappa = 2.81 \times 10^{-3} \frac{\text{cm}^2}{\text{s}}$, respectively [182]. Because the bone mineral content steadily increases into adolescence, the thermal diffusivity of fetal bone for gestational ages of 60–150 *days* is likely to be only a few times that of the soft tissue value, as opposed to five and one-half times greater as in the case of adult cortical bone. The results of the next section will show that these issues are not of serious concern

and that approximating the region as homogeneous is sufficient. A sufficient estimate of the error can be obtained by employing the infinite, homogeneous, isotropic medium Green's function previously used in Chapter 4 in the analysis.

An approximation for the difference in the temperature between the ideal case with no hole in the bone and the actual case can be obtained by integrating the product of the equivalent heat source resulting from absorption and the infinite, isotropic, and homogeneous medium Green's function over the entire source region and subtracting away the temperature increase resulting from an equivalent heat source over the hole. The temperature increase over the entire heating volume representing the bone specimen and the volume representing the hole are [36], [156]

$$T_0(\bar{r}, t) = Q_0 \int_0^t d\theta F(\theta) \int_{V_0} d\bar{r}' f(\bar{r}') G(\bar{r} - \bar{r}', t - \theta) \quad (5.35)$$

and

$$T_h(\bar{r}, t) = Q_0 \int_0^t d\theta F(\theta) \int_{V_h} d\bar{r}' f(\bar{r}') G(\bar{r} - \bar{r}', t - \theta) \quad (5.36)$$

where

$$G(\bar{r} - \bar{r}', t - \theta) = \frac{e^{-\frac{|\bar{r} - \bar{r}'|^2}{4\kappa(t - \theta)}}}{[4\pi\kappa(t - \theta)]^{\frac{3}{2}}}$$

and the 0 and h subscripts pertain to the entire volume and the hole source regions, respectively, and Q_0 is the rate of the temperature increase as $t \rightarrow 0$. The difference between the temperature increase for the case in which no hole is introduced T_0 and that where the source region has a hole, expressed as a percent of T_0 , is

$$\delta T = \frac{T_0 - (T_0 - T_h)}{T_0} \times 100\% = \frac{T_h}{T_0} \times 100\% \quad (5.37)$$

The percent difference in the derivative of the temperature increase is defined similarly as

$$\delta T' = \frac{\frac{\partial T_0}{\partial t} - \left(\frac{\partial T_0}{\partial t} - \frac{\partial T_h}{\partial t} \right)}{\frac{\partial T_0}{\partial t}} \times 100\% \quad (5.38)$$

If the heating due to ultrasonic absorption in the bone is modeled with a Gaussian shape as was done in Chapter 4 in soft tissue, and the source region given by the bone volume is approximated as a rectangular parallelepiped, the volume integral in Eq. (5.35) can be performed analytically resulting in

$$T_0(\bar{r}) = Q_0 e^{-2\alpha d} v(\bar{r}, t, \beta_r, \beta_z, \alpha) \quad (5.39)$$

where the source region boundaries are defined as in Section 4.1, and $v(\bar{r}, t, \beta_r, \beta_z, \alpha)$ is given by Eq. (4.15). The coordinate system used is shown in Figure 5.1. The volume integral over the cylindrical region defined by the hole in the bone can also be performed analytically for $r = \sqrt{y^2 + z^2} = 0$, and $x = 0$ as

$$\begin{aligned} T(0, 0, t) &= Q_0 t \int_0^1 d\xi \frac{1}{2\kappa t \xi} \int_0^{r_0} r' dr' e^{-\frac{r'^2}{4\kappa t \xi}} \int_{x_1}^{x_2} dx' \frac{e^{-\frac{x'^2}{4\kappa t \xi} - \frac{x'}{\beta_z}}}{\sqrt{4\pi\kappa t \xi}} \\ &= Q_0 t \int_0^1 d\xi \left[1 - e^{-\frac{r_0^2}{4\kappa t \xi}} \right] \\ &\quad \times \frac{1}{2} \left\{ \operatorname{erf} \left[\frac{x_2}{\sqrt{4\kappa t \xi}} \left(1 + \frac{4\kappa t \xi}{\beta_r} \right)^{\frac{1}{2}} \right] \right. \\ &\quad \left. - \operatorname{erf} \left[\frac{x_1}{\sqrt{4\kappa t \xi}} \left(1 + \frac{4\kappa t \xi}{\beta_r} \right)^{\frac{1}{2}} \right] \right\} \end{aligned} \quad (5.40)$$

where the change of variables $t\xi = t - \theta$ has been introduced. The remaining integrals for T_0 and T_h can then be evaluated numerically to determine δT and $\delta T'$.

Three cases were analyzed for different sizes of the source region V_0 , corresponding to the dimensions of the fetal femur specimens for 59, 89, and 108 *days* of gestation. The percent difference δT is shown as a function of time in Figure 5.4 for these three cases. The decay of the heat distribution in the source region was taken to be zero.

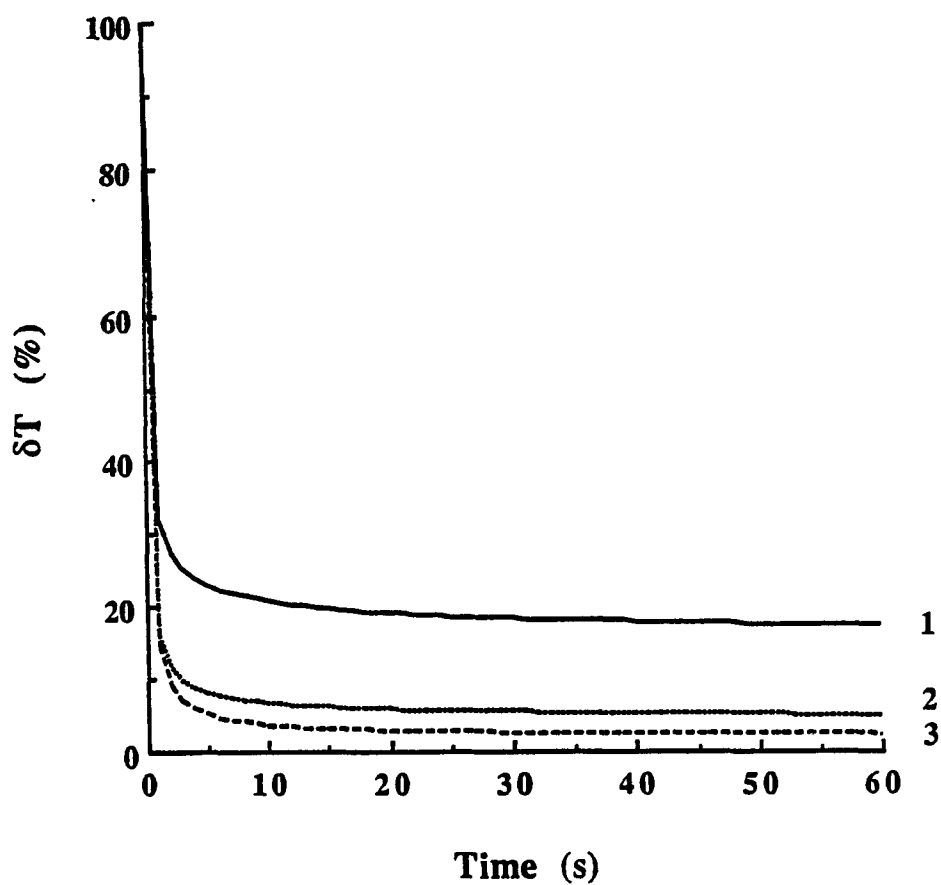


Figure 5.4: δT versus time for source region dimensions corresponding to the dimensions of fetal femur specimens of 59 (curve 1), 89 (curve 2), and 108 (curve 3) *days* (see Table 5.1 on page 127).

While δT is significant during the first two seconds, the asymptotic value is reached quickly thereafter. Although δT is 5% or less for the cases representing the 89 and 108 *day* specimens, it is 20% for the case representing the 59 *day* specimen. The size of this error or difference may initially seem significant; however, the temperature increase for the corresponding specimen is very small. The temperature elevation in the 59 *day* specimen upon exposure to 1 *MHz* ultrasound at a SPTA intensity of $1 \frac{W}{cm^2}$ is $0.10 \text{ }^\circ C$ after 20 *s*. Thus, even if δT were 100 %, i.e., $T_0 = 2(T_0 - T_h)$, the temperature elevation in the femur specimen resulting from ultrasonic exposure is less than $1 \text{ }^\circ C$, a normal diurnal variation in the body temperature of the mother.

The time rate of change of the temperature elevation is also considered to be important as shown in the Section 5.4. The percent difference between the derivative of the temperature elevation with the hole for the thermocouple present and the derivative of the temperature that would result with no hole in the source region is then also of interest. This difference, given by $\delta T'$, is shown in Figure 5.5.

It is necessary to evaluate the derivative before significant heat conduction takes place, as indicated in Appendix C, to obtain a reasonable estimate of the magnitude of the rate of temperature increase Q_0 . The time derivative of the temperature elevation is evaluated at 0.2 *s* for the measurements presented. The percent difference $\delta T'$ at 0.2 *s* is approximately 37% for the case representing the 59 *day* specimen and 31% for the cases representing the 89 and 108 *day* specimens. Although $\delta T'$ is significantly less at later times, e.g., 0.5 *s*, the measurements show that significant heat conduction occurs between 0.2 *s* and 0.5 *s*. For example, the time derivative of the temperature elevation per unit of exposure intensity of an 89 *day* specimen is $0.46 \frac{^\circ C}{s} \frac{cm^2}{W}$ and $0.36 \frac{^\circ C}{s} \frac{cm^2}{W}$ at 0.2 *s* and 0.5 *s*, respectively.

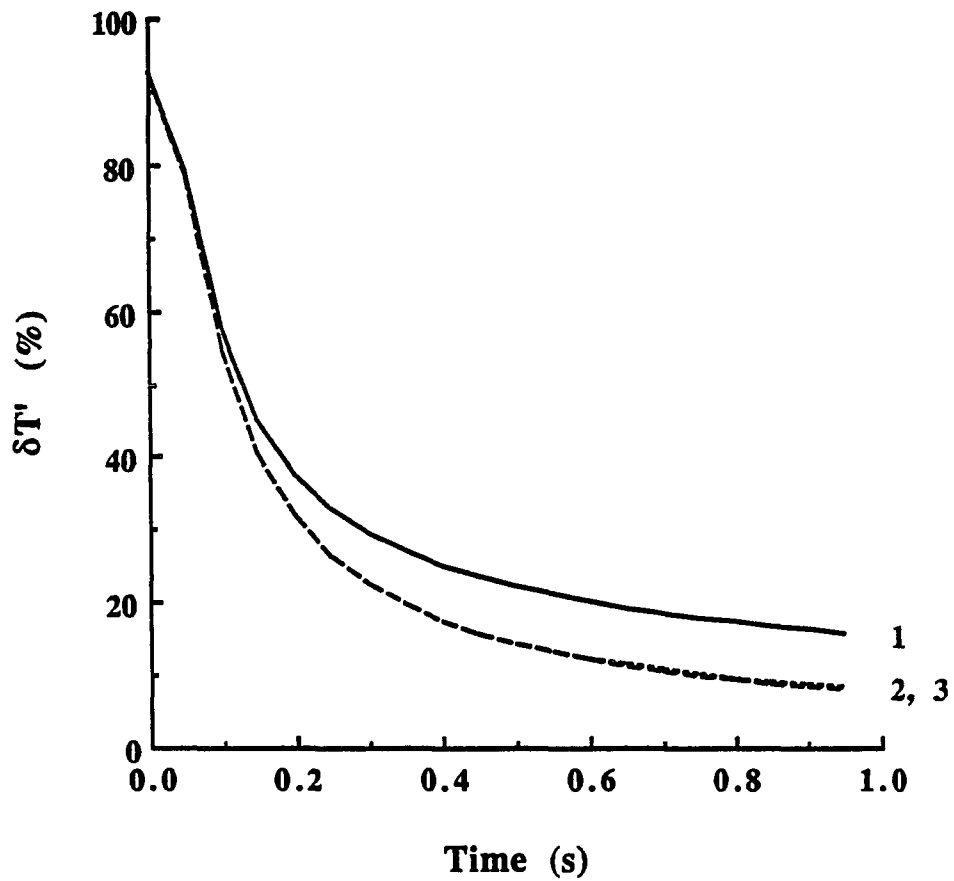


Figure 5.5: $\delta T'$ versus time for source region dimensions corresponding to the dimensions of fetal femur specimens of 59 (curve 1), 89 (curve 2), and 108 (curve 3) *days*.

The limit of $\delta T'$ as $t \rightarrow 0$ approaches 100% even though the curve in Figure 5.5 does not indicate this. The curve shown does not go to 100% as $t \rightarrow 0$ because the derivative is evaluated numerically from Eqs. (5.39) and (5.40), with a central difference at all but the endpoints [52]. A forward and backward difference is taken at the endpoints. Alternatively, the integral-differential relation between the impulse and unit step response can be employed as was done in Chapter 4 to avoid numerical integration and differentiation in order to obtain $\delta T'$. In this case $\frac{\partial T_h}{\partial t}$ and $\frac{\partial T_0}{\partial t}$ are simply the integrands of Eqs. (5.39) and (5.40) with $\xi = 1$. Then, upon taking the limit $t \rightarrow 0$, it is seen that $\delta T'$ is 100 %.

Figures 5.4 and 5.5 show the relative difference for δT and $\delta T'$ for the worst case of the thermocouple junction positioned at the center of the hole, i.e., $r = 0$. However, as a result of the method by which the specimen is prepared for the measurement, the thermocouple junction may be positioned next to the bone at the hole boundary. To avoid a double numerical integration in the analysis, the hole was approximated as having a square cross-section with sides equal to the hole diameter, and δT and $\delta T'$ were evaluated for the three cases under consideration. The results comparing δT and $\delta T'$ for the observation located at the center of the hole and at the hole periphery (square hole in both cases) are shown in Figures 5.6 and 5.7. The difference for both δT and $\delta T'$ is discernible only for the analysis representing the 59 *day* specimen, in which case, it is approximately a 5% change for both δT and $\delta T'$.

The results presented in this section assume the decay of the heat source function to be zero in computing T_0 . This corresponds to no attenuation of the intensity across the bone diameter. The temperature elevation measurements in the fetal bone irradiated with 1 *MHz* ultrasound show the center of the bone diameter to be approximately the maximum

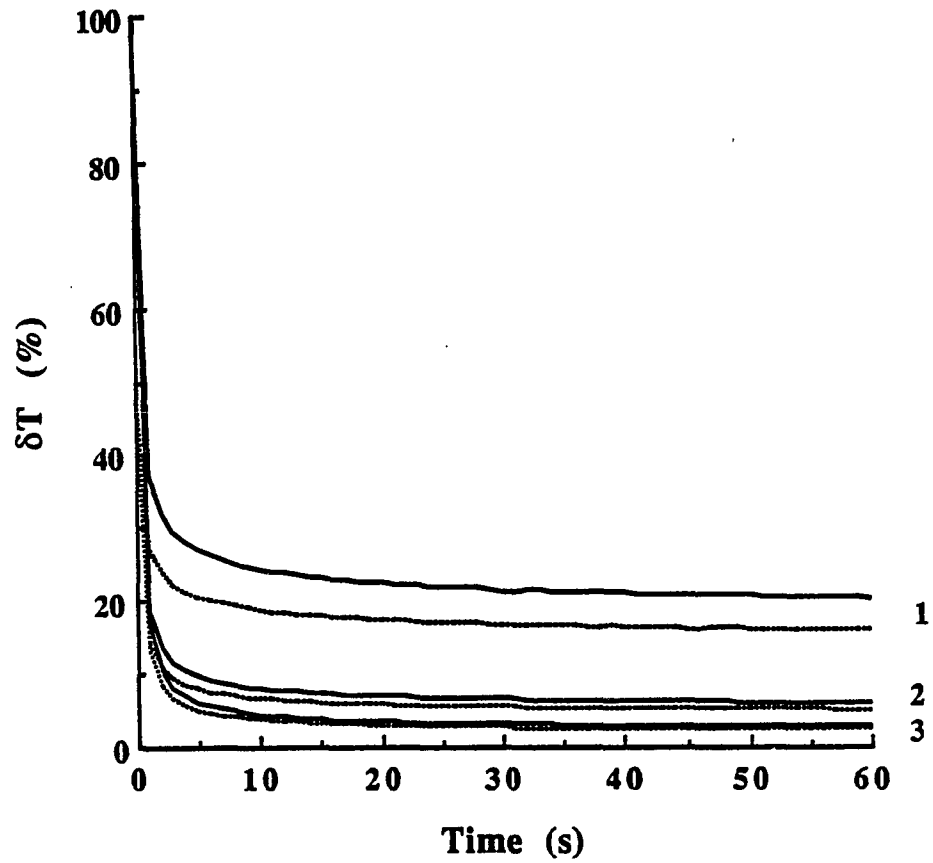


Figure 5.6: Comparison of δT versus time for the observation point at the hole center (solid lines) and at the hole/heat source boundary (dashed lines) for source region dimensions corresponding to the dimensions of fetal femur specimens of 59 (curve 1), 89 (curve 2), and 108 (curve 3) days.

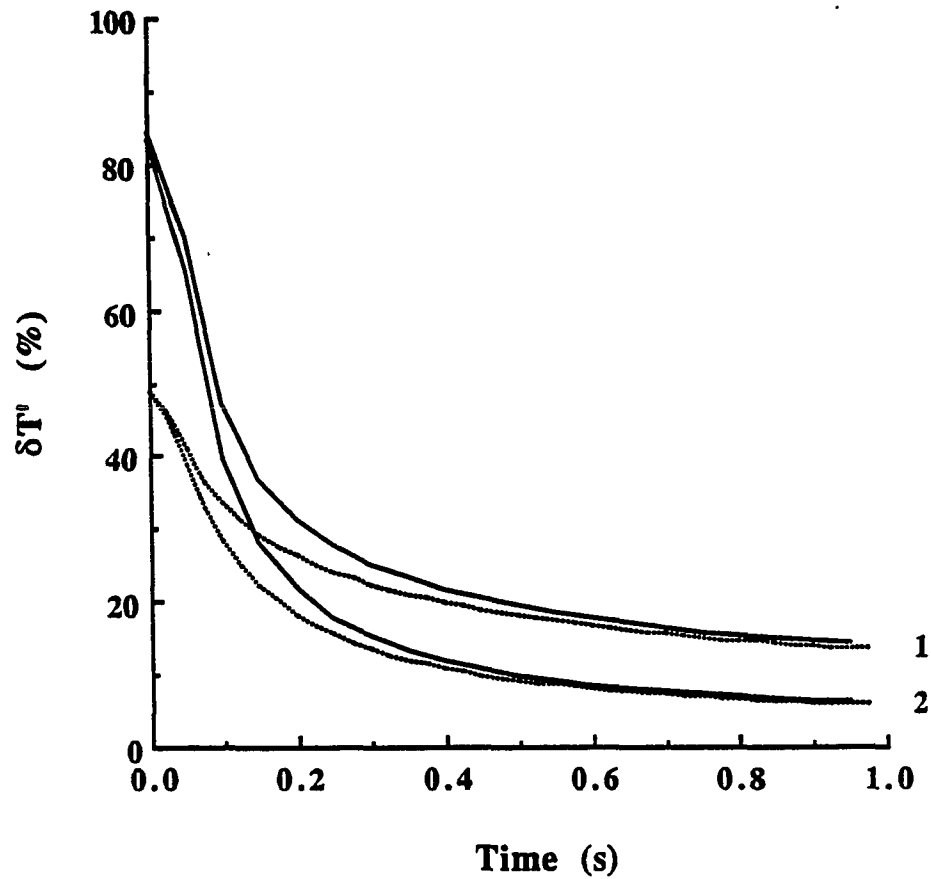


Figure 5.7: Comparison of $\delta T'$ versus time for the observation point at the hole center (solid lines) and at the hole/heat source boundary (dashed lines) for source region dimensions corresponding to the dimensions of fetal femur specimens of 59 (curve 1), 89 (curve 2), and 108 (curve 3) *days*.

of the heat source function. This is determined by evaluating the derivative of the measured temperature increase and verifying that heat flow is away from the point of the measurement. At higher frequencies the attenuation across the bone diameter is likely to be significant and should not be neglected.

5.4 Temperature Increase Measurements at 1 MHz

Two transducers were used to obtain the data presented in Table 5.1. The 59 and 89 *day* specimens were irradiated at the focal point of a 1 MHz, 5.08 cm aperture, focused PZT-4 transducer, with a radius of curvature of 15 cm and 3 and 6 dB beamwidths of 0.5 and 0.6 cm, respectively. All remaining specimens were irradiated with an unfocused, 1 MHz, 2.54 cm aperture, PZT-4 transducer with 3 and 6 dB beamwidths of 1 and 1.5 cm, respectively, at a distance of 93λ from the transducer face. The beam profiles for these transducers are shown in Appendix B. Because of the small diameter of the 59 *day* specimen, less than 1 mm, relative to the half-power beamwidth of the focused transducer, the difference between the temperature increase that would have been measured with the unfocused transducer and that measured with the focused transducer is negligible for the exposure time shown. To determine the difference in the temperature elevation upon exposure for the two transducers in the heating of the later gestational age specimens, the temperature increase was measured in an 83 *day* specimen irradiated first with the focused and then the unfocused transducer. The spatial peak, temporal average (SPTA) intensities were the same in both cases. It was found, for example, that the temperature increase resulting from irradiation with the focused transducer was 24 % less, after a 60 s irradiation, than that measured using the unfocused transducer.

Table 5.1: Temperature Elevation in Fetal Femurs Exposed *In Vitro* to 1 Megahertz CW Ultrasound ($^{\circ}C$)

Gestational age (days)	Irradiation time (s)	Diameter (± 0.5 mm)	Length (± 2 mm)	Intensity ($\frac{W}{cm^2}$)				
				0.1	0.5	1	5	10
				Temperature Elevation ($^{\circ}C$)				
59	20	0.5	11		0.05	0.10	0.48	0.96
67	20	0.75	15		0.13	0.27	1.60	3.35
	35			0.03	0.15	0.31	1.83	3.89
78	20	1.2	17	0.06	0.34	0.69	3.94	8.7
	35			0.07	0.39	0.79	4.6	10.2
	50			0.08	0.42	0.85	5.0	11.3
83	20	1.2	24		0.66	1.31	6.5	14.0
	35			0.78	1.53	7.6	16.3	
	50			0.86	1.68	8.3	17.8	
	60			0.90	1.74	8.7	18.4	
89	20	1.5	27		0.69	1.39	7.0	14.1
	35			0.78	1.55	7.9	15.6	
	50			0.82	1.64	8.4	16.8	
	60			0.84	1.69	8.6	17.2	
91	20	1.8	30		0.89	1.79	8.9	19.3
	35			1.07	2.14	10.6	23.0	
	50			1.19	2.39	11.8	25.4	
	60			1.26	2.54	12.4	26.6	
	180			1.59	3.19	15.3	32.6	
108	20	3.3	38	0.31	1.48	2.92	14.9	28.1
	35			0.38	1.75	3.49	18.3	35.0
	50				1.92	3.85	20.4	40.0
	60			0.41	2.01	4.00	21.3	43.1

Table 5.1 lists the temperature elevation measured in the specimens at specific exposure intensities, as well as the length and diameter of the various gestational age specimens studied. The femur cross-section is approximately elliptical and the dimension given for the diameter is the average of the major and minor axes. The error in the measured temperature is less than 3% as indicated in Section 2.3. The temperature increase was measured for two different 108 *day* gestational age specimens in order to assess the repeatability of the entire procedure, which yielded a difference in the temperature increase between the two specimens of approximately 6% for the range of times listed in Table 5.1.

The temperature increase of the 78 and 89 *day* specimens, irradiated with the unfocused and focused transducers, respectively, versus intensity is shown in Figure 5.8. It is apparent that the temperature increase is linear with exposure intensity for linear acoustic fields at the exposure site in the range of 0.1–10 $\frac{W}{cm^2}$. The deviation of the 5 and 10 $\frac{W}{cm^2}$ values for the 78 *day* specimen is a result of nonlinear acoustic propagation as explained below. Although the linearity of the temperature increase with intensity is expected, the result is fortuitous. The temperature increase can then be measured at any intensity, assuming a linear acoustic field, and scaled to the desired intensity. The same conclusion will hold for the temperature increase in a nonlinear field for a given harmonic development, i.e., shock parameter σ [20], [26], [27], [99], [149], [179]. Pressure amplitude measurements with a wideband hydrophone (NTR Systems, Inc.), with a 1–20 *MHz* bandwidth, in degassed mammalian Ringer's solution, showed the second harmonic component in the field of the unfocused transducer to be down 10 *dB* from the fundamental at an intensity of 10 $\frac{W}{cm^2}$, while the second harmonic was down 24 *dB* from the fundamental at 0.5 $\frac{W}{cm^2}$. The linearity of the temperature rise with intensity for the two specimens irradiated with the focused transducer, shown in Figure 5.8 for the

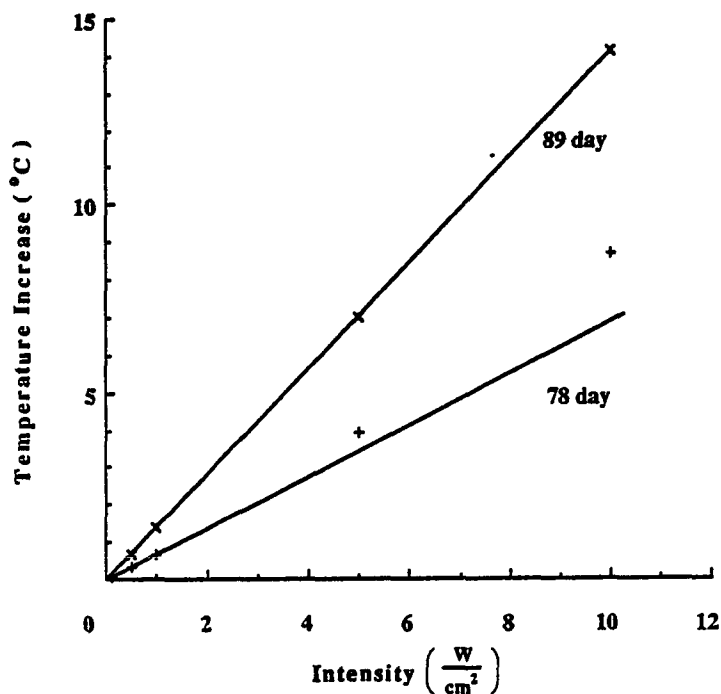


Figure 5.8: Temperature increase at 20 s following the initiation of the ultrasound exposure versus intensity for 78 and 89 *day* specimens

89 *day* specimen, is a result of the second harmonic component being down 25 *dB* from the fundamental at $10 \frac{W}{cm^2}$ at the focal point.

The increased absorption of ultrasound in soft tissue in a nonlinear ultrasound field over that for linear propagation has been studied [12], [39], [41], [84]. It is evident from the data in Table 5.1 for the specimens irradiated with the unfocused transducer that an incident ultrasound field with developed harmonics impinging on bone will also result in increased heating under some circumstances. For example, the temperature elevation in the 78 *day* specimen at the " $10 \frac{W}{cm^2}$ " intensity is 26 % greater than that expected by extrapolating from the 0.1, 0.5, and $1 \frac{W}{cm^2}$ intensities. The absorption of ultrasound in bone is expected to be a function of the bone mineral content, hence, gestational age, as well as the frequency. As a consequence, the development of harmonics in the acoustic field is not expected to

affect the temperature elevation resulting from such exposures for those gestational ages and frequencies at which all the energy is absorbed near the surface. It should be noted that the higher harmonics will scatter from the bone in a fashion different from that of the fundamental, with a resulting change in the intensity distribution in the bone.

The quotation marks around the $10 \frac{W}{cm^2}$ intensity value above indicates that the linear relation between the intensity and the square of the voltage applied to the transducer determined from the calibration procedure at low acoustic intensities (linear fields) has been extrapolated. Thus, since the device is known to be linear, the output power at this " $10 \frac{W}{cm^2}$ " is ten times that at $1 \frac{W}{cm^2}$. However, because the shape of the beam changes as the acoustic wave propagates and the higher harmonics develop, and the higher harmonics can be significantly attenuated [20], [40], the intensity cannot be accurately determined by extrapolating the low-intensity, linear-field calibrations. Experimental results given by Carstensen et al. [40] indicate this difference to be only a few percent at 1 MHz and 93λ from the transducer.

The values of temperature increase in Table 5.1 for specimens irradiated at $1 \frac{W}{cm^2}$ at 20, 35, and 50 s are shown as a function of gestational age in Figure 5.9. The temperature elevation is seen to increase rapidly as a function of gestational age. The temperature increase at 20 s in the 59 day femur is only 0.10 °C. At this gestational age the bone is still very soft and ossification is just beginning. As was shown in Section 5.3, δT is 20% for the approximate analysis corresponding to this gestational age. However, it is clear from Figure 5.9 that even doubling the resulting value yields a temperature increase of only 0.2 °C at $1 \frac{W}{cm^2}$ (SPTA). A normal diurnal temperature variation for a pregnant woman is approximately 1°C [6]. Temperature elevations in the fetus resulting from exposure to ultrasound that are less than

1°C are then considered safe [6]. The temperature elevation in the 108 *day* specimen at 60 s and $1 \frac{\text{W}}{\text{cm}^2}$ exposure intensity is 4°C , and is no longer insignificant.

It is interesting to note that this value of the measured temperature increase is in the same range as that measured by Carstensen et al. [38] in the mouse skull irradiated with 3.6 MHz focused ultrasound at $1.5 \frac{\text{W}}{\text{cm}^2}$, which was approximately 3.5°C for young mice ($< 17 \text{ week}$) and 5.2°C for old mice ($> 6 \text{ months}$). It is not surprising that the temperature increases for the femur and mouse exposures are in the same range, even though the frequencies, as well as the beam sizes, differ. At some gestational age the bone is expected to become so highly absorbing that all the power transmitted into the bone will be absorbed and converted to heat. At that point, the temperature elevation will be frequency dependent only in so far as the heating volume is affected. Explicitly, the incident energy will be absorbed within a smaller distance of the bone surface as the frequency is increased. The beam size will also influence the temperature elevation. If the 108 *day* fetal femur temperature-increase value irradiated at $1 \frac{\text{W}}{\text{cm}^2}$ is scaled to $1.5 \frac{\text{W}}{\text{cm}^2}$, the intensity used by Carstensen et al., the resulting temperature increase at 60 s is 6°C . This higher value, as opposed to that measured by Carstensen et al., is consistent with the sizes of the beams employed in the two studies. In the work presented here, the HPBW is five times that used in the study by Carstensen et al.

The temperature increase measured at long times in the femur specimens is a function of the intensity at the point of measurement, thermal diffusivity, amount of acoustic energy converted to heat, i.e., absorption, and the total heating volume of the specimens. The thermal diffusivity and absorption are expected to vary with gestational age. A quantity is desired to identify the portion of the temperature increase that is not dependent on the heating volume of the specimen, as gestational age increases. For soft tissue, the temperature

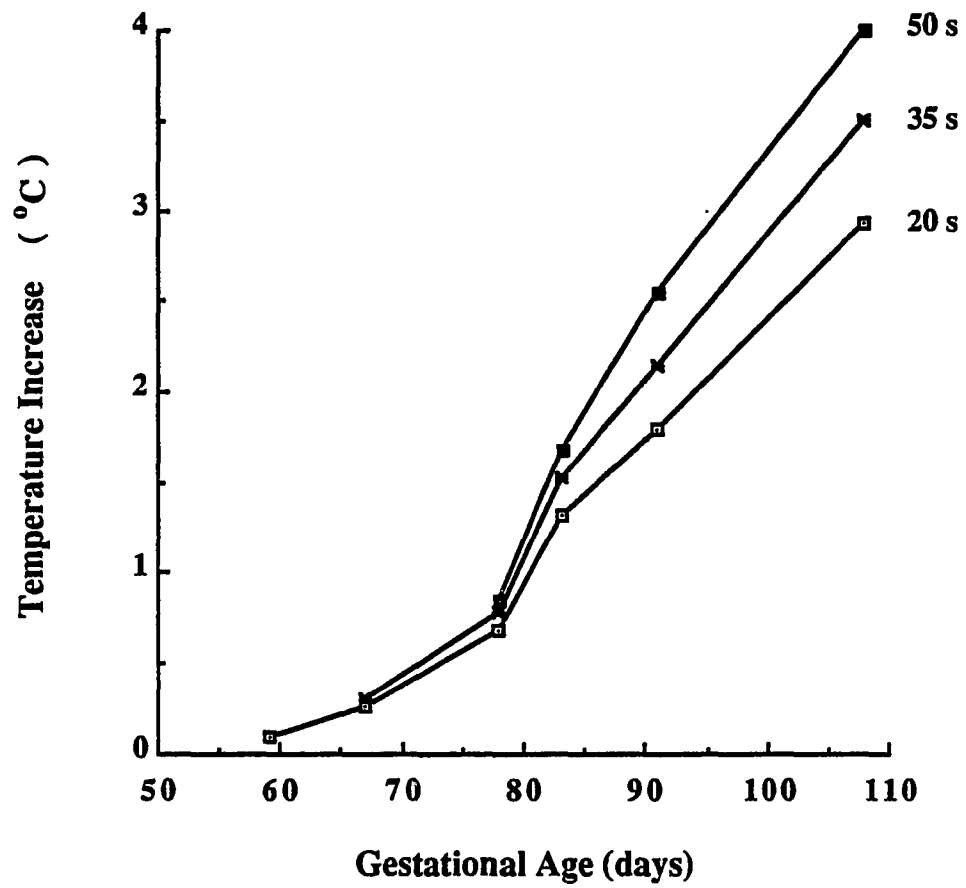


Figure 5.9: Temperature increase in the fetal femurs versus gestational age at 20, 35, and 50 s following the initiation of ultrasonic exposure at $1 \frac{W}{cm^2}$ (SPTA).

increase due to absorption is separated from the tissue volume and intensity by assuming a knowledge of the acoustic intensity in the tissue and evaluating $\frac{dT}{dt}$, the time derivative of the measured temperature increase, at a time at which heat conduction is negligible, to determine the ultrasonic absorption coefficient, as was discussed in Chapter 4. The problem is more complex in the case of a fetal femur specimen. The acoustic intensity at the site of the temperature measurement will vary with gestational age because of the changing acoustic properties as well as the changing dimensions of the bone. The ultrasonic intensity distribution in the specimen is unknown because of the complexities of the propagation in an anisotropic material and the difficult scattering problem, and absorption in compact bone is expected to be different than that in the inner bone lumen. In the absence of specific knowledge of the absorption as a function of the mode of propagation and the propagation direction, and lacking analytical or numerical solutions for the scattering from an elliptical, anisotropic cylinder, the rate of heating as $t \rightarrow 0$, i.e., $Q_0 = \frac{\partial T}{\partial t} |_{t \rightarrow 0}$, in the fetal bone is considered to be useful as shown in Appendix C. Although the quantity $I_0^{-1} \frac{dT}{dt}$, where I_0 is the free-field SPTA intensity, evaluated when heat conduction is negligible, is not independent of the specimen size or shape, it provides a useful measure of the variation in heat deposition with gestational age that is not dependent on the total heating volume of the specimen. The quantity $Q_0 = \frac{\partial T}{\partial t} |_{t \rightarrow 0}$ (negligible heat conduction) will be a function of the bone mineral content, heat capacity, density, and intensity at the site of the temperature measurement, all of which vary with gestational age.

A second-order polynomial curve is fit to the digitized measured temperature over the first 0.5 s for the 59 and 67 day gestational age specimens, and over the first 1 s for the remaining specimens [19]. The derivative of the temperature increase at 0.2 s, normalized to

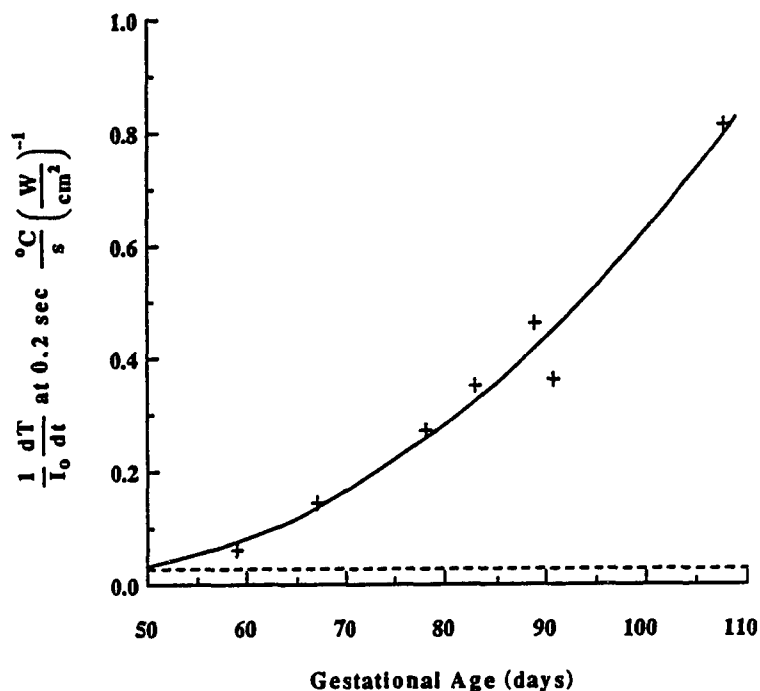


Figure 5.10: Time derivative of the temperature, normalized to the incident intensity, versus the gestational age of the specimens. The solid curve is a quadratic least-squares fit to the measured data. The dashed line is the value obtained for soft tissue with an absorption coefficient of 0.05 cm^{-1} .

the SPTA intensity incident on the specimen, as a function of the gestational age, is shown in Figure 5.10, where the quantity $I_0^{-1} \frac{dT}{dt}$ at 0.2 s has been measured for a single specimen of the gestational ages available; thus, no error bars are shown. The error in the determination of the gestational ages is ± 2 to 4 days, depending on the gestational age [183].

In order to minimize errors introduced by heat conduction, the time derivative of the temperature is evaluated at 0.2 s herein, as opposed to the more common 0.5 s delay when using the transient thermoelectric method to measure the absorption coefficient in soft tissue [57], [91]. It has been shown for soft tissues that appreciable errors can result in evaluating the derivative of the temperature, while assuming no heat conduction, if the thermocouple junction is placed too near the boundary between the absorbing specimen and nonabsorbing

coupling medium [57], [162]. It has been determined that a thermocouple junction placed 1 *mm* or deeper in soft tissue is consistent with the assumption concerning negligible heat conduction away from the junction at 0.5 s [57], [91], [162]. In evaluating the time derivative of the temperature of the fetal femur specimens, the important dimension is the diameter of the bone at the location at which the temperature is measured. The diameters of the fetal femurs range from 0.5 to 3.3 *mm* for the gestational ages studied. The small size of the specimens causes the value of $I_0^{-1} \frac{dT}{dt}$ to be sensitive to the placement of the thermocouple junction in the specimen. The placement of the thermocouple junction too near the bone surface can result in a significantly different measured $I_0^{-1} \frac{dT}{dt}$. In addition, the functional variation of the intensity over the femur, in the vicinity of temperature measurement, although unknown, may not be slowly varying, and, hence, would shorten the linear portion of the temperature increase after the initiation of the ultrasonic exposure.

The contribution of the viscous heating, which results from the relative motion of the thermocouple wire and the bone, to the temperature derivative at 0.2 s is negligible. The size of the hole left by the insertion of the thermocouple in the bone is several times larger than the diameter of the thermocouple wire. Contact between the bone and the thermocouple wire occurs over only a fraction of the circumference of the wire. The resulting heating distribution is appreciably smaller than would occur in the case of soft tissue where the tissue is presumed to relax to its original conformation to make contact around the entire periphery of the thermocouple wire. The time dependence of the viscous heating in the case of the bone specimens should then be small at exposure times shorter than the 0.2 s of the same response obtained for soft tissue [86], [87]. The measurements show the rapid rise time in the temperature response associated with the viscous heating to be approximately 0.05 s,

which is 25 % of the time at which the derivative of the temperature is evaluated. The above ratio of the fast rise time to the time at which the derivative is evaluated is comparable to the ratio for measurements in soft tissues.

It has been suggested that the temperature increase at a particular time for a given femur specimen might be normalized to the square of the radius of the femur, in an attempt to discern the degree of the increase in absorption with gestational age that is independent of the total heating volume [49]. Analytical results for a uniform, infinite, cylindrical heat source in an infinite, isotropic, and homogeneous medium given by Filipczynski provides some impetus for this normalization [75]. The bone however is not infinite, and the ultrasound beam and hence the equivalent heat source are reduced from the beam maximum over the length of the bone. In addition, the equivalent heat source resulting from absorption at higher frequencies is not expected to be a uniform cylinder [38]. Asymptotic results at short times, given by Filipczynski in an earlier paper [74], for the temperature increase resulting from an infinite uniform cylindrical heat source show that $\frac{\partial T}{\partial t}|_{t \rightarrow 0} = \frac{q_{v0}}{\rho C_p}$ (see Eq. (1.5) for notation). This result is entirely expected as is clear from the discussion in Appendix C. The same result is obtained for a shaped equivalent heat source approximating an ultrasound beam. For example, if $\beta_z \rightarrow \infty$ in Eq. (4.16), the integral can be performed analytically. Taking the derivative of the Taylor series expansion and keeping only the leading-order term for small time yield $\frac{\partial T}{\partial t}|_{t \rightarrow 0} = \frac{2\alpha I_0}{\rho C_p} = \frac{q_{v0}}{\rho C_p}$.

The temperature-increase data reported in this study can be compared to that expected for soft tissue by computing $I_0^{-1} \frac{dT}{dt} = \frac{2\alpha}{\rho C_p}$, where I_0 is the SPTA intensity, for nominal soft tissue values of α , ρ , and C_p [97], [98], [182]. For $\alpha = 0.05 \text{ cm}^{-1}$ and $\rho C_p = 3.78 \frac{\text{J}}{\text{cm}^3 \cdot \text{C}}$, $I_0^{-1} \frac{dT}{dt} = 0.026 \frac{\text{C}}{\text{s}} (\frac{\text{W}}{\text{cm}^2})^{-1}$. This value of $I_0^{-1} \frac{dT}{dt}$ can then be compared directly with the

values measured for the fetal bone studied as shown in Figure 5.10. The values measured for the 59 and 108 *day* specimens are approximately 2 and 30 times greater, respectively, than the soft tissue value. The temperature increase measurements presented have been for a single orientation of the femur specimen with respect to the incident ultrasound field. It is likely that the quantity $I_0^{-1} \frac{dT}{dt}$, for negligible heat conduction, will be different for other orientations. Preliminary results in fetal pig femurs exposed to ultrasound indicate that the temperature elevation is a function of the direction of the incident wave on the elliptical cross-section [15]. This is expected to be the case for the fetal femur exposures also. The angle of incidence is likely to influence the value of $I_0^{-1} \frac{dT}{dt}$ and the temperature elevation also. Chan et al. analytically studied the heat generated by ultrasound in fat-muscle-bone layers and found the heating in and around the bone to be dependent on the angle of incidence of the ultrasound beam [45]. This is expected since the energy transmitted into the highly absorbing bone is a function of the angle of incidence.

The time required for the temperature to increase 1 °C for a specified set of ultrasonic exposure conditions is considered important in view of the fact that the diurnal variation in the body temperature of the mother is of this magnitude. Thus, ultrasonic exposure conditions, in which the primary consideration for deleterious effects to the fetus is heat deposition, are considered to be without risk if such a temperature increase is not exceeded. The irradiation time necessary for the temperature to increase 1 °C in the specimens studied is shown in Figure 5.11 for incident intensities of 1 and 5 $\frac{W}{cm^2}$.

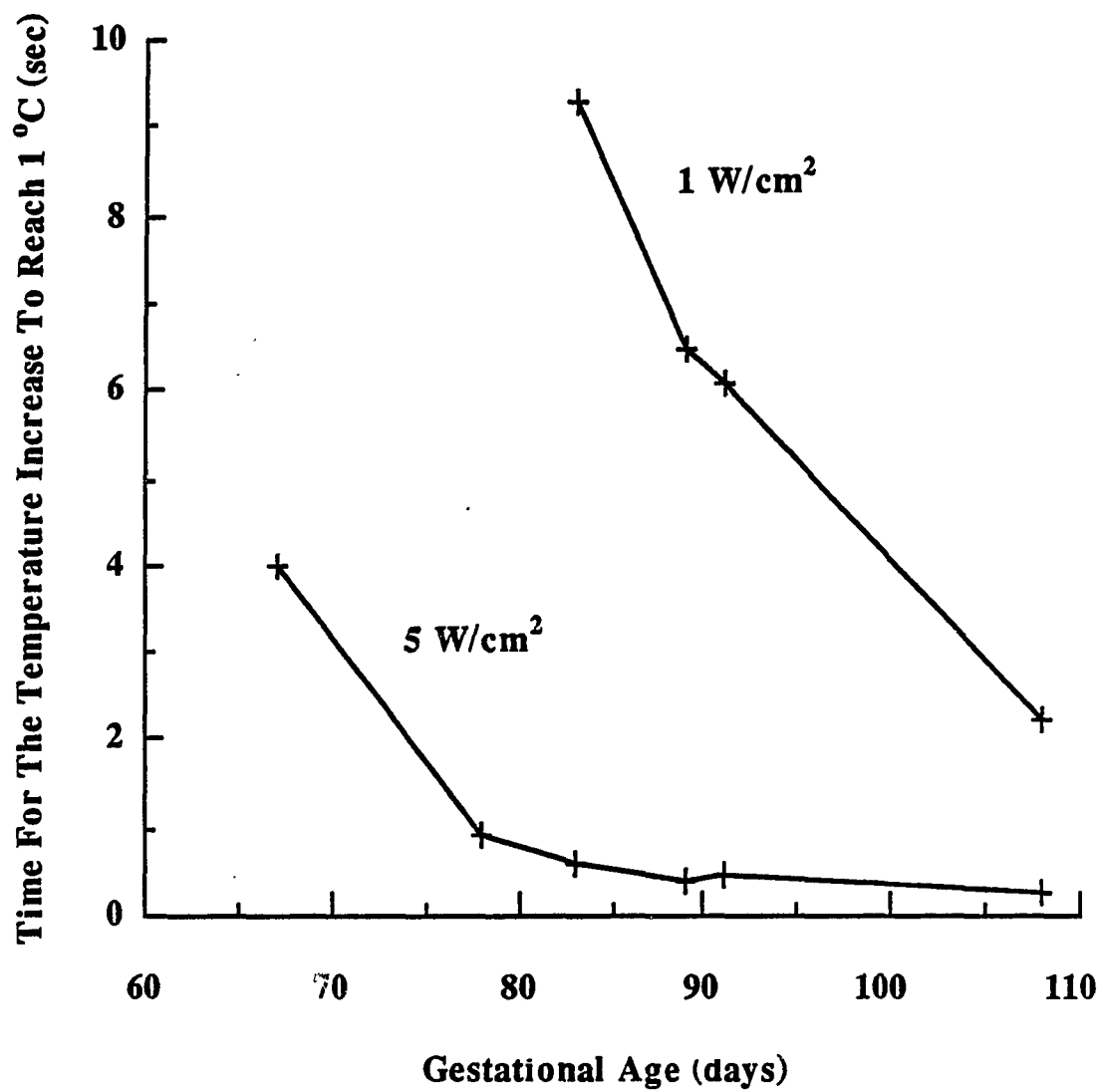


Figure 5.11: Time of ultrasonic exposure required for the temperature increase to reach 1°C versus gestational age.

CHAPTER 6

SUMMARY AND RECOMMENDATIONS FOR FUTURE WORK

The temperature elevation in the fetus resulting from absorption of ultrasound in diagnostic exposures is of concern because of the well-established teratogenicity of hyperthermia, and the possibility of more subtle, as yet undetermined, effects of elevated fetal temperatures. The absorption of ultrasound and the resulting temperature elevation in soft and hard fetal tissues have been addressed in this study.

The temperature increase in fetal mice exposed *in utero* to 1 MHz ultrasound was presented in Chapter 3. Temperature elevations between 1.5 °C and 4 °C were measured for exposure intensities between 0.5 and 10 $\frac{W}{cm^2}$. A simple analytical model was given that allowed for different absorption coefficients in the dam and the fetus; however, only uniform perfusion throughout was considered. Values of absorption and perfusion were chosen to yield reasonable, although not exact, agreement between the calculated and measured values of temperature increase. Values assumed for the absorption coefficient were extrapolated from available experimental data, and qualitative arguments were given for the assumed values of perfusion. The analytical results presented employed a very simple model for heat transfer; however, more complex models require information regarding the absorption coefficient and perfusion in the fetal tissues not presently available.

Future work in the study of *in utero* temperature increases upon exposure to ultrasound would include the measurement of the absorption coefficient in fetal soft tissue. Also, temperature increase measurements at medical diagnostic frequencies with narrow beams would provide more clinically relevant information. Finally, an improvement in the experimental

method to minimize the movement of the dam during the measurement procedure would possibly increase the precision of the measurements.

An analytical analysis of the transient thermoelectric method (TTM) for determining the ultrasonic absorption coefficient in soft tissue was given in Chapter 4. The ultrasound beam was approximated with a Gaussian function, and the temperature increase resulting from the absorption of acoustic energy was analytically determined from the Green's function representation of the solution of the heat equation. A Gaussian source heating in an infinite, isotropic and homogeneous medium was assumed in the analysis. An error was defined that represented the percent difference between the ideal case without heat conduction and that of the analytical model, which included heat conduction due to the finite dimensions of the beam and tissue specimen. The error was then investigated as a function of the transducer beamwidth, tissue specimen dimensions, position, and time.

The analytical results of the error as a function of HPBW were found to compare well with published experimental data. An analytical expression for the temperature increase was given also for a Gaussian source heating in a halfspace bounded by a medium of differing thermal diffusivity. It was shown in Chapter 4 that the error in the measurement of the absorption coefficient in soft tissue resulting from heat conduction can be kept small for sufficiently broad HPBWs. For example, an HPBW of 5.0 *mm* and tissue dimensions greater than 3.0 *mm* result in an error of less than 5% due to heat conduction, if the time derivative of the temperature is evaluated at 0.5 *s*. A critical depth was defined for implanting the thermocouple in the tissue such that heat flow to the boundary would have no effect at the time the derivative is evaluated. The critical depth was found to be 1.0, 1.5, and 1.75 *mm* when the time derivative of the temperature is evaluated at 0.5, 1.0, and 1.5 *s*, respectively.

Previously, the time derivative of the temperature has been evaluated at 0.5 s when applying the TTM. The analysis presented in Chapter 4 has shown that the time derivative of the temperature can be evaluated at later times with an error due to heat conduction less than 10%. This is particularly advantageous in low absorbing soft tissues, such as fetal soft tissue, for minimizing the viscous heating artifact associated with the thermocouple.

Future work in the analysis of the TTM would include further experimental work to obtain additional support for the analysis. Absorption coefficient measurements at times different from 0.5 s and at shallow depths in a material would provide information on the defined error as a function of time and depth of thermocouple placement. Absorbing oils or polymethylmethacrylate are possible materials from which this information might be obtained. Absorption coefficient measurements in soft tissue as a function of frequency are also needed for further comparison with those for the pulse-decay method.

Acoustic absorption in fetal bone was discussed in Chapter 5. The difficulties in determining the absorption in bone as a function of the direction of propagation and the mode of propagation were enumerated. In the absence of specific knowledge concerning acoustic absorption in fetal bone, the temperature elevation can be measured, and is useful for assessing thermal effects. The temperature elevation in fetal femurs resulting from exposure to 1 MHz ultrasound was measured for gestational ages between 59 and 108 days. The measured temperature increase at an exposure intensity of $1 \frac{W}{cm^2}$ at 20 s for the 59 day specimen was 0.10 °C, and the value for the 108 day specimen was 2.9 °C. The latter value of temperature increase is clinically of concern, because it exceeds the 1°C temperature elevation generally considered to be safe [6]. The time derivative of the temperature increase was evaluated to obtain an equivalent heat source for ultrasonic absorption in fetal bone. The initial rates of

temperature increase in the 59 and 108 *day* gestational age specimens were found to be 2 and 30 times that expected for an adult soft tissue such as liver.

Little information regarding the temperature elevation upon exposure to ultrasound has been available for human fetal bone. Although this study provides insight into the problem, a great deal of work remains to be done. The temperature elevation upon exposure to ultrasound was studied for only a single orientation of the bone specimen with respect to the ultrasound beam. It is likely that the temperature increase and the initial rate of temperature increase depend upon the orientation of the bone with respect to the ultrasound beam. Further work is necessary to determine this variation and the maximum temperature increase. Temperature elevation measurements are also needed at higher frequencies, as a function of gestational age, particularly at clinical frequencies. Temperature increase measurements in and around the bone with the surrounding tissue left attached to the bone would also be informative. The significantly greater absorption in bone as compared to soft tissue is presumed to result from the collagen and mineral matrix of bone. The density and bone-mineral density of the bone specimens can be measured to determine a possible correlation between the temperature elevation and the mineral content. The data presented in Chapter 5 gave the femur length as a function of gestational age, and the temperature elevation was measured in the ossified region. To establish a more accurate equivalent heat source, the length of the ossified region alone should also be measured. An analytical investigation of the intensity distribution in absorbing, cylindrically layered media would provide approximate information on the spatial distribution of the heating in the bone. This spatial variation combined with the measured initial rate of the temperature increase would provide a more realistic source term in the bioheat equation. Numerical

calculations could then be performed to estimate the temperature elevation in the fetal bone and the surrounding tissues. Biot's theory of acoustic propagation in porous media may be applicable for determining the attenuation in bone and merits consideration in the future study of acoustic wave propagation in bone [18], [23], [24], [25].

APPENDIX A

**INTEGRAL-DIFFERENTIAL RELATION BETWEEN THE IMPULSE AND
UNIT STEP RESPONSES**

Let L denote the general, linear, ordinary differential operator

$$L = a_p \frac{d^p}{dt^p} + \dots + a_1 \frac{d}{dt} + a_0 \quad (\text{A.1})$$

where the coefficients $\{a_p, \dots, a_0\}$ are constant. Let $E(t - \tau)$ be the impulse response satisfying

$$LE(t - \tau) = \delta(t - \tau) \quad E \equiv 0, \quad t < \tau \quad (\text{A.2})$$

and $F(t - \tau)$ be the unit step response satisfying

$$LF(t - \tau) = U(t - \tau) \quad F \equiv 0, \quad t < \tau \quad (\text{A.3})$$

Because the operator L has constant coefficients, the impulse and unit step responses are time invariant, i.e., $E(t, \tau) = E(t - \tau, 0) = E(t - \tau)$, and $F(t, \tau) = F(t - \tau, 0) = F(t - \tau)$.

Then it is easily shown that

$$-\frac{\partial F(t, \tau)}{\partial \tau} = E(t, \tau) \quad (\text{A.4})$$

and further, since L has constant coefficients

$$-\frac{\partial F(t - \tau)}{\partial \tau} = \frac{\partial F(t - \tau)}{\partial t} = E(t - \tau) \quad (\text{A.5})$$

i.e., the time derivative of the unit step response is the impulse response. Let the distribution f be denoted by $\langle f, \phi \rangle$, where ϕ is a testing function [116]. Then

$$\begin{aligned}
\langle L \left(-\frac{\partial F(t, \tau)}{\partial \tau} \right), \phi(t) \rangle &= \int_{-\infty}^{\infty} L \left(-\frac{\partial F(t, \tau)}{\partial \tau} \right) \phi(t) dt \\
&= \int_{-\infty}^{\infty} -\frac{\partial}{\partial \tau} L F(t, \tau) \phi(t) dt \\
&= -\frac{\partial}{\partial \tau} \int_{-\infty}^{\infty} U(t - \tau) \phi(t) dt \\
&= -\frac{\partial}{\partial \tau} \int_{\tau}^{\infty} \phi(t) dt \\
&= \phi(\tau) \\
&= \langle \delta(t - \tau), \phi(t) \rangle \\
&= \langle LE(t, \tau), \phi(t) \rangle
\end{aligned} \tag{A.6}$$

or in the distributional sense $-\frac{\partial F(t, \tau)}{\partial \tau} = E(t, \tau)$.

APPENDIX B

TRANSDUCER BEAM PROFILES

The ultrasound beam profiles for the transducers employed in the experimental measurements are given in this appendix. The beam profiles for each transducer were plotted using the ultrasound irradiation system shown in Figure 2.1. All field plots were measured with small voltages applied to the transducer, and the second harmonic was measured to be 15 – 20 *dB* below the fundamental in all cases shown. Two plots superimposed for two orthogonal directions relative to the acoustic axis of propagation are shown for each transducer. Circular PZT-4 crystals were used in the transducer design. The beam profile for the focused 1 *MHz* transducer is shown in Figure B.1. The diameter of the transducer is 5.08 *cm*, and the experimentally determined focal length is 15 *cm*. The HPBW is 4.76 *cm*. The field plots for the plane-piston, 1 *MHz*, unfocused transducer, # 101, at 93 λ from the crystal face (slightly beyond the near-field, far-field transition region) are shown in Figure B.2. The diameter is 2.54 *cm*, and the HPBW is 1.1 *cm*. The field plot at 193 λ from the crystal face of the same transducer is shown in Figure B.3. Finally, field plots for the Gaussian transducer, # 201B, at 3, 5, and 7 *MHz* are shown in Figure B.4. The crystal aperture is 2.54 *cm* with the contact electrode on the back surface being 7.5 *mm*. The transducer has a fundamental frequency of 1 *MHz*. The distances of the plots from the crystal face are 5.0, 8.0, and 13.0 *cm* at 3, 5, and 7 *MHz*, respectively. The field plot for the 1 *MHz*, focused transducer is also shown. The HPBW at all frequencies is approximately 4.5 *mm*.

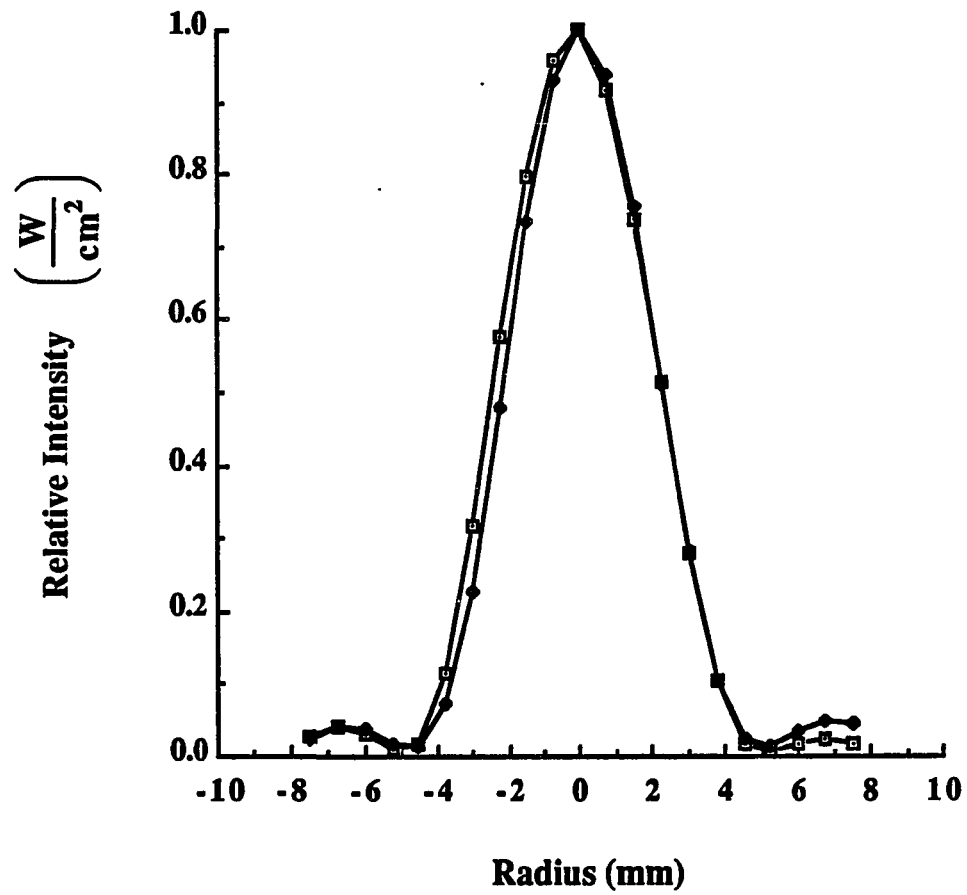


Figure B.1: Ultrasound beam profile for the 1 MHz, focused transducer.

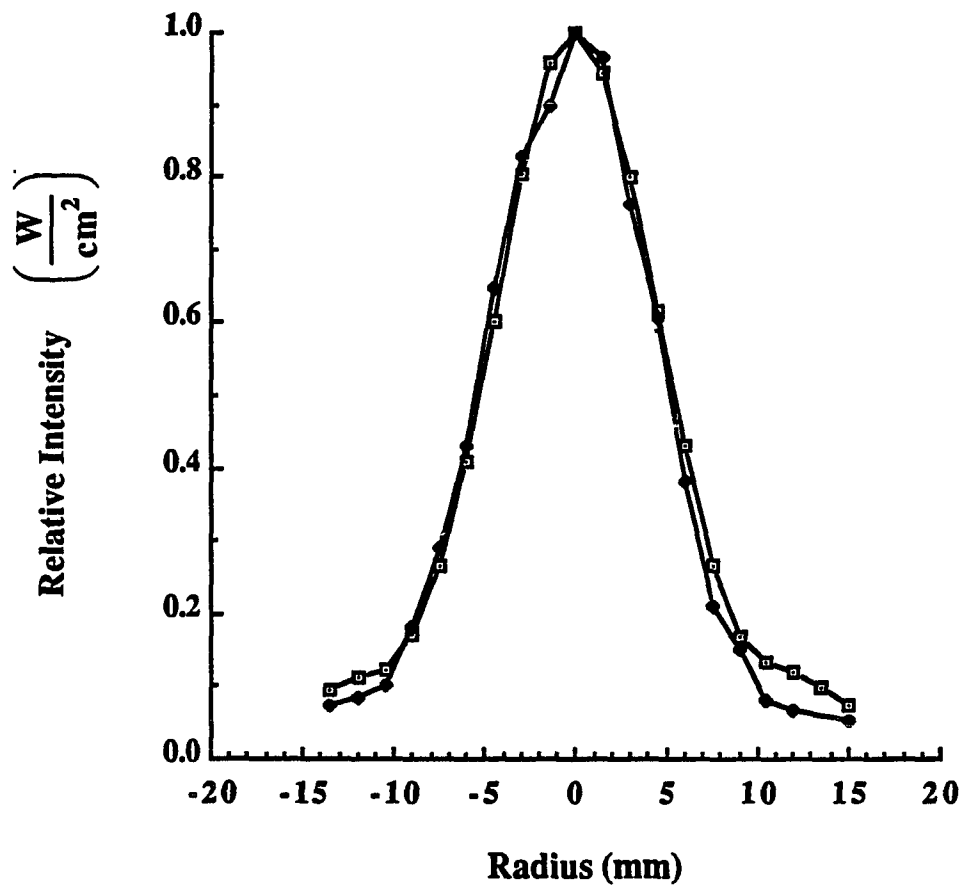


Figure B.2: Ultrasound beam profile for the 1 MHz, unfocused transducer # 101, 93λ from the crystal face.

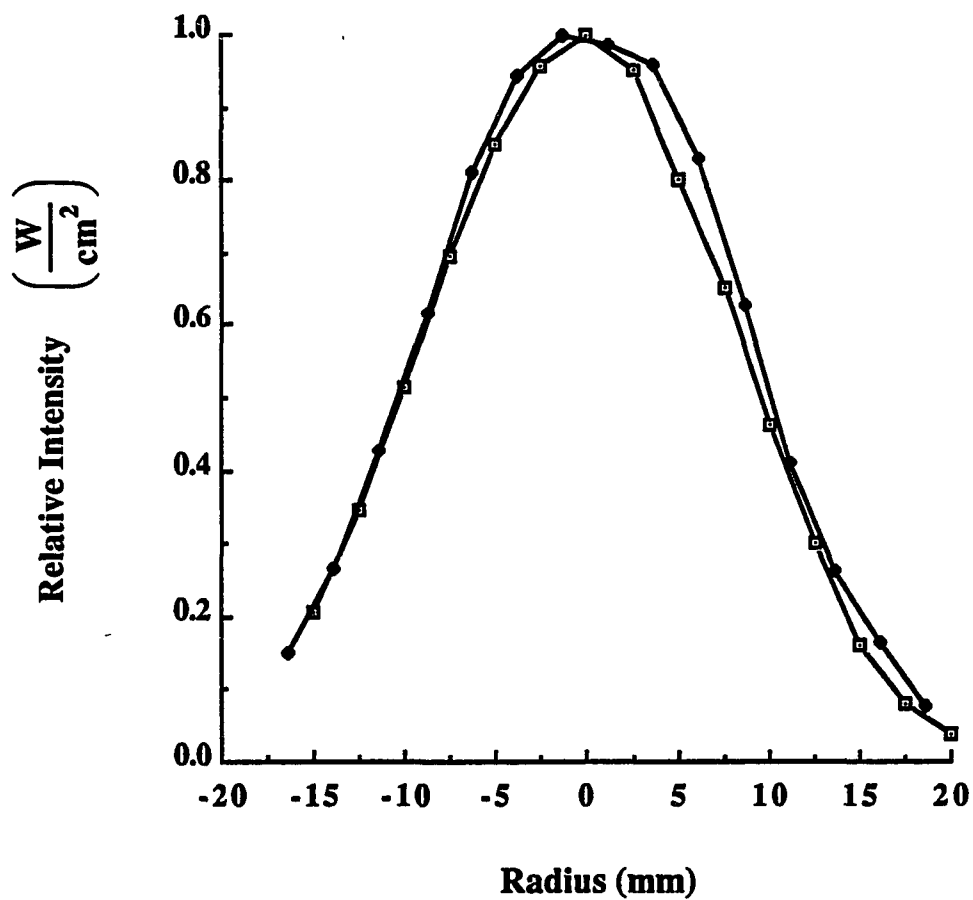


Figure B.3: Ultrasound beam profile for the 1 MHz, unfocused transducer # 101, 193λ from the crystal face.

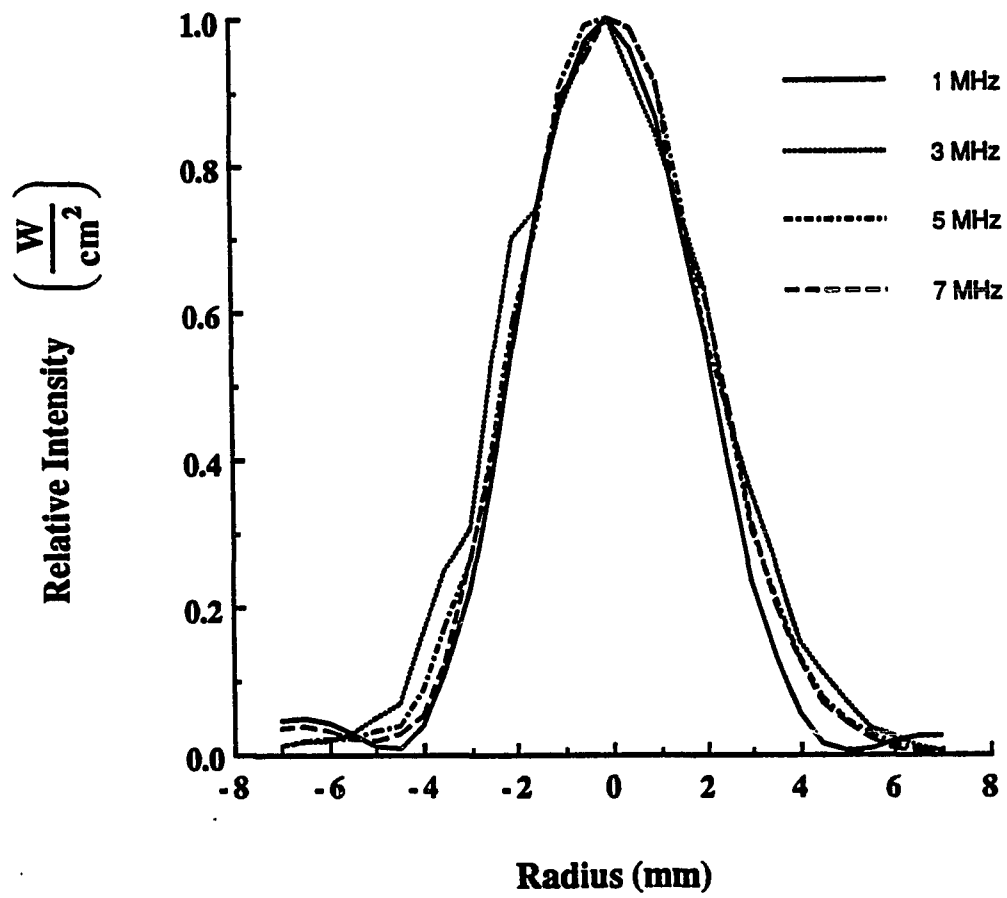


Figure B.4: Ultrasound beam profile for the Gaussian transducer # 201B, at 3, 5, and 7 MHz.

APPENDIX C

**A SIMPLE INTERPRETATION OF THE EQUIVALENT HEAT SOURCE
RESULTING FROM THE ABSORPTION OF ULTRASOUND BY
BIOLOGICAL TISSUE**

The acoustic propagation properties of fetal bone are as yet unknown, in particular, the absorption. Another quantity that characterizes the equivalent heat source resulting from absorption is therefore needed. The temperature elevation in the bone and surrounding tissues can then be estimated using numerical or analytical methods, and the subsequent thermal risk to the developing tissues assessed. In the absence of perfusion, and at short times such that heat conduction is negligible, the bioheat equation Eq. (1.1) becomes

$$\left. \frac{\partial T(\bar{\mathbf{r}}, t)}{\partial t} \right|_{t \rightarrow 0} = \frac{q_v(\bar{\mathbf{r}}, t)}{\rho C_p} \quad (\text{C.1})$$

If the acoustic properties of the medium are known, the volumetric rate of energy deposition is given as in Eq. (5.18) [45]

$$q_v(\bar{\mathbf{r}}) = -\frac{1}{2} \nabla \cdot \Re e [\bar{\mathbf{v}} \cdot \bar{\mathbf{T}}] \quad (\text{C.2})$$

In the absence of specific knowledge of the acoustic properties of fetal bone, Eq. (C.1) indicates an experimental method for determining an equivalent heat source for ultrasonic absorption in fetal bone. A simple example is given below.

Let the source function to the bioheat equation be written as

$$\frac{q_v(\bar{\mathbf{r}}, t)}{\rho C_p} = \frac{q_{v0} f(\bar{\mathbf{r}}) F(t)}{\rho C_p} = Q_0 F(t) f(\bar{\mathbf{r}}) \quad (\text{C.3})$$

where Q_0 ($\frac{^\circ\text{C}}{\text{s}}$) is the magnitude of the rate of the temperature increase, q_{v0} is the volumetric rate of energy deposition, and $f(\bar{\mathbf{r}})$ and $F(t)$ are the spatial and temporal variations of $q_v(\bar{\mathbf{r}}, t) = q_{v0} F(t) f(\bar{\mathbf{r}})$, respectively.

The nature of the equivalent heat source as given in Eq. (C.3), when the source of the heating is ultrasonic absorption, can be seen by investigating the solution to a uniform heat distribution of infinite length, with a cylindrical cross section of radius r_0 , in an infinite, homogeneous medium. In this case the appropriate Green's function is given by

$$G(r, r', t - \theta) = e^{-\frac{(t-\theta)}{r}} \frac{1}{2\kappa(t-\theta)} e^{-\frac{r^2-r'^2}{4\kappa(t-\theta)}} I_0 \left(\frac{rr'}{2\kappa(t-\theta)} \right) \quad (\text{C.4})$$

where $r^2 = x^2 + y^2$. The temperature increase at the radial coordinate r and time t is then given by

$$T(r, t) = Q_0 \int_0^t d\theta F(\theta) \frac{e^{-\frac{(t-\theta)}{r}}}{2\kappa(t-\theta)} \int_0^{r_0} r' dr' e^{-\frac{r^2-r'^2}{4\kappa(t-\theta)}} I_0 \left(\frac{rr'}{2\kappa(t-\theta)} \right) \quad (\text{C.5})$$

The spatial variables can be integrated analytically if the temperature is observed at $r = 0$, resulting in

$$T(0, t) = Q_0 \int_0^t d\theta F(\theta) e^{-\frac{(t-\theta)}{r}} \left\{ 1 - \exp \left[-\frac{r_0}{4\kappa(t-\theta)} \right] \right\} \quad (\text{C.6})$$

If the material characteristics of the medium ρ and C_p are known, as well as the magnitude of the heat source q_{v_0} , the maximum temperature (which occurs at $r = 0$) as a function of time can be computed from Eq. (C.6). In the case of ultrasonic absorption in soft tissue irradiated by a traveling plane wave, q_{v_0} is proportional to the acoustic intensity. The proportionality constant is determined experimentally for soft tissues as discussed in Chapter 4. The situation is considerably more complex in bone because the acoustic absorption in bone as a function of the mode and the direction of propagation is unknown. The constant Q_0 is comprised of thermal constants and quantities characterizing the conversion of acoustic energy to heat. In the case of soft tissue, these quantities can easily be separated; however, as seen by Eq. (C.6) this is not entirely necessary for determining the temperature in this

example. If Q_0 itself can be determined experimentally, the temperature in this example can still be calculated from Eq. (C.6).

Let the absorbing cylinder be exposed to a unit step *CW* ultrasonic exposure, i.e., $F(t) = U(t)$, where $U(t)$ is the unit step function. For the sake of this simple example, the ultrasound "beam" is assumed to heat the cylinder uniformly. The temperature increase at $r = 0$ is then given by

$$T(0, t) = Q_0 \int_0^t d\theta e^{-\frac{(t-\theta)}{\tau}} \left\{ 1 - \exp \left[-\frac{r_0}{4\kappa(t-\theta)} \right] \right\} \quad (\text{C.7})$$

In soft tissue, the ultrasonic absorption coefficient is determined from the derivative of Eq. (C.7) (with no perfusion) at short times. The derivative of the unit step response is the impulse response and no integration is necessary in this case. A general proof of this is given in Appendix A. Since measurements of the ultrasonic absorption coefficient in soft tissue are typically performed *in vitro*, the perfusion time constant goes to infinity, and

$$\frac{\partial T}{\partial t} = Q_0 \left[1 - e^{-\frac{r_0}{4\kappa t}} \right] \quad (\text{C.8})$$

The relationship between the temperature and Q_0 is established as $\frac{\partial T}{\partial t} \Big|_{t \rightarrow 0} = Q_0$, by evaluating the derivative of the temperature at $t = 0$. The temperature increase for this example can then be computed without specific knowledge of the absorption coefficient. It is, however, necessary to know κ , the thermal diffusivity of the medium, and τ if the medium is perfused, in order to calculate the temperature elevation. It should be noted that the observation point taken in this example is at the heat source maximum; hence, the heat flow is away from the observation point. If the heat source had the shape of an ultrasound beam and it is desired to measure $Q_0 = \frac{\partial T}{\partial t} \Big|_{t \rightarrow 0}$, it would be necessary to make the observation

at the maximum of the heat source to obtain an estimate of Q_0 , if no other information regarding the ultrasound field in the tissue was available.

The ultrasonic absorption coefficient can be measured directly for soft tissues and an analysis of the procedure is given in Chapter 4. Hence, lumping the acoustic and thermal properties of the medium together in the quantity Q_0 is unnecessary. However, determining an ultrasonic absorption coefficient for bone presents a formidable problem as discussed in Chapter 5. In this case, the quantity Q_0 , which can be measured directly, will be useful for numerical and analytical calculations of the temperature in the fetal bone and surrounding tissues.

REFERENCES

- [1] V. Abraham, M. C. Ziskin, and S. Heynen, "Temperature elevation in the rat fetus due to ultrasound exposure," *Ultrasound Med. & Biol.* **15**, 443-449 (1989).
 - [2] M. A. Abramowitz and I. A. Stegun, *Handbook of Mathematical Functions* (Dover Publications, Inc., New York, NY, 1967), pp. 297-299.
 - [3] J. D. Achenbach, *Wave Propagation in Elastic Solids* (North Holland Publishing Company, New York, NY, 1973).
 - [4] AIUM, *1985 Acoustical Data for Diagnostic Ultrasound Equipment* (American Institute of Ultrasound in Medicine, Bethesda, MD, 1985).
 - [5] AIUM, *1987 Acoustical Data for Diagnostic Ultrasound Equipment* (American Institute of Ultrasound in Medicine, Bethesda, MD, 1987).
 - [6] AIUM, "Bioeffects considerations for the safety of diagnostic ultrasound," *J. Ultrasound Med.* (Supplement 9) **7**, S1-S38 (1988).
 - [7] R. B. Ashman and J. Y. Rho, "Elastic modulus of trabecular bone material," *J. Biomech.* **21**, 177-181 (1988).
 - [8] B. A. Auld, "Application of microwave concepts to the theory of acoustic fields and waves in solids," *IEEE Trans. Microwave Theory Tech.* **MTT-17**, 800-811 (1969).
 - [9] B. A. Auld, *Acoustic Fields and Waves in Solids - Vol. I* (John Wiley and Sons, Inc., New York, NY, 1973).
 - [10] O. Axelsson and V. A. Barker, *Finite Element Solution of Boundary Value Problems* (Academic Press, Inc., New York, NY, 1984).
 - [11] D. R. Bacon, "Characteristics of a pvdf membrane hydrophone for use in the range 1-100 MHz," *IEEE Trans. Sonics Ultrason.* **SU-29**, 18-25 (1982).
 - [12] D. R. Bacon and E.L. Carstensen, "Increased heating by diagnostic ultrasound due to nonlinear propagation," *J. Acoust. Soc. Am.* **88**, 26-34 (1990).
 - [13] I. L. Bajak, A. McNab, J. Richter, and C. W. D. Wilkinson, "Attenuation of acoustic waves in lithium niobate," *J. Acoust. Soc. Am.* **69**, 689-695 (1981).
 - [14] H. D. Baker, E. A. Ryder, and N. H. Baker, *Temperature Measurement in Engineering - Vol. 1* (Omega Press, Stamford, CT, 1975).
 - [15] S. Barnett, results presented at the Conference for Ultrasonics in Biophysics and Bioengineering, University of Illinois (1990).
 - [16] K. Beissner, "On the plane wave approximation of acoustic intensity," *J. Acoust. Soc. Am.* **71**, 1406-1411 (1982).
-

- [17] P. J. Benkeser, L. A. Frizzell, K. R. Holmes, and S. A. Goss, "A perfused tissue phantom for ultrasound hyperthermia," *IEEE Trans. Biomed. Eng.* **BME-37**, 425-428 (1990).
 - [18] J. G. Berryman, "Confirmation of Biot's theory," *Appl. Phys. Lett.* **37**, 382-384 (1980).
 - [19] P. R. Bevington, *Data Reduction and Error Analysis for the Physical Sciences* (McGraw-Hill Book Company, New York, NY, 1969).
 - [20] R. T. Beyer, *Nonlinear Acoustics* (Naval Sea Systems Command, Washington, DC, 1974).
 - [21] A. B. Bhatia, *An Introduction to the Theory of Sound Absorption and Dispersion in Gases, Liquids and Solids* (Dover Publications, Inc., New York, NY, 1967).
 - [22] B. M. Bindon, "Blood flow in the reproductive organs of the mouse after hypophysectomy, after gonadotrophin treatment, during the estrous cycle, and during early pregnancy," *J. Endocr.* **44**, 523-536 (1969).
 - [23] M. A. Biot, "Theory of propagation of elastic waves in a fluid-saturated porous solid. I. Low-frequency range," *J. Acoust. Soc. Am.* **28**, 168-178 (1956).
 - [24] M. A. Biot, "Theory of propagation of elastic waves in a fluid-saturated porous solid. II. Higher frequency range," *J. Acoust. Soc. Am.* **28**, 179-191 (1956).
 - [25] M.A. Biot, "Generalized theory of acoustic propagation in porous dissipative media," *J. Acoust. Soc. Am.* **34**, 1254-1264 (1962).
 - [26] D. T. Blackstock, "Thermoviscous attenuation of plane, periodic, finite-amplitude sound waves," *J. Acoust. Soc. Am.* **36**, 534-539 (1964).
 - [27] D. T. Blackstock, "Connection between the Fay and Fubini solutions for plane sound waves of finite amplitude," *J. Acoust. Soc. Am.* **39**, 1019-1026 (1966).
 - [28] W. Bloom and D. W. Fawcett, *A Textbook of Histology* (W. B. Saunders Company, Philadelphia, PA, 1975).
 - [29] F. E. Borgnis, "Specific directions of longitudinal wave propagation in anisotropic media," *Phys. Rev.* **98**, 1000-1005 (1955).
 - [30] H. F. Bowman, "Heat Transfer Mechanisms and Thermal Dosimetry", in *Third International Symposium: Cancer Therapy by Hyperthermia, Drugs, and Radiation*, edited by L. Dethlefsen, National Cancer Institute Monograph No. 61, (US Department of Health and Human Services, Washington, DC, 1982), pp. 437-445.
 - [31] M. A. Breazeale, F. D. Martin, and B. Blackburn, "Reply to : Radiation pattern of partially electroded piezoelectric transducers," *J. Acoust. Soc. Am.* **70**, 1791-1793 (1981).
 - [32] K. A. Brix, "Environmental and occupational hazards to the fetus," *J. Reprod. Med.* **27**, 577-583 (1982).
-

- [33] K. Brugger, "Pure modes for elastic waves in crystals," *J. Appl. Phys.* **36**, 759-768 (1965).
 - [34] M. M. Burlew, E. L. Madsen, J. A. Zagzebski, R. A. Banjavic, and S. W. Sum, "A new ultrasound tissue-equivalent material," *Radiology* **134**, 517-520 (1980).
 - [35] K. I. Carnes and F. Dunn, "Absorption of ultrasound by mammalian ovaries," *J. Acoust. Soc. Am.* **84**, 434-437 (1988).
 - [36] H. S. Carslaw and J. C. Jaeger, *Conduction of Heat in Solids* (Oxford University Press, Inc., New York, NY, 1959).
 - [37] E. L. Carstensen, S. A. Becroft, W. K. Law, and D. B. Barbee, "Finite amplitude effects on the thresholds for lesion production in tissues by unfocused ultrasound," *J. Acoust. Soc. Am.* **70**, 302-309 (1981).
 - [38] E. L. Carstensen, S. Z. Child, S. Norton, and W. Nyborg, "Ultrasonic heating of the skull," *J. Acoust. Soc. Am.* **87**, 1310-1317 (1990).
 - [39] E. L. Carstensen, D. Dalecki, K. J. Parker, D. R. Bacon, and D. Blackstock, "Nonlinear aspects of ultrasonic heating," *J. Acoust. Soc. Am.* **86** (Supplement 1), S27 (1989).
 - [40] E. L. Carstensen, W. K. Law, N. D. McKay, and T. G. Muir, "Demonstration of nonlinear acoustical effects at biomedical frequencies and intensities," *Ultrasound Med. & Biol.* **6**, 359-368 (1980).
 - [41] E. L. Carstensen, N. D. McKay, D. Dalecki, and T. G. Muir, "Absorption of finite amplitude ultrasound in tissues," *Acustica* **51**, 116-123 (1982).
 - [42] E. L. Carstensen, K. J. Parker, and D. B. Barbee, "Temporal peak intensity," *J. Acoust. Soc. Am.* **74**, 1057-1058 (1983).
 - [43] T. J. Cavicchi and W. D. O'Brien, Jr., "Heat generated by ultrasound in an absorbing medium," *J. Acoust. Soc. Am.* **76**, 1244-1245 (1984).
 - [44] T. J. Cavicchi and W. D. O'Brien, Jr., "Acoustic scattering of an incident cylindrical wave by an infinite circular cylinder," *IEEE Trans. Ultrason. Ferroelectr. Freq. Contr.* **UFFC-35**, 78-80 (1980).
 - [45] A. K. Chan, R. A. Sigelmann, and A. W. Guy, "Calculations of therapeutic heat generated by ultrasound in fat-muscle-bone layers," *IEEE Trans. Biomed. Eng.* **BME-21**, 280-284 (1974).
 - [46] A. K. Chan, R. A. Sigelmann, A. W. Guy, and J. F. Lehman, "Calculation by the method of finite differences of the temperature distribution in layered tissues," *IEEE Trans. Biomed. Eng.* **BME-20**, 86-90 (1973).
 - [47] Z. P. Chang, "Pure transverse modes for elastic waves in crystals," *J. Appl. Phys.* **39**, 5669-5681 (1968).
 - [48] P. C. Chou and N. J. Pagano, *Elasticity* (D. Van Nostrand, Princeton, NJ, 1967).
-

- [49] Conference for Ultrasonics in Biophysics and Bioengineering, University of Illinois (1990).
 - [50] R.V. Churchill and J. W. Brown, *Complex Variables and Applications* (McGraw-Hill Book Company, New York, NY, 1984).
 - [51] H. F. Cooper, Jr., "Reflection and transmission of oblique plane waves at a plane interface between viscoelastic media," *J. Acoust. Soc. Am.* **42**, 1064-1069 (1967).
 - [52] G. Dahlquist and A. Bjorck, *Numerical Methods* (Prentice-Hall, Inc., Englewood Cliffs, NJ, 1974).
 - [53] D. Dalecki, E. L. Carstensen, K. J. Parker, and D. R. Bacon, "Overview of absorption of finite amplitude, focused ultrasound," in *Frontiers of Nonlinear Acoustics: Proceedings of the 12th ISNA*, edited by M. F. Hamilton and D. T. Blackstock (Elsevier Science Publishers Ltd., London, 1990), pp. 125-130.
 - [54] B. Davies, *Integral Transforms and Their Applications* (Springer-Verlag, New York, NY, 1978).
 - [55] V. A. Del Grosso and C. W. Maden, "Speed of sound in pure water," *J. Acoust. Soc. Am.* **52**, 1442-1446 (1972).
 - [56] J. L. Drewniak, K. I. Carnes, and F. Dunn, "*In vitro* ultrasonic heating of fetal bone," *J. Acoust. Soc. Am.* **86**, 1254-1258 (1989).
 - [57] J. L. Drewniak, L. A. Frizzell, and F. Dunn, "Errors resulting from finite beamwidth and sample dimensions in the determination of the ultrasonic absorption coefficient," *J. Acoust. Soc. Am.* **88**, 967-977 (1990).
 - [58] G. Du and M. A. Breazeale, "The ultrasonic field of a Gaussian transducer," *J. Acoust. Soc. Am.* **78**, 2083-2086 (1985).
 - [59] G. Du and M. A. Breazeale, "Harmonic distortion of a finite amplitude Gaussian beam in a fluid," *J. Acoust. Soc. Am.* **80**, 212-217 (1986).
 - [60] G. Du and M. A. Breazeale, "Theoretical description of a focussed Gaussian ultrasonic beam in a nonlinear medium," *J. Acoust. Soc. Am.* **81**, 51-57 (1987).
 - [61] F. A. Duck and H. C. Starritt, "Acoustic shock generation by ultrasonic imaging equipment," *Br. J. Radiology* **57**, 231-240 (1984).
 - [62] F. A. Duck, H. C. Starritt, J. D. Aindow, M. A. Perkins, and A. J. Hawkins, "The output of pulse-echo ultrasound equipment: A survey of powers, pressures and intensities," *Br. J. Radiology* **58**, 989-1001 (1985).
 - [63] F. Dunn, A. J. Averbuch, and W. D. O'Brien, Jr., "A primary method for the determination of ultrasonic intensity with the elastic sphere radiometer," *Acustica* **38**, 58-61 (1977).
-

- [64] F. Dunn, P. D. Edmonds, and W. J. Fry, "Absorption and dispersion of ultrasound in biological media," in *Biological Engineering*, edited by H.P. Schwan (McGraw-Hill Book Company, New York, NY, 1969), Chap. 3, pp. 205-332.
- [65] F. Dunn, J. E. Lohnes, and F. J. Fry, "Frequency dependence of threshold ultrasonic dosages for irreversible structural changes in the mammalian brain," *J. Acoust. Soc. Am.* **58**, 512-514 (1975).
- [66] E. S. Ebbini, *Deep Localized Hyperthermia with Ultrasound Phased Arrays Using the Pseudoinverse Pattern Synthesis Method* (Ph.D. Thesis, University of Illinois, Urbana, IL, 1990).
- [67] E. S. Ebbini, S. Umemura, M. Ibbini, and C. Cain, "A cylindrical-section ultrasound phased array applicator for hyperthermia cancer therapy," *IEEE Trans. Ultrason. Ferroelectr. Freq. Contr.* **UFFC-35**, 561-572 (1988).
- [68] R. C. Eberhart, A. Shitzer, and E. J. Hernandez, "Thermal dilution methods: estimation of tissue blood flow and metabolism," *Ann. NY Acad. Sci.* **335**, 107-132 (1980).
- [69] E. R. Eckert and R. M. Drake, *Analysis of Heat and Mass Transfer*, (McGraw-Hill Book Company, New York, NY, 1972), Chap. 1.
- [70] P. D. Edmonds, S. J. Stolzenberg, C. A. Torbin, S. M. Maden, and D. E. Pratt, "Postpartum survival of mice exposed *in utero* to ultrasound," *J. Acoust. Soc. Am.* **66**, 590-593 (1979).
- [71] M. J. Edwards, "Hyperthermia as a teratogen: a review of experimental studies and their clinical significance," *Terat. Carcinog. Mutag.* **6**, 568-582 (1986).
- [72] J. J. Faran, "Sound scattering by solid cylinders and spheres," *J. Acoust. Soc. Am.* **23**, 405-418 (1951).
- [73] J. J. Faran, "Scattering of cylindrical waves by a cylinder," *J. Acoust. Soc. Am.* **25**, 155-156 (1953).
- [74] L. Filipczynski, "Thermal effects in soft tissues developed under the influence of focused ultrasonic fields of short duration," *Archives Acoust.* **1**, 309-322 (1976).
- [75] L. Filipczynski, "Thermal effects in soft tissues developed under the action of ultrasonic fields of long durations," *Archives Acoust.* **2**, 297-303 (1977).
- [76] L. Filipczynski, "Absorption of longitudinal and shear waves and generation of heat in soft tissues," *Ultrasound Med. & Biol.* **12**, 223-228 (1986).
- [77] B. R. Fisher, *Biological Effects of Hyperthermia and Potential Risk Associated With Ultrasound Exposure*, FDA CDRH Publ. PB90 10 070 (Washington, DC, 1989).
- [78] L. Flax and W. G. Neubauer, "Acoustic reflection from layered elastic absorptive cylinders," *J. Acoust. Soc. Am.* **61**, 307-312 (1977).
- [79] L. Flax, V. K. Varadan, and V. V. Varadan, "Scattering of an obliquely incident acoustic wave by an infinite cylinder," *J. Acoust. Soc. Am.* **68**, 1832-1835 (1980).
-

- [80] L. A. Frizzell, "Threshold dosages for damage to mammalian liver by high intensity focused ultrasound," *IEEE Trans. Ultrason. Ferroelectr. Freq. Contr.* **UFFC-35**, 578-581 (1988).
 - [81] L. A. Frizzell, E. L. Carstensen, and J. F. Dyro, "Shear properties of mammalian tissues at low megahertz frequencies," *J. Acoust. Soc. Am.* **60**, 1409-1411 (1976).
 - [82] L. A. Frizzell, C. A. Linke, E. L. Carstensen, and C. W. Fridd, "Thresholds for focal lesions in rabbit kidney, liver, and testicle," *IEEE Trans. Biomed. Eng.* **BME-24**, 393-396 (1977).
 - [83] F. J. Fry and J. E. Barger, "Acoustical properties of the human skull," *J. Acoust. Soc. Am.* **63**, 1576-1590 (1978).
 - [84] F. J. Fry, K. A. Dines, C. R. Rielly, and S. A. Goss, "Losses in tissue associated with finite amplitude ultrasound transmission," *Ultrasound Med. & Biol.* **15**, 481-497 (1989).
 - [85] W. J. Fry and F. Dunn, "Ultrasound: analysis and experimental methods in biological research," in *Physical Techniques in Biological Research*, edited by W.L. Nastuck (Academic Press, Inc., New York, NY, 1962), vol. 4, Chap. 6.
 - [86] W. J. Fry and R. B. Fry, "Determination of absolute sound levels and acoustic absorption coefficients by thermocouple probes - theory," *J. Acoust. Soc. Am.* **26**, 294-310 (1954).
 - [87] W. J. Fry and R. B. Fry, "Determination of absolute sound levels and acoustic absorption coefficients by thermocouple probes - experiment," *J. Acoust. Soc. Am.* **26**, 311-317 (1954).
 - [88] F. J. Fry, G. Kossoff, R. C. Eggleton, and F. Dunn, "Threshold ultrasonic dosages for structural changes in the mammalian brain," *J. Acoust. Soc. Am.* **48**, 1413-1417 (1970).
 - [89] B. J. Garcia, R. S. C. Cobbold, F. S. Foster, and K. G. McNeill, "Ultrasonic attenuation in bone," *IEEE Ultrasonics Symposium Proceedings* (Institute of Electrical and Electronics Engineers, New York, NY, 1978), pp. 327-330.
 - [90] M. Germain, W. S. Webster, and M. J. Edwards, "Hyperthermia as a teratogen: parameters determining hyperthermia-induced head defects in the rat," *Teratology* **31**, 265-272 (1985).
 - [91] S. A. Goss, J. W. Cobb, and L. A. Frizzell, "Effect of beam width and thermocouple size on the measurement of ultrasonic absorption using the thermoelectric technique," *IEEE Ultrasonics Symposium Proceedings* (Institute of Electrical and Electronics Engineers, New York, NY, 1977), pp. 206-211.
 - [92] S. A. Goss and F. Dunn, "Ultrasonic propagation properties of collagen," *Phys. Med. Biol.* **25**, 827-837 (1980).
-

- [93] S. A. Goss, L. A. Frizzell, and F. Dunn, "Frequency dependence of ultrasonic absorption in mammalian testis," *J. Acoust. Soc. Am.* **63**, 1226-1229 (1978).
- [94] S. A. Goss, L. A. Frizzell, and F. Dunn, "Ultrasonic absorption and attenuation in mammalian tissues," *Ultrasound in Med. & Biol.* **5**, 181-186 (1979).
- [95] S. A. Goss, L. A. Frizzell, F. Dunn, and K. A. Dines, "Dependence of the ultrasonic properties of biological tissue on constituent proteins," *J. Acoust. Soc. Am.* **67**, 1041-1044 (1980).
- [96] S. A. Goss and F. J. Fry, "Nonlinear acoustic behavior in focused ultrasonic fields: observations of intensity dependent absorption in biological tissue," *IEEE Trans. Sonics Ultrason.* **SU-28**, 21-26 (1981).
- [97] S. A. Goss, R. L. Johnston, and F. Dunn, "Comprehensive compilation of empirical ultrasonic properties of mammalian tissues," *J. Acoust. Soc. Am.* **64**, 423-457 (1978).
- [98] S. A. Goss, R. L. Johnston, and F. Dunn, "Compilation of empirical ultrasonic properties of mammalian tissues. II," *J. Acoust. Soc. Am.* **68**, 93-108 (1980).
- [99] M. F. Hamilton, "Fundamentals and applications of nonlinear acoustics," in *Nonlinear Wave Propagation in Mechanics*, edited by T. W. Wright (The American Society of Mechanical Engineers, New York, NY, 1986).
- [100] G. R. Harris, "A discussion of procedures for ultrasonic intensity and power calculations from miniature hydrophone measurements," *Ultrasound Med. & Biol.* **11**, 803-817 (1985).
- [101] G. R. Harris, "A model of the effects of hydrophone and amplifier frequency response on ultrasound exposure measurements," *IEEE Ultrasonics Symposium Proceedings* (Institute of Electrical and Electronics Engineers, New York, NY, 1989), pp. 1061-1065.
- [102] J. G. Harris and J. Pott, "Further studies of the scattering of a Gaussian beam from a fluid-solid interface," *J. Acoust. Soc. Am.* **78**, 1072-1080 (1985).
- [103] T. Hasegawa and Y. Watanabe, "Acoustic radiation pressure on an absorbing sphere," *J. Acoust. Soc. Am.* **63**, 1733-1737 (1978).
- [104] T. Hasegawa and K. Yosioka, "Acoustic radiation force on a solid elastic sphere," *J. Acoust. Soc. Am.* **46**, 1139-1143 (1969).
- [105] T. Hasegawa and K. Yosioka, "Acoustic radiation force on fused silica spheres, and intensity determination," *J. Acoust. Soc. Am.* **58**, 581-585 (1975).
- [106] E. G. Henneke II and G. L. Jones, "Critical angle for reflection at a liquid solid interface in single crystals," *J. Acoust. Soc. Am.* **59**, 204-205 (1976).
- [107] K. F. Herzfeld and T. A. Litovitz, *Absorption and Dispersion of Ultrasonic Waves* (Academic Press, Inc., New York, NY, 1959).
-

- [108] B. Hosten, M. Deschamps, and B. R. Tittman, "Inhomogeneous wave generation and propagation in lossy anisotropic solids. Application to the characterization of viscoelastic composite materials," *J. Acoust. Soc. Am.* **82**, 1763-1770 (1987).
- [109] D. K. Hsu, F. J. Margentan, M. D. Hasselbusch, S. J. Wormley, M. S. Hughes, and D. O. Thompson, "Technique for nonuniform poling of piezoelectric element and fabrication of Gaussian transducers," *UFFC-37*, 404-410 (1990).
- [110] K. H. Huebner, *Finite Element Method for Engineers* (John Wiley & Sons, Inc., New York, NY, 1975).
- [111] K. Hynynen, "Present status of ultrasound hyperthermia," *IEEE Ultrasonics Symposium Proceedings* (Institute of Electrical and Electronics Engineers, New York, NY, 1988), pp. 941-946.
- [112] K. Hynynen and D. DeYoung, "Temperature elevation at muscle-bone interface during scanned, focused ultrasound hyperthermia," *Int. J. Hyperthermia* **4**, 267-279 (1988).
- [113] Y. Jaluria and K. E. Torrance, *Computational Heat Transfer* (Hemisphere Publishing, Washington, DC, 1986).
- [114] H. Jansons, A. Tatarimov, V. Dzenis, and A. Kregers, "Constructional peculiarities of the human tibia defined by reference to ultrasound measurement data," *Biomaterials* **5**, 221-226 (1984).
- [115] R. L. Johnston and F. Dunn, "Ultrasonic absorbed dose, dose rate, and produced lesion volume," *Ultrasonics* **14**, 153-155 (1976).
- [116] R. P. Kanwal, *Generalized Functions: Theory and Technique* (Academic Press, Inc., New York, NY, 1983).
- [117] J. L. Katz and K. Ukraincik, "On the anisotropic elastic properties of hydroxyapatite," *J. Biomech.* **4**, 221-227 (1971).
- [118] J. L. Katz and S. B. Yoon, "The structure and anisotropic mechanical properties of bone," *IEEE Trans. Biomed. Eng.* **BME-31**, 878-884 (1984).
- [119] D. R. S. Kirby and S. Bradbury, "The hemo-chorial mouse placenta," *Anat. Rec.* **152**, 279-282 (1965).
- [120] I. I. Konopatskaya, "Theoretical investigation of the local heating of biological tissue under the action of focused ultrasound," *Sov. Phys. Acoust.* **34**, 384-387 (1988).
- [121] J. Kushibiki and N. Chubachi, "Material characterization by line-focus-beam acoustic microscope," *IEEE Trans. Sonics Ultrason.* **SU-32**, 189-212 (1985).
- [122] J. Kushibiki, T. Ueda, and N. Chubachi, "Determination of elastic constants by LFB acoustic microscope," *IEEE Ultrasonics Symposium Proceedings* (Institute of Electrical and Electronics Engineers, New York, NY, 1987), pp. 817-824.
-

- [123] J. Kushibiki, K. L. Ha, N. Chubachi, and F. Dunn "Application of acoustic microscopy to dental material characterization," *IEEE Ultrasonics Symposium Proceedings* (Institute of Electrical and Electronics Engineers, New York, NY, 1987), pp. 837-842.
- [124] R. Lakes, H. S. Yoon, and J. L. Katz, "Ultrasonic wave propagation and attenuation in wet bone," *J. Biomed. Eng.* **8**, 143-148 (1986).
- [125] S. B. Lang, "Ultrasonic method for measuring elastic coefficients of bone and results on fresh and dried bovine bones," *IEEE Trans. Biomed. Eng.* **BME-2**, 101-105 (1970).
- [126] F. Lee, "Scattering of a cylindrical wave of sound by an elastic cylinder," *Acustica* **13**, 397-402 (1963).
- [127] C. S. Lee, *Ultrasonically Induced Functional Changes in the Neonatal Mouse Central Nervous System* (M.S. Thesis, University of Illinois, Urbana, IL, 1982).
- [128] S. Lees, J. M. Ahern, and M. Leonard, "Parameters influencing the sonic velocity in compact calcified tissues of various species," *J. Acoust. Soc. Am.* **74**, 28-33 (1983).
- [129] S. F. Lees, P. F. Cleary, J. D. Heeley, and E. L. Gariepy, "Distribution of sonic pleiovelocity in a compact bone sample," *J. Acoust. Soc. Am.* **66**, 644-646 (1979).
- [130] S. Lees and F. R. Rollins, "Anisotropy in hard dental tissues," *J. Biomech.* **5**, 557-566 (1972).
- [131] J. F. Lehman, "Heating produced by ultrasound in bone and soft tissue," *Arch. Phys. Med Rehabil.* **48**, 397-401 (1967).
- [132] P. P. Lele, "A simple method for production of trackless focal lesions with focused ultrasound; physical factors," *J. Physiol.* **160**, 494-511 (1962).
- [133] P. P. Lele, "Ultrasonic teratology in mouse and man," in *Proceedings of the Second European Congress on Ultrasonics in Medicine*, International Congress Series No. 363 (Excerpta Medica, Amsterdam, 1975) pp. 22-27.
- [134] P. P. Lele, "Safety and potential hazards in the current applications of ultrasound in obstetrics and gynecology," *Ultrasound Med. & Biol.* **5**, 307-320 (1979).
- [135] R. M. Lerner, E. L. Carstensen, and F. Dunn, "Frequency dependence of thresholds for ultrasonic production of thermal lesions in tissues," *J. Acoust. Soc. Am.* **54**, 504-506 (1973).
- [136] T. Li and M. Ueda, "Sound scattering of a plane wave obliquely incident on a cylinder," *J. Acoust. Soc. Am.* **86**, 2363-2368 (1989).
- [137] F. L. Lizzi, D. J. Coleman, J. Driller, M. Ostromogilsky, S. Chang, and P. Greenall, "Ultrasonic hyperthermia for ophthalmic therapy," *IEEE Trans. Sonics Ultrason.* **SU-31**, 473-481 (1984).
- [138] F. L. Lizzi, J. Driller, M. Ostromogilsky, and D. J. Coleman, "Thermal model for ultrasonic treatment of glaucoma," *Ultrasound Med. & Biol.* **10**, 289-298 (1984).
-

- [139] F. L. Lizzi and M. Ostromogilsky, "Analytical modeling of ultrasonically induced tissue heating," *Ultrasound Med. & Biol.* **13**, 607-618 (1987).
 - [140] L. A. Longley and W. D. O'Brien, Jr., "Ultrasonic heating distribution in lossy cylinders and spheres," *IEEE Trans. Sonics Ultrason.* **SU-29**, 69-78 (1982).
 - [141] M. E. Lyons and K. J. Parker, "Absorption and attenuation in soft tissues: II - experimental results," *IEEE Trans. Ultrason. Ferroelectr. Freq. Contr.* **UFFC-35**, 511-521 (1988).
 - [142] E. L. Madsen, H. J. Sathoff, and J. A. Zagzebski, "Ultrasonic shear wave properties of soft tissues and tissuelike materials," *J. Acoust. Soc. Am.* **74**, 1346-1355 (1983).
 - [143] F. D. Martin and M. A. Breazeale, "A simple way to eliminate diffraction lobes emitted by ultrasonic transducers," *J. Acoust. Soc. Am.* **49**, 1668-1669 (1971).
 - [144] W. P. Mason, *Physical Acoustics and the Properties of Solids* (D. Van Nostrand, New York, NY, 1958).
 - [145] T. W. McGrail and R. C. Seagrave, "Application of the bioheat transfer equation in fetal placental studies," *Ann. NY Acad. Sci.* **335**, 161-172 (1980).
 - [146] M. W. Miller and M. C. Ziskin, "Biological consequences of hyperthermia," *Ultrasound Med. & Biol.* **15**, 707-722 (1989).
 - [147] E. G. Moros, R. B. Roemer, and K. Hynynen, "Simulations of scanned focused ultrasound hyperthermia: the effects of scanning speed and pattern on the temperature fluctuations at the focal depth," *IEEE Trans. Ultrason. Ferroelectr. Freq. Contr.* **UFFC-35**, 552-560 (1988).
 - [148] P. M. Morse and K. U. Ingard, *Theoretical Acoustics* (McGraw-Hill Book Company, New York, NY, 1968), Chap. 8.
 - [149] T. G. Muir and E. L. Carstensen, "Prediction of nonlinear acoustic effects at biomedical frequencies and intensities," *Ultrasound Med. & Biol.* **6**, 345-347 (1980).
 - [150] National Council for Radiation Protection, *Exposure Criteria for Medical Diagnostic Ultrasound - Part 1: Exposure Based on Thermal Mechanisms*, in preparation (1991).
 - [151] W. H. Newman and P. P. Lele, "Measurement and sensitivity characteristics of transient, focused ultrasound for tissue perfusion measurements," in *Heat and Mass Transfer in the Microcirculation and Thermally Significant Vessels*, edited by K. R. Diller and R. B. Roemer (American Society of Mechanical Engineers, New York, NY, 1986).
 - [152] W. L. Nyborg, *Physical Mechanisms for Biological Effects of Ultrasound*, Department of Health Education and Welfare Publication No. (FDA) 78-8062 (Washington, DC, 1977).
 - [153] W. L. Nyborg, "Heat generation by ultrasound in a relaxing medium," *J. Acoust. Soc. Am.* **70**, 310-312, 1981.
-

- [154] W. L. Nyborg, "Solutions of the bio-heat transfer equation," *Phys. Med. Biol.* **33**, 785-792 (1988).
- [155] W. L. Nyborg and R. B. Steele, "Temperature elevation in a beam of ultrasound," *Ultrasound Med. & Biol.* **9**, 611-620 (1983).
- [156] N. M. Ozisik, *Heat Conduction* (John Wiley and Sons, Inc., New York, NY, 1980).
- [157] E. P. Papadakis, "Ultrasonic attenuation caused by scattering in polycrystalline media," in *Physical Acoustics*, edited by W. P. Mason (Academic Press, Inc., New York, NY, 1968), vol. 4B.
- [158] A. Papoulis, *Probability, Random Variables, and Stochastic Processes* (McGraw-Hill Book Company, New York, NY, 1965)
- [159] K. J. Parker, "The thermal pulse decay technique for measuring ultrasonic absorption coefficients," *J. Acoust. Soc. Am.* **74**, 1356-1361 (1983).
- [160] K. J. Parker, "Ultrasonic attenuation and absorption in liver tissue," *Ultrasound in Med. & Biol.* **9**, 363-369 (1983).
- [161] K. J. Parker, "Observation of nonlinear acoustic effects in a B-Scan imaging instrument," *IEEE Trans. Sonics Ultrason.* **SU-32**, 4-8 (1985).
- [162] K. J. Parker, "Effects of heat conduction and sample size on ultrasonic absorption measurements," *J. Acoust. Soc. Am.* **77**, 719-725 (1985).
- [163] K. J. Parker and E. M. Friets, "On the measurement of shock waves," *IEEE Trans. Ultrason. Ferroelectr. Freq. Contr.* **UFFC-34**, 454-460 (1987).
- [164] K. J. Parker and M. E. Lyons, "Absorption and attenuation in soft tissues: I - calibration and error analyses," *IEEE Trans. Ultrason. Ferroelectr. Freq. Contr.* **UFFC-35**, 242-252 (1988).
- [165] A. D. Pierce, *Acoustics: An Introduction to Its Physical Principles and Applications* (McGraw-Hill Book Company, New York, NY, 1981).
- [166] H. H. Pennes, "Analysis of tissue and arterial blood temperatures in resting human forearm," *J. Appl. Physiol.* **2**, 93-122 (1948).
- [167] J. B. Pond, *A Study of the Biological Action of Focused Mechanical Waves (Focused Ultrasound)* (Ph.D. Thesis, University of London, London, 1968).
- [168] J. B. Pond, "The role of heat in the production of ultrasonic focal lesions," *J. Acoust. Soc. Am.* **47**, 1607-1611 (1970).
- [169] P. D. Pollock, *The Theory and Properties of Thermocouple Elements*, ASTM Special Technical Publication No. 492 (American Society for Testing and Materials, Philadelphia, PA, 1971).
- [170] J. Pott and J. G. Harris, "Scattering of an acoustic Gaussian beam from a fluid-solid interface," *J. Acoust. Soc. Am.* **76**, 1829-1838 (1984).
-

- [171] R. L. Powell, W. J. Hall, C. H. Hyink, L. L. Sparks, G. W. Burns M. G. Scroger, and H. H. Plumb, *Thermocouple Reference Tables Based on the IPTS-68*, National Bureau of Standards Monograph No. 125 (Omega Press, Stamford, CT, 1975).
- [172] R. C. Preston, D. R. Bacon, A. J. Livett, and K. Rajendran, "PVDF membrane hydrophone performance properties and their relevance to the measurement of acoustic output of medical ultrasonic equipment," *J. Phys. E: Sci. Instrum.* **16**, 786-796 (1983).
- [173] C. R. Reilly and K. J. Parker, "Finite amplitude effects on ultrasound beam patterns in attenuating media," *J. Acoust. Soc. Am.* **86**, 2339-2348 (1989).
- [174] R. Resnik, "Anatomic alterations in the reproductive tract," in *Maternal-Fetal Medicine: Principles and Practice*, edited by R. K. Creasy and R. Resnik (W. B. Saunders Co., Philadelphia, PA, 1989).
- [175] T. C. Robinson and P. P. Lele, "An analysis of lesion development in the brain and plastics by high-intensity focused ultrasound at low-megahertz frequencies," *J. Acoust. Soc. Am.* **51**, 1333-1351 (1972).
- [176] G. Roberts and H. Kaufman, *Table of Laplace Transforms* (Sanders, Philadelphia, PA, 1966).
- [177] R. B. Roemer, W. Swindell, S. T. Clegg and R. L. Kress, "Simulation of focused, scanned ultrasonic heating of deep-seated tumors: the effect of blood perfusion," *IEEE Trans. Sonics Ultrason.* **SU-31**, 457-466 (1984).
- [178] W. M. Roshenow and H. Choi, *Heat, Mass, and Momentum Transfer* (Prentice-Hall, Inc., Englewood Cliffs, NJ, 1961), p. 106.
- [179] O. V. Rudenko and S. I. Soluyan, *Theoretical Foundations of Nonlinear Acoustics*, translated from the Russian by R. T. Beyer (Consultants Bureau, New York, NY, 1977).
- [180] R. Rugh, *The Mouse: Its Reproduction and Development* (Burgess Publishing Company, Minneapolis, MN, 1968).
- [181] D. G. Schombert, S. W. Smith, and G. K. Harris, "Angular response of miniature ultrasonic hydrophones," *Med. Phys.* **9**, 484-492 (1982).
- [182] K. M. Sekins and A. F. Emery, "Thermal science for physical medicine," in *Therapeutic Heat and Cold*, edited by J. F. Lehman (Williams and Wilkins, Baltimore, MD, 1982), Chap. 3.
- [183] T. Shephard, private communication (1989).
- [184] A. Shitzer, "Studies of bioheat transfer in mammals," in *Topics in Transport Phenomena*, edited by C. Gutfinger (Halstead Press, New York, NY, 1975), pp. 211-341.
- [185] M. R. Sikov, D. H. Collins, and D. B. Carr, "Measurement of temperature rise in prenatal rats during exposure of the exteriorized uterus to ultrasound," *IEEE Trans. Sonics Ultrason.* **SU-31**, 497-503 (1984).
-

- [186] B. S. Singh and A. Dybbs, "Error in temperature measurements due to conduction along the sensor leads," *Trans. ASME J. Heat Transfer* **98**, 491-495 (1976).
- [187] R. A. Smith and D. R. Bacon, "A multiple-frequency hydrophone calibration technique," *J. Acoust. Soc. Am.* **87**, 2231-2243 (1990).
- [188] D. W. Smith, S. K. Clarren, and M. A. S. Harvey, "Hyperthermia as a possible teratogenic agent," *J. Ped.* **92**, 878-883 (1978).
- [189] N. B. Smith, T. H. Shepard, and W. D. O'Brien, Jr., "Ultrasonically induced temperature rise in rat embryos," submitted for publication to the *J. Acoust. Soc. Am.*
- [190] I. Stakgold, *Green's Functions and Boundary Value Problems* (John Wiley and Sons, Inc., New York, NY, 1979), Chap. 3.
- [191] T. K. Stanton, "Sound scattering by cylinders of finite length. I. Fluid cylinders," *J. Acoust. Soc. Am.* **83**, 55-63 (1988).
- [192] T. K. Stanton, "Sound scattering by cylinders of finite length. II. Elastic cylinders," *J. Acoust. Soc. Am.* **83**, 64-67 (1988).
- [193] T. K. Stanton, "Sound scattering by cylinders of finite length. III. Deformed cylinders," *J. Acoust. Soc. Am.* **86**, 691-705 (1989).
- [194] H. C. Starritt, M. A. Perkins, F. A. Duck, and V. F. Humphrey, "Evidence for ultrasonic finite amplitude distortion in muscle using medical equipment," *J. Acoust. Soc. Am.* **77**, 302-306 (1985).
- [195] S. J. Stolzenberg, C. A. Torbit, P. D. Edmonds, and J. C. Taenzer, "Effects of ultrasound on the mouse exposed at different stages of gestation: acute studies," *Rad. and Envir. Biophys.* **17**, 245-270 (1980).
- [196] K. Theiler, "Embryology," in *The Mouse in Biomedical Research Vol. III: Normative, Biology, Immunology, and Husbandry*, edited by H. L. Foster, T. D. Small, and J. Fox (Academic Press, Inc., New York, NY, 1983).
- [197] W. S. Webster, M. Germain, and J. J. Edwards, "The induction of microphthalmia, encephalocele, and other head defects following hyperthermia during the gastrulation process in the rat," *Teratology* **31**, 73-82 (1985).
- [198] P. N. T. Wells, M. A. Bullen, and H. F. Freundlich, "Milliwatt ultrasonic radiometry," *Ultrason.* **2**, 124-128 (1964).
- [199] D. G. Whittingham and M. J. Wood, "Reproductive physiology," in *The Mouse in Biomedical Research Vol. III: Normative, Biology, Immunology, and Husbandry*, edited by H. L. Foster, T. D. Small, and J. Fox (Academic Press, Inc., New York, NY, 1983).
- [200] P. G. Wilkin, "Organogenesis of the human placenta," in *Organogenesis*, edited by R. L. DeHaan and H. Ursprung (Holt, Rinehart, and Winston, Inc., Chicago, IL, 1965).
- [201] J. Wu and G. Du, "Temperature elevation in tissues generated by finite-amplitude tone bursts of ultrasound," *J. Acoust. Soc. Am.* **88**, 1562-1577 (1990).
-

- [202] J. Wu and G. Du, "Temperature elevation generated by a focused Gaussian beam of ultrasound," *Ultrasound Med. & Biol.* **16**, 489-498 (1990).
 - [203] S. B. Yoon and J. L. Katz, "Ultrasonic wave propagation in human cortical bone - I. Theoretical considerations for hexagonal symmetry," *J. Biomech.* **9**, 407-412 (1976).
 - [204] S. B. Yoon and J. L. Katz, "Ultrasonic wave propagation in human cortical bone - II. Measurements of elastic properties and micro-hardness," *J. Biomech.* **9**, 459-464 (1976).
 - [205] H. S. Yoon and J. L. Katz, "Ultrasonic wave propagation in human cortical bone - III. Piezoelectric contribution," *J. Biomech.* **9**, 537-540 (1976).
 - [206] H. S. Yoon and J. L. Katz, "Dispersion of the ultrasonic velocities in human cortical bone," *IEEE Ultrasonics Symposium Proceedings* (Institute of Electrical and Electronics Engineers, New York, NY, 1976), pp. 48-50.
-

VITA

James Lewis Drewniak was born in Beach, North Dakota, on July 13, 1962. He attended the University of North Dakota from 1979 to 1981, and received the B. S. degree with highest honors in 1985, and the M.S. degree from the University of Illinois in 1987. From 1985 to 1987 he was a Graduate Research Assistant in the Electromagnetics Laboratory at the University of Illinois investigating broadband, circularly-polarized, radiating-line antennas and arrays. He was a Graduate Research Assistant in the Bioacoustics Research Laboratory at the University of Illinois from 1987 to 1990 studying ultrasonic properties of tissue. Mr. Drewniak was awarded the General Electric Teaching Incentive Grant in 1988, the Ernest A. Reid Teaching Incentive Fellowship in 1989, and the Knowles Fellowship in Acoustics in 1990. He is a member of Eta Kappa Nu, Tau Beta Pi, and Phi Kappa Phi. Mr. Drewniak has been a member of IEEE since 1985. His journal and symposium papers and presentations include:

J.L. Drewniak and P.E. Mayes, "ANSERLIN: A broadband, low-profile, circularly polarized antenna," *IEEE Trans. Antennas Propag.*, vol. 37, pp. 281-288, March 1989.

J.L. Drewniak, K.I. Carnes, and F. Dunn, "*In vitro* ultrasonic heating of fetal bone," *J. Acoust. Soc. Am.*, vol. 86, pp. 1254-1258, October 1989.

J.L. Drewniak, L.A. Frizzell and F. Dunn, "Errors resulting from finite beamwidth and sample dimensions in the determination of the ultrasonic absorption coefficient," *J. Acoust. Soc. Am.*, vol. 88, pp. 967-977, August 1990.

J.L. Drewniak and P.E. Mayes, "The synthesis of patterns using a series-fed array of ANnular SEctor Radiating LINE (ANSERLIN) elements: low-profile, circularly polarized radiators," to be published in the *IEEE Trans. Antennas Propag.*, January 1991.

K.I. Carnes, J.L. Drewniak, and F. Dunn, "*In utero* measurements of ultrasonically induced fetal mouse temperature increases," accepted for publication in *Ultrasound Med. & Biol.*, August 1990.

P.E. Mayes, D. Tanner, R. Waller, J.L. Drewniak, T. Szmurlo, A. Boris, and D. Kunkee, "Some broadband, low-profile antennas," *Proc. 1985 Antenna Applications Symposium*, University of Illinois, Urbana, IL, September 1985.

J.L. Drewniak, P.E. Mayes, D. Tanner, and R. Waller, "A log-spiral, radiating-line antenna," *IEEE AP-S International Symposium Digest*, pp. 773-776, June 1986.

J.L. Drewniak and P.E. Mayes, "Power division by element design in a circularly polarized, series-fed array," *IEEE AP-S International Symposium Digest*, pp. 798-801, June 1987.

J.L. Drewniak, P.E. Mayes, D. Tanner, and J. Woodruff, "A dual circular polarization, radiating-line antenna," *IEEE AP-S International Symposium Digest*, pp. 348-351, June 1987.

P.E. Mayes, J.L. Drewniak, J. Bowen, and J. Gentle, "Simple, low-profile, circularly polarized arrays," presented at the Jet Propulsion Laboratory Mobile Satellite Conference, May 1988.

J.L. Drewniak, K.I. Carnes, and F. Dunn, "Measured temperature rise in fetal bone exposed, *in vitro*, to ultrasound," *Journal of Ultrasound In Medicine, Proceedings of the 1988 World Federation for Ultrasound in Medicine and Biology Meeting*, vol. 7 (supplement), p. 263, October 1988.

J.L. Drewniak, K.I. Carnes, and F. Dunn, (invited) "*In vitro* ultrasonic heating of fetal bone," *J. Acoust. Soc. Am.*, vol. 86 (S1), p. S28, November 1989.

K.I. Carnes, J.L. Drewniak, and F. Dunn, "*In utero* measurement of fetal mouse temperature increases", presented at the American Institute of Ultrasound in Medicine Conference, March 1990.

J.L. Drewniak, (invited) "The synthesis of patterns using a series-fed array of ANnular SEctor Radiating LINE (ANSERLIN) elements: low profile, circularly polarized radiators," The Ohio State Electroscience Laboratory, May 1990.